universitätbonn igg

Institut für
Geodäsie und Geoinformation

Schriftenreihe

54

Proceedings of the First International Workshop on VLBI Observations of Near-field Targets

October 5 - 6, 2016

Edited by A. Nothnagel and F. Jaron

First International Workshop on VLBI Observations of Near-field Targets Proceedings

universitätbonn igg

Institut für Geodäsie und Geoinformation

Schriftenreihe

54

Proceedings of the First International Workshop on VLBI Observations of Near-field Targets

October 5 - 6, 2016

Edited by A. Nothnagel and F. Jaron

Diese Veröffentlichung erscheint anlässlich des
First International Workshop on VLBI Observations of Near-field Targets,
der am 4 · 5. Oktober 2016 im Institut für Geodäsie und Geoinformation stattfand.

Schriftenreihe des Instituts für Geodäsie und Geoinformation
der Rheinischen Friedrich-Wilhelms-Universität Bonn

Herausgeber: Prof. Dr. Jan-Henrik Haunert
Prof. Dr.-Ing. Theo Kötter
Prof. Dr.-Ing. Heiner Kuhlmann
Prof. Dr.-Ing. Jürgen Kusche
Prof. Dr. techn. Wolf-Dieter Schuh
Prof. Dr. Cyrill Stachniss

Die Aufnahme dieser Arbeit in die Schriftenreihe wurde von den Herausgebern
der Reihe einstimmig beschlossen.

Bonn 2017 ISSN 1864-1113

Preface

Geodetic and astrometric Very Long Baseline Interferometry (VLBI) observations of satellites and other near-field targets have come to the attention of more and more scientists dealing with a variety of applications. One of the main goals of performing and analyzing such observations is to establish and improve the direct link between the quasi-inertial celestial reference frame of compact extra-galactic objects, such as the International Celestial reference Frame (ICRF), and the dynamical reference frames of Earth orbiting satellites. Another body of interest is the Moon with its kinematics, so far mostly observed with Lunar Laser Ranging (LLR).

VLBI and DeltaDOR (Differential One-way Ranging) observations are well established for solar system spacecraft tracking but just start to be employed for other applications nearer to Earth as well. For this, first VLBI observations of artificial satellites and the Moon were carried out in recent years. As a consequence, the research areas of near-field VLBI observations are manifold including technical developments for components of scheduling, observations, correlation, fringe fitting and data analysis.

To bring together scientists working on topics related to near-field VLBI observations and to explore current possibilities and future opportunities, the *First International Workshop on VLBI Observations of Near-field Targets* was held at the Institute of Geodesy and Geoinformation, University of Bonn, Bonn, Germany, on October 5 - 6, 2016. The workshop was sponsored by the IVS Working Group 7: Satellite Observations with VLBI (`http://ivscc.gsfc.nasa.gov`).

The two-day workshop was dedicated to the presentations of the current status and of recent results in the form of oral and poster presentations. Considering that this was the first workshop of this kind, the 45 participants from Europe as well as from overseas delivering 25 talks and 4 posters are a very good indication of the interest in these topics. The workshop certainly helped to exchange ideas and solutions on the personal level and produced a number of exciting new results.

In order to make available the descriptions of the activities and the respective results to a wider group, we decided to call for manuscripts and print the documents in the *Schriftenreihe des Instituts für Geodäsie und Geoinformation der Universität Bonn*. We are grateful to all authors who have submitted their manuscripts for publication in these proceedings and hope that many more readers will draw interesting information from the papers.

Axel Nothnagel, Frédéric Jaron

Bonn, February 28, 2017

First International Workshop on VLBI Observations of Near-Field Targets
October 5-6, 2016, Bonn, Germany

Contents

Scheduling of VLBI Satellite Observations with VieVS

Hellerschmied A, Plank L, McCallum J, Sun J, Böhm J

Abstract In order to enable VLBI observations of satellite targets on a regular basis, proper scheduling procedures need to be in place. The Vienna VLBI Software VieVS has been used to schedule about 40 of these test sessions, triggering large developments in the scheduling tools. We report on the current capabilities of the available software and discuss present difficulties when preparing a new experiment. In the second part we concentrate on the scheduling of VLBI sessions observing the very low APOD satellite with the Australian AuScope array.

Keywords Space tie, Co-location in space, VLBI satellite tracking, VieVS, scheduling, APOD

1 Introduction

Scheduling depicts the process of generating suitable observation plans. This is defining the time sequence of a VLBI experiment under consideration of the telescopes specific capabilities. The result is a schedule in a standardized format, e.g. .SKD or .VEX.

The new challenge hereby is the cross-eyed observation geometry, meaning that the directions from the participating telescopes to the target cannot be considered as parallel any more, as is the case for quasar VLBI. The satellite targets are moving, requiring active tracking of the telescope. In general, accurate timing and antenna steering is more critical.

We use the Vienna VLBI Software (VieVS, Böhm et al., 2012) for scheduling.

2 Scheduling satellite observations with VieVS

The satellite scheduling module of VieVS[1] is described in Hellerschmied et al. (2015a) and Hellerschmied et al. (2015b). All antenna specifications and steering are treated as for standard geodetic scheduling (Sun, 2013). The coordinates for the satellite targets are implemented via public two-line element (TLE) orbit data. Running in Matlab, the scheduler works interactively, where the operator can choose the best target - a visible quasar or a satellite - and add it to the schedule. An intuitive program design and interactive sky plots support this manual process. The program then internally manages antenna slewing, on source times for quasars and observation timing requiring common visibilities. In order to allow tracking tests at individual stations, the scheduler also works for a single telescope to be scheduled.

This interactive mode is very suitable for short test sessions. Over the past years, about 40 of those sessions were scheduled with this program (see Figure 1).

A. Hellerschmied, J. Böhm
Technische Universität Wien, Gußhausstraße 27-29, 1040, Vienna, Austria

L. Plank, J. McCallum, J. Lovell
University of Tasmania, Private Bag 37, 7001, Hobart, Australia

J. Sun
Beijing Aerospace Control Center, Beijing, China

[1] More information including a user manual is available at `http://vievs.geo.tuwien.ac.at/`

date	duration	name	stations	targets
16.01.2014	1h	G140116a	O8, Wz	Glonass
16.01.2014	1h	G140116b	O8, Wz	Glonass
21.01.2014	1h	G140121a	O8, Wz	Glonass
21.01.2014	1h	G140121b	O8, Wz	Glonass
15.06.2015	1h	615aHo	Ho	GPS + Glonass
18.06.2015	1h	169cHo	Ho	GPS + Glonass
18.06.2015	2h	169cCd	Cd	GPS + Glonass
28.06.2015	2h	179a	Ho, Cd	GPS + Glonass + quasars
19.08.2015	28 min	ex1	Wz, Wn, Wd	GPS + Glonass
20.08.2015	25 min	ex2	Wz, Wn, Wd	GPS + Glonass
24.08.2015	11 min	ex3a	Wz, Wn, Wd	GPS
24.08.2015	4h	236a	Ho, Cd	GPS + quasars
26.08.2015	4h	238a	Ho, Cd	GPS + Glonass + quasars
12.11.2015	30 min	ex4a	Wd, Wn	GPS + Glonass
23.11.2015	33 min	23a1	Mc, Wd	GPS + Galileo + Glonass
23.11.2015	2h 15min	23b1	Mc, Wd	GPS + Galileo + Glonass + quasars
23.11.2015	2h 30 min	23c1	Mc, Wd	GPS + Galileo + Glonass + quasars
18.04.2016	9 min	ex5a	Wz, Wn, Wd	Glonass
05.05.2016	6h	126b	Ho, Cd	GPS + quasars
10.05.2016	6h	131a	Ho, Cd	GPS + quasars
11.05.2016	6h	132a	Ho, Cd	GPS + quasars
17.05.2016	12 min	ex6b	Wn, Wz	Glonass
23.05.2016	12 min	ex7a	Wn, Wz	Glonass
23.05.2016	3h	144b	Mc, O8, Sr	GPS + Galileo + Glonass + Beidou + quasars
23.05.2016	40 min	144d	Mc, O8, Sr	GPS + Galileo + Glonass + Beidou
30.05.2016	12 min	ex8a	Wn, Wz	Glonass
06.07.2016	6 min	ap01	On	APOD
06.07.2016	9 min	ap02	On	APOD
06.07.2016	8 min	ap03	On	APOD
14.07.2016	7 min	196b	On	APOD
14.07.2016	9 min	196c	On	APOD
15.07.2016	9 min	197c	On	APOD
18.07.2016	10 min	200a	Yg, Ke	APOD
20.07.2016	9 min	202	Yg, Ke	APOD
25.07.2016	6 min	207a	On	APOD
25.07.2016	5 min	207b	On, Wn, Wz	APOD
19.09.2016	6 min	263a	On	APOD
19.09.2016	6 min	263b	On, Wn, Wz	APOD
19.09.2016	5 min	263c	On, Wn, Wz	APOD
11.11.2016	33 min	316a	Ke, Yg	APOD + quasars
12.11.2016	41 min	317a	Hb, Ho, Ke	APOD + quasars
12.11.2016	35 min	317b	Hb, Ke, Yg	APOD + quasars
13.11.2016	26 min	318b	Hb, Ho, Ke, Yg	APOD + quasars
13.11.2016	26 min	318c	Hb, Ho, Ke	APOD + quasars
13.11.2016	23 min	318d	Yg, Ke	APOD + quasars
14.11.2016	40 min	319a	Hb, Ho, Ke, Yg	APOD + quasars
23.11.2016	1 h	328a	Wa	GPS
27.11.2016	24 h	a333	Hb, Ke, Yg	APOD + quasars
01.12.2016	3h 10 min	g336	Ho, Cd, Wa	GPS + quasar (pol. calibrator)

Fig. 1 List of scheduled satellite VLBI sessions with VieVS.

2.1 Automatic scheduling mode

Prompted by the aim to observe longer sessions of a few hours duration, VieVS now also allows for automated scheduling of combined observations of satellites and quasars. It uses the station-based scheduling approach (Sun et al., 2014), optimising for sky coverage and slew times at each site equally for quasar and satellite scans. One can define alternating blocks in a defined time duration for a preselected list of satellite and quasar targets. Following simulations by Plank et al. (2016), we chose a mix of 10 minutes of quasar observations every 50 minutes in experiments 126b, 131a, and 132a. We also found it useful to restrict the observed GNSS satellites to only a handful, since re-observing the same targets allows for better interpretation of the results (see Plank et al. , this volume).

This newly developed automatic scheduling mode is suitable for longer sessions of satellite observations as well as it supports the integration of satellite scans into a geodetic schedule.

2.2 Challenges

Having scheduled numerous sessions, we express our thanks to all our collaborators and stations contributing to the experiments. It really was the request for actual sessions' schedules that triggered the rapid development.

Looking back we can say that the only real challenge in creating a new schedule (for a new station) is the definition of the correct observing mode in the .VEX files. While the schedule itself could be made within a few hours, collecting the necessary information about the station's equipment and capabilities was the hardest part. One reason for this is the fact that the observations of GNSS satellites are performed in L-band, often using different equipment (and telescopes) than typically used in geodetic VLBI. In addition, with VLBI being such a complex technique, the local knowledge of the scheduler is often not sufficient to thoroughly control the selected mode whether it is suitable for the individual stations.

As a consequence, we have identified the communication and feedback loop between station personnel, correlator staff and the scheduler as an item for future improvement. This will allow an easy integration of new telescopes into future observing efforts in VLBI satellite tracking.

2.3 Observing APOD

The APOD satellite mission (Tang et al, 2016) is a Chinese CubSat carrying a dedicated VLBI transmitter sending tones in S- and X-band. The orbit is extremely low, at about 470 km orbital height. This makes common visibility between two or more VLBI telescopes challenging. VieVS was used for tracking tests using the telescopes in Australia, Onsala and Wettzell. In November 2016 intensive observing was done using

the Australian AuScope telescopes in Hobart, Katherine and Yarragadee. The novelty hereby was the successful application of continuous tracking as well as the integration into a full 24 hour geodetic schedule observing quasars.

For the scheduling of APOD, again orbit information provided by the public TLE was used. Before the actual tracking, the antenna steering information in terms of azimuth (Az) and elevation (El) at one second intervals was calculated using the latest orbit prediction provided by the APOD mission control centre BACC, the Beijing Aerospace Control Center.

Initial test sessions in July 2016 showed that the TLE tracking features implemented in recent Field System (FS) versions are not suitable to track this fast satellite with the AuScope antennas. The shortest available position update interval of 1 second could not be maintained (blocked all other FS commands) and larger intervals were not suitable for keeping the target within the antenna beam. Alternatively, the continuous tracking mode provided by the antenna control units (ACU) of the AuScope antennas was used for satellite tracking. Using this option, the ACU interpolates positions and adjusts slew speeds between AzEl tracking points directly loaded from an ASCII table. At the moment, this mode can only be controlled manually by changing the tracking mode and loading the AzEl files via the ACU interface.

Practically the APOD scheduling was done as follows:

- Define a session time window and search for satellite passes and common visibilities using the latest TLE (several days in advance). VieVS provides convenient features to check for mutual visibility and to determine possible observation times while taking into account various observation restrictions. The visibility graphs in VieVS (as shown in Figure 2) ease this process.
- Select suitable passes and request the VLBI signal switched on at the APOD BACC (minimum two days in advance). BACC may also provide predicted APOD ephemeris shortly before the actual observations. These ephemeris are preferred for tracking as they are assumed to be more accurate than TLE data.
- Build the schedule. Be aware that final scan times may change up to a few seconds with updated satellite ephemeris. The APOD scans were either fully embedded into a geodetic schedule (e.g. session a333) or at least a block of sveral minutes of quasar observations was added before and after the APOD block. While the quasar scans were scheduled automatically, the observations of APOD needed manual interaction. In order to allow for the switch between the automatic observations controlled by the FS for the quasar scans and the direct AzEl tracking mode for APOD, gap times of five minutes were included in the schedule. Result of the schedule is a VEX file defining the observing mode (see Figure 3), which in our case was identical for the satellite and quasar scans. Furthermore, it triggers the recording for both types of scans and provides the source coordinates of quasars.
- Once the latest orbit information was received by the APOD BACC, the AzEL tracking files were prepared. These are essentially simple ASCII tables containing AzEl tracking points at one second intervals. Additional care had to be taken to provide Az values within the cable wrap limits of the antenna.

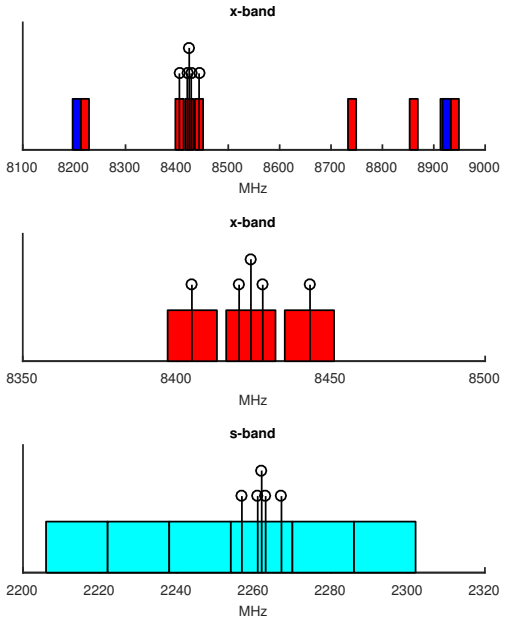

Fig. 3 Observing mode in APOD experiments 316 to 333. We observed 16 channels with 16 MHz bandwidth at two-bit sampling. In X-band, the DOR tones are covered by channels 2 to 4 with the carrier at 8424.04 MHz. In S-band, all satellite tones lie within one channel. Due to RFI, all S-band channels were allocated contiguous to cover a continuous band.

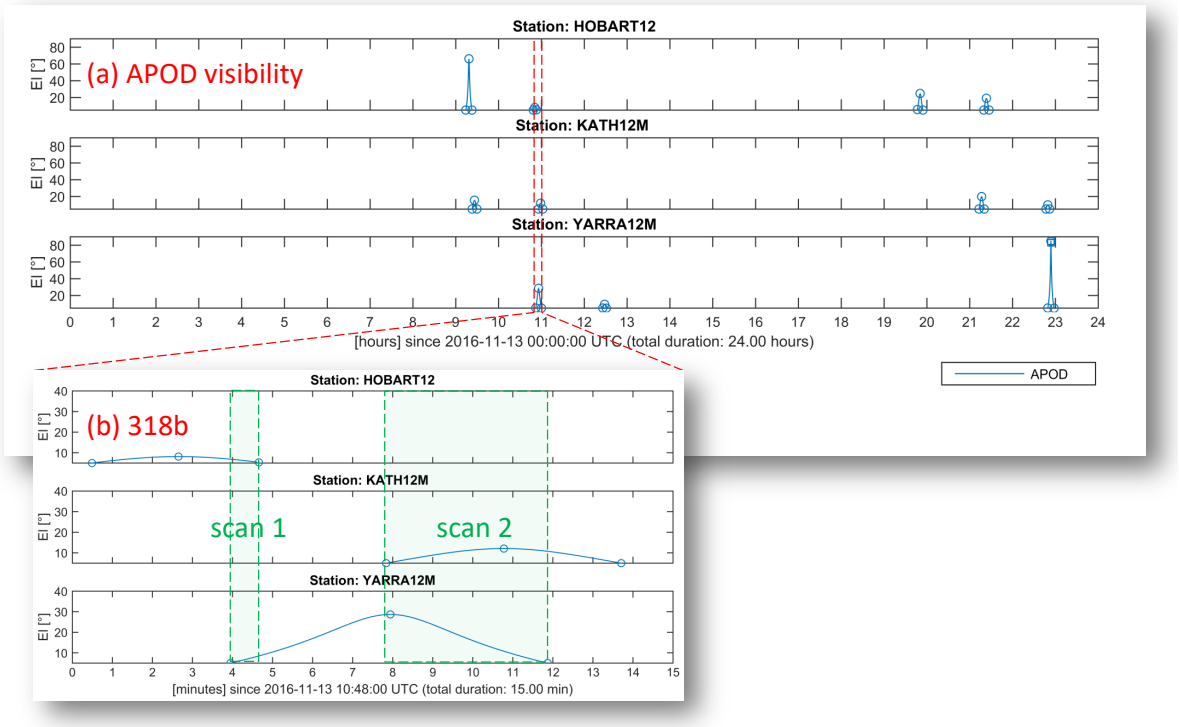

Fig. 2 Graphical illustration of the APOD visibilities in VieVS (satellite elevation at stations versus time). After checking (a) APOD visibility roughly for the whole day (Nov. 12, 2016) and selecting suitable passes, (b) definite scan times were accurately determined. Scan durations for common visibilities are a few minutes at most.

3 Conclusions

The VieVS satellite scheduling module has been repeatedly applied for generating observing files for VLBI satellite observations. The newly developed mode now allows for automatic scheduling of combined sessions including satellite targets and quasars, suitable for scheduling sessions of longer duration. While the scheduling process is easy to run, the most difficult part of generating a schedule was identified to be the correct implementation of a selected observing mode, considering station specific back-ends and equipment.

Latest developments in VieVS were dedicated to observing the very low APOD satellite. Hereby the connection between antenna steering using the field system and satellite tracking directly via the ACU revealed new challenges for our scheduling module.

Keep up to date with the latest developments at the IVS Working Group 7 "Observation of satellites using VLBI" Wiki: `http://auscope.phys.utas.edu.au/opswiki/doku.php?id=wg7:home`.

Acknowledgements

This study made use of AuScope VLBI infrastructure. AuScope Ltd is funded under the National Collaborative Research Infrastructure Strategy (NCRIS), an Australian Commonwealth Government Programme.

The authors thank the Austrian Science Fund (FWF) for funding projects SORTS I 2204 and J 3699-N29. This work was supported by the Australian Research Council (FS1000100037 and FS110200045).

4 References

Böhm J, Böhm S, Nilsson T, Pany A, Plank L, Spicakova H, Teke K, Schuh H (2012) The new Vienna VLBI Software VieVS. In: Proceedings of the 2009 IAG Symposium, Buenos Aires, Argentina, International Association of Geodesy Symposia, vol 136, doi:10.1007/978-3-642-20338-1_126, 31 August - 4 September 2009

Hellerschmied A, Böhm J, Neidhardt A, Kodet J, Haas R, Plank L (2015a) Scheduling VLBI Observations to Satellites with VieVS. International Association of Geodesy Symposia, Springer Berlin Heidelberg, pp 1–6, doi:10.1007/1345_2015_183

Hellerschmied A, Böhm J, Neidhardt A, Kodet J, Haas R, Plank L (2015b) Scheduling of VLBI observbations to satellites with the Vienna VLBI Software (VieVS). In: "Proceedings of the 22nd European VLBI for Geodesy and Astrometry Meeting", issued by: R. Haas, F. Colomer; European VLBI Group for Geodesy and Astrometry, 2015, ISBN: 978-989-20-6191-7, pp 102–106

Plank L, McCallum J, Hellerschmied A, Böhm J, Lovell J (this volume) Observing GNSS satellites with VLBI on the baseline Hobart-Ceduna.

Plank L, Böhm J, Schuh H (2016) Simulated VLBI satellite tracking of the GNSS constellation: Observing strategies. In: Rizos C, Willis P (eds) IAG 150 Years: Proceedings of the IAG Scientific Assembly in Postdam, Germany, 2013, Springer International Publishing, Berlin, Heidelberg, pp 85–90, doi:10.1007/1345_2015_87

Sun J (2013) VLBI scheduling strategies with respect to VLBI2010. Geowissenschaftliche Mitteilungen 92, Schriftenreihe der Studienrichtung Vermessung und Geoinformation, Technische Universität Wien, ISSN 1811-8380

Tang G, Sun J, Li X, Liu S, Chen G, Ren T, Wang G (2016) APOD Mission Status and Observations by VLBI. In: International VLBI Service for Geodesy and Astrometry 2016 General Meeting Proceedings, in press

Technical Challenges in VLBI Observations of GNSS Sources

McCallum J, Plank L, Hellerschmied A, Böhm J, Lovell J

Abstract We have conducted a series of VLBI satellite tracking experiments using the Hobart (Tasmania) and Ceduna (South Australia) antennas. In this contribution we comment on some technical challenges that had to be resolved for successful observation and correlation and point out some other effects that were identified in the data. Some of the discussed items are connected to existing procedures which are not optimised for these observations, while others are more directly connected to the different nature of satellite signals. Certainly the findings suggest further modification in observation and data processing, with improved results to be expected.

Keywords Space tie, Co-location in space, VLBI satellite tracking

1 Introduction

In geodetic VLBI we usually observe natural, far-field broad-band radiation with low polarisation, emitted from quasars at vast distances, at very low amplitudes (typically about a few thousandths of the system noise). The signals emitted from an artificial satellite on the other hand are near-field, narrow-band and highly polarised, and in the case of GNSS, are dramatically stronger. This generates many challenges in implementing VLBI observations of GNSS satellites, and in the data processing of such observations.

In this manuscript we report on some issues connected to the series of single-baseline experiments performed on the Australian Hobart-Ceduna baseline. The interested reader is referred to Plank et al. (this volume) and Plank et al. (2016) for more details and background information about these experiments.

J. McCallum, L. Plank, J. Lovell
University of Tasmania, Private Bag 37, 7001, Hobart, Australia

A. Hellerschmied, J. Böhm
Technische Universität Wien, Gußhausstraße 27-29, 1040, Vienna, Austria

2 Results

2.1 Observations

The discussed experiments were performed using the radio telescopes in Ceduna (30m) and Hobart (26m), both operated by the University of Tasmania. Both telescopes are equipped with L-band receivers, with a nominal operating range between 1.2 and 1.7 GHz. The slew speeds are relatively slow (40°/min in each axis) with slow accelerations (0.03°/min^2 in each axis). In the current observations, a 10 second repositioning interval was used when tracking the spacecraft and this, combined with the low acceleration of the drives, leads to a largely continuous tracking. For the recording, DBBCs and Mark5 recorders were used as a sampler and recorder (and in the case of Hobart also a Mark4 rack was used). The data were recorded in two linear polarisations. Having nominal antenna sensitivities of about 400 Jy for Hobart and 1600 Jy for Ceduna, no obvious signs of compression in the IF due to saturation were found while tracking GNSS sources. The recording was made with two-bit resolution, with dual linear polarisations in four frequencies of 16 MHz bandwidth each.

2.2 Correlation

Correlation was done using DiFX (Deller et al., 2011), with a combined VEX file and modified IM files for the GNSS sources (see Plank et al. , this volume). After determining the a priori clock model using the quasar scans, the GNSS observations were thoroughly studied with varying time and spectral resolution. For the creation of the final results we opted for 0.1 second integration time and 62.5 kHz channel width. This gives 256 channels over the 16 MHz bandwidth. The output was then converted to the FITS and Mark4 format for fringe-fitting and further analysis.

In Figure 1 typical signal spectra of three different satellites are shown for L1 and L2.

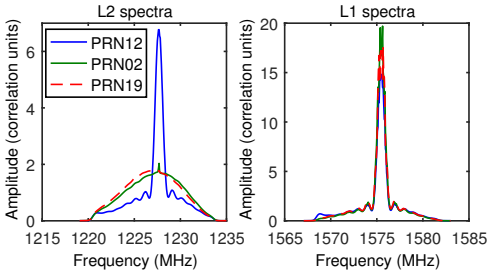

Fig. 1 Typical signal spectra (autocorrelation) of three satellites. The amplitudes are normalized using template spectra on the quasar sources.

The signal in L1 is dominated by a clear peak of the carrier, largely of consistent amplitude between different GPS satellites. This is not the case for L2, where we find significant differences in the transmitted signals of various satellites. The difference is linked to the generation of the satellite. Older generation satellites, such as PRN19 and PRN02 transmit the unmodulated L2 carrier while the newer generation, such as PRN12 transmits the L2C signal (Figure 1).

The cross-correlation spectrum of the data shows continuous phase against frequency. The residual bandpass phase shows some structure (Figure 2) and good agreement between the quasar and satellite response. While the extreme ends of the bandpass have essentially no signal and highly variable phase these do not contribute strongly towards the delay estimation. These findings suggest bandpass calibration a viable technique for these observations, although this has not been performed for this data set.

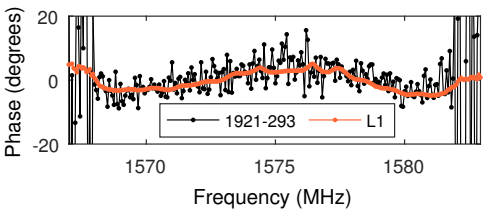

Fig. 2 Typical cross-correlation spectrum in L1, averaged over one scan. The residual phase after delay calibration is shown. One clearly sees a residual bandpass phase with good agreement between the quasar and satellite response.

2.3 Fringe-fitting

To estimate total delays in the usual geodetic frame, *fourfit* (part of the HOPS package) was used to estimate single-band delays per IF. No multiband delay estimation was attempted between the L2 and L1 bands of the satellite, or for the quasar sources. The FRING task in AIPS was also used to examine the data, which proved particularly useful in examining effects at time resolutions less than the 10 second scan time.

Figure 3 shows the output from *fourfit* after fitting to a single 10 second scan. Note that while the peak channels are dominant in fitting for the total delay, the results are consistent with the fit to the broader carrier. The variable phase in the band edges is due to low signal to noise at these frequencies. This is due to the filters in the DBBC.

2.4 Gain variations

The visibilities show a large amplitude variation with a period of two seconds. We have traced this back to an effect of the automatic gain control (AGC) within the DBBC, which struggled to maintain an optimal sampling level in the presence of the very strong narrowband GPS signals. This varying gain causes a delay 'noise' with a peak-to-peak amplitude of almost 1 ns, through the relative amplitude of the peak channels with respect to the total bandwidth. These variations are not present in the data recorded using the Mark4 system at Hobart, which uses fixed attenuation settings.

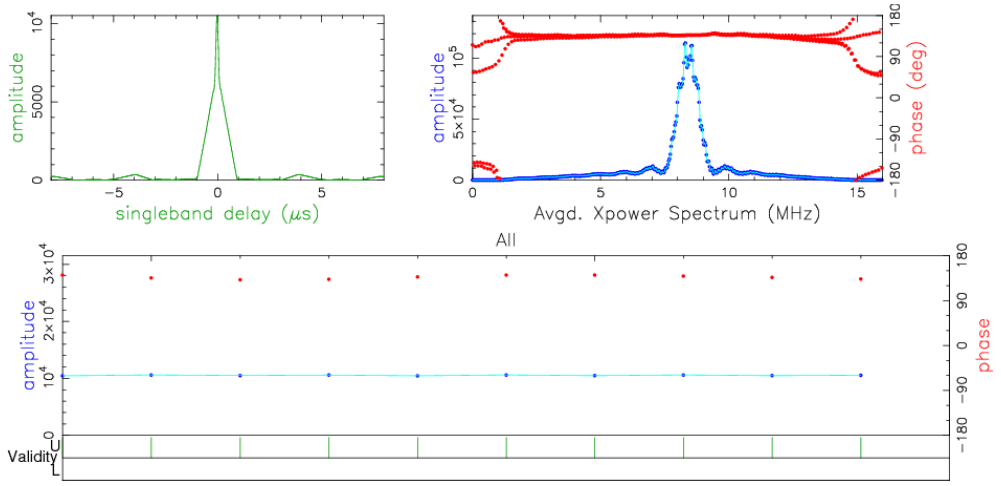

Fig. 3 Fourfit fringe-fit outputs of a GPS scan in L1. The upper left panel shows the single-band delay resolution function while the upper right shows the averaged amplitude and phase against frequency after applying the fitted delay and rate. The lower panel shows the residual phase and amplitude against time, after applying the fitted delay and rate.

2.5 Tracking effect

At sub-integration times the effects of the stepwise tracking are clearly apparent, both in amplitude and in the estimated delay. The amplitude of these delay variations are typically between 40 and 400 ps (less than those caused by the AGC issue), we assume that they largely cancel out in the data when integrating over the entire scan length of 10 seconds.

2.6 Polarisation

The signal emitted from the GPS satellites is strongly circularly polarised (RCP), while the data were recorded in dual linear polarisation. This signal should be able to be reconstructed by applying proper polarisation calibration of the differential delay, gain and the leakage terms per station. Unfortunately neither Hobart nor Ceduna is currently well calibrated or well suited to polarisation calibration. They have different and unusual receiver mountings, are expected to have moderately high leakage terms and potentially variable gains. As a results, no polarisation combination has been done so far. All results are from the XX correlation product, though the same conclusions hold for the other polarisation products. The differences between the XX and YY product are at the level of 1-2 ns, different for each observed satellite.

One alternative would be to use the quadrature hybrid feeds existent at both stations. However, they are known to only work over a relatively small frequency range and thus are not suitable for observing both the L2 and L1 bands simultaneously.

3 Conclusions

Standard tools from geodetic quasar VLBI have been adopted and used for VLBI satellite observations. While a general process chain was successfully developed and applied, thorough investigations of the recorded signal in auto- and cross correlation revealed some unforeseen effects. In addition, the application of fringe fitting in AIPS has proven beneficial in order to reveal some hidden effects of gain variations.

These investigations have enabled us to identify several procedural modifications that we will apply to future observations:

- The implementation of a proper continuous tracking mode instead of 10 second step wise tracking. In a first step, applying a different update interval (e.g. 9 seconds) may confirm whether the observed effects are indeed caused by the step-wise tracking.

- 8-bit instead of 2-bit sampling. A higher resolution in the sampling of the signal shall enable a better capture of the varying amplitude, minimising the effects on the measured delay that are observed in the present data. The 8-bit mode is implemented in the DBBC2, which our observatories are equipped with at the moment.
- AGC usage. We suggest to use fixed attenuation settings in the DBBC and disable active AGC during recording (pulsar mode). The prominent 2 second loop was not seen in the data when the Mark4 rack was used in Hobart.
- Improve quasar observations. Due to a mismatch in the recording mode no quasar signal was detected in the two extra bands. Hence a bandwidth synthesis for improved delay precision has not been successful for the quasar scans.
- In improving the understanding of the residual fringe delays and solving the remaining issues with the polarisation, the final aim is a proper combination of the L1 and L2 signals, in order to generate an ionosphere free linear combination.

Following the observations described here, Australian VLBI observations of GNSS satellites were continued in December 2016, this time enlarging the network with the 30 m radio telescope in Warkworth, New Zealand (Petrov et al., 2015).

Acknowledgments

This study made use of AuScope VLBI infrastructure. AuScope Ltd is funded under the National Collaborative Research Infrastructure Strategy (NCRIS), an Australian Commonwealth Government Programme. Parts of the correlation have been carried out on the Vienna Scientific Cluster (VSC).

The authors thank the Austrian Science Fund (FWF) for funding projects J 3699-N29 and SORTS I 2204. This work was supported by the Australian Research Council (FS1000100037 and FS110200045).

4 References

Deller A, Brisken W, Phillips C, Morgan J, Alef W, Capallo R, Middelberg E, Romney J, Rottmann H, Tingay S, Wayth R (2011) Difx-2: a more flexible, efficient, robust and powerful software correlator. PASP 123:275–287

Petrov L, Natusch T, Weston S, McCallum J, Ellingsen S, Gulyaev S (2015) First Scientific VLBI Observations Using New Zealand 20 Meter Radio Telescope WARK30M. PASP 127:952,516–522

Plank L, McCallum J, Hellerschmied A, Böhm J, Lovell J(this volume) Observing GNSS satellites with VLBI on the baseline Hobart-Ceduna.

Plank L, Hellerschmied A, McCallum J, Böhm J, Lovell J (2016) VLBI observations of GNSS satellites: from scheduling to analysis. J Geod, submitted

Co-Location on the Ground and in Space

Kodet J, Schreiber U, Neidhardt A, Eckl J, Herold G, Kronschnabl G, Plötz C, Mähler S, Schüler T, Klügel T, Riepl S

Abstract The classical approach for co-locations of the space geodetic instrumentation, namely SLR, VLBI, GNSS and DORIS is to regularly measure local ties between the reference points. At the Geodetic Observatory Wettzell (GOW) we reestablish the local ties every other year, which do not show displacements larger than 1mm. However one can identify noticeable discrepancies between the local survey the measurements of the techniques of space geodesy. The cause are systematic measurement biases, which are not correlated with the local ties measurements and are not captured by the established calibrations techniques.To observe near Earth objects like GNSS satellites using classical geodetic VLBI network is a challenging task. Observing the same satellites using VLBI, SLR and GNSS will greatly improve local ties because it provides a tie both in space and on the ground. The ties can be further improved by multi-technique ground targets, which are concentrating the different measurement systems at a single point on the observatory. The goal is to overcome the problem that local ties monitor only geometric distances between the reference points of the instruments. Multi-technique ground targets use the same signal originating from a common clock and the known respective path delay for tying the instruments to a single point of reference on the observatory. This provides both, intra- and inter- technique comparisons and delay control. The talk summaries the ongoing activities at the GO Wettzell leading to observe GNSS satellites by the VLBI systems on a regular bases and outlines the concept of the multi-technique ground target. Furthermore we show the first experimental results.

Keywords SLR, VLBI, GNSS, Calibration

Jan Kodet, Ulrich Schreiber, Alexander Neidhardt
Technische Universitaet Muenchen, Geodetic Observatory Wettzell

Johann Eckl, Günther Herold, Gerhard Kronschnabl, Christian Plötz, Swetlana Mähler, Torben Schüler, Thomas Klügel, Stefan Riepl
Federal Agency for Cartography and Geodesy, Geodetic Observatory Wettzell

1 Introduction

The combination of space geodetic techniques, e.g. GNSS (Global Navigation Satellite System), SLR (Satellite Laser Ranging), and VLBI (Very Long Baseline Interferometry) is important in creation of International Terrestrial Reference Frame (Altamimi et al., 2011), geophysics and studding of new observations techniques. All the major measurement techniques are providing very high measurement precision, while precision still contains biases and not calibrated delays. These measurement errors are minimized in preprocessing process as parameter estimation. However such a process does not often represents physical origin of the biases.

In this context geodetic observatories including more then one space geodetic technique are very important, because we can measure geometric distances between the reference points of different space geodetic techniques. On the another hand this characterization has disadvantage, because it doses include only geometry and do not use the signal origin of the measurement techniques. At Geodetic Observatory Wettzell we are investigating local ties on regular basis every second year. During last 30 years the reference points at the observatory do not

show significant movements. However realization of reference systems shows inconsistency between the different space geodetic techniques.

2 Observing GNSS satellits

One possibility is to observe GNSS satellites with all relevant techniques at the same time. In the path we have modified Wettzell 20m radio telescope such a way, that we can observe L1 GNSS signals using S/X receiver. The biggest disadvantage of this modification is a large attenuation of approximately 60 dB in S band feed, which is compensated by large parabolic antenna gain of 47 dBi. Such a large attenuation does not allow to observe GNSS satellites and quasars at the same frequency. Additionally, one must consider large delay dependency around GNSS frequencies, because the S band feed attenuation is dropping very rapidly and one can expect also large signal delay dependency.

The Wettzell North radio telescope is the first telescope from TWIN, which was put in to a regular operation. Because of the feed and waveguide cut off frequency is much higher then the GNSS L1 we use standard GNSS antenna connected to in house build VLBI GNSS receiver, which mix down L1 and L2 signals to IF band. The IF band is then recorded using standard Mark5 VLBI system. The small baseline geometry is

Fig. 1 Geodetic Observatory Wettzell, 20m radio telescope Wettzell is equipped with modified VLBI L1 receiver, which enables observation of the GNSS L1 signals using S band feed. Wettzell TWIN North telescope do not enable the same receiver modification. Therefor we use GNSS antenna installed on the roof of the VLBI building to observe satellites.

shown in Fig. 1. The GNSS antenna installed on the roof of the VLBI building has retro-reflector in reference point, which was added in to a local ties measurement.

Observation of the Glonass and GPS satellites were tested in a series of experiments using local VLBI network at Wettzell observatory. We found cross correlation in all made experiment.

3 Multi-technique Ground Target

Another activity at Geodetic Observatory Wettzell is the realization of new timing system, which will keep all the important signal paths constant or the signal delayes can be measured and recorded. The future goal of this activity is to keep time as a new and independent tie between the different space geodetic techniques. Closure measurements over several measurement systems using a clock as the origin and endpoint reveal even small time delays thus going beyond the currently applied calibration schemes.

For new closure calibration purposes, we have designed a new Multi-technique Ground Target, which is combining all relevant measurement techniques in to a central reference point at the observatory. The target is accessible to the local ground survey and its electronic will be synchronized to the new timing system. The current prototype of the multi-technique target is shown in Fig. 2. The target is installed on the top of the 5.5 meter tall tower near WLRS laser ranging station. It provides a good visibility for both SLR systems and all radio-telescopes.

The GNSS receiver on the target is used for monitoring of the target reference point. The GNSS solution demonstrates the solid construction of the monument. There is no significant target movement in the weekly GNSS solutions, see Fig. 3.

The SLR reflector is mounted on a turnabl table and integrated into SLR operations as a target for local tie measurements and as an external calibrating target for both SLR stations. We have modified WLRS SLR station such a way that we can use retro reflector mounted on the Multi-technique Ground Target as an external target and to range to this target in an eye save mode. The second SLR station SOS-W uses a bistatic mount with separated transmit and receive telescopes. In such a system the calibration target is too close to see it from both telescopes, therefor the transmit telescope will be used for transmitting and receiving of the

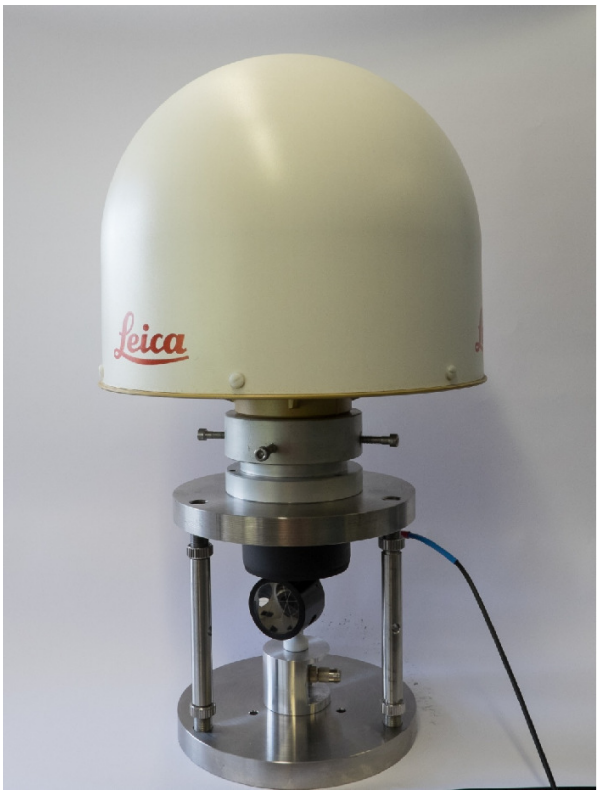

Fig. 2 The development version of multi-technique ground target. On top there is a GNSS antenna, the SLR retro reflector, which will be used as a SLR calibration target and for local ties measurement, is mounted below the GNSS antenna and at the bottom there is a X-band antenna, which will be used for VLBI calibration.

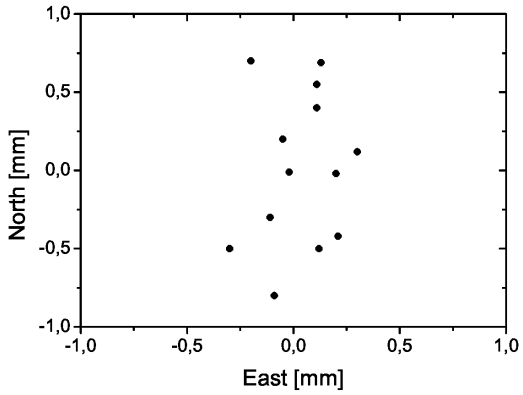

Fig. 3 North and East components of weekly GNSS solutions of the multi-technique ground target during the 13 weeks in the year 2015 (start day 200).

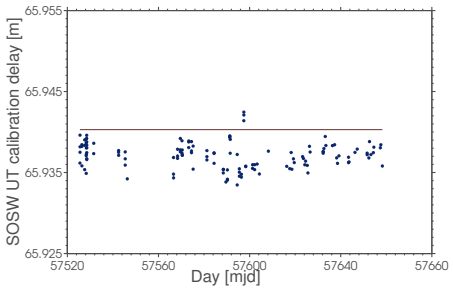

Fig. 4 Calibration delay to Multi-technique Ground Target of SOS-W SLR station (dots) compared to local ties measurement (solid line).

optical signal. In Fig. 4 is shown calibration delay to Multi-technique Ground Target of SOS-W SLR station compared to local ties measurement. One can see a discrepancy between local ties measurement and SOS-W calibration delay. The reason of the measurement bias is under investigation.

The most challenging task is to establish the multi-technique ground target for VLBI calibration purposes. For that purpose we are using a small X-band antenna to transmit a microwave frequency comb with 1 MHz tone spacing. In Fig. 5 is shown experimental concept with marked all important delays. The idea is to extract phase (φ_1 and φ_2) of the comb transmitted from the target. This phase carries information about the VLBI range to the target. The VLBI instrumental delay is measured using another microwave comb, which is installed in the VLBI technique and is standardly used in the VLBI measurement. The target extracted phases φ_1 and φ_2 contain delay inside target microwave comb generator, therefor in the first experiment it was possible to measure only phase difference between the telescopes ($\varphi_1 - \varphi_2$). The experiment was further complicated, because 20 m radio-telescope Wettzell was connected to maser EFOS 18 and TWIN North was connected to maser EFOS 60. We have estimated maser time difference using TWOTT technique.

The resulting phase difference with distracted all known delays is in Fig. 6. The telescope instrumental delays were monitored using radio-telescopes pCal systems. The cable delay distributing reference frequency for the pCal systems was monitored only in 20 m radio-telescope. In the graph in Fig. 6 the phase difference varies in range of $\pm$ 2 mm with 2.8 ps rms. The goal of this experiment is to run such measurement

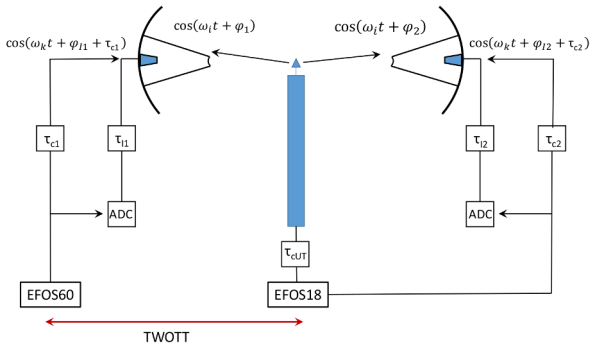

Fig. 5 Experimental setup of VLBI calibration.

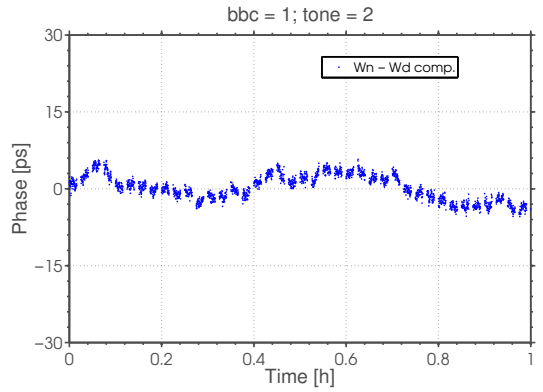

Fig. 6 The resulting calibration VLBI phase difference between 20 m and TWIN radio-telescopes Wettzell.

on everyday bases. This results can be further used for mapping and understanding of the VLBI uncompensated delays.

4 Conclusions

We are systematically working on improving the local ties at the Geodetic Observatory Wettzell. Long-term measurements of the geodetic markers at the station (spanning more than 30 years) do not show significant displacements. We are therefore focusing on the co-location and comparison of the different geodetic instruments among each other and across the various techniques. A promising approach is the observation of GNSS satellites using VLBI technique. We have modified VLBI radio-telescopes at Wettzell observatory to be able to track the GNSS satellites.

Another approach is the use of a multi-technique ground target for the calibration of all space geodetic techniques. The goal is to establish one central geodetic reference point for all the geodetic techniques and relate instrumental reference points to this common point in order to capture measurement biases in the form of time delays that otherwise would go unnoticed. In this way the space geodetic techniques in conjunction with a delay compensated clock distribution are used for the monitoring of the local ties.

Acknowledgements

This work has been supported by the Technische Universitaet Muenchen, the Bundesamt für Kartographie und Geodasie. We acknowledge funding through the Forschergruppe DFG FOR1503.

5 References

J. Kodet and K.U. Schreiber and Ch. Pltz and A. Neidhardt and G. Kronschnabl and R. Haas and G. Molera Calvs and S. Pogrebenko and M. Rothacher and B. Maennel and L. Plank and A. Hellerschmied.: Co-location of space geodetic techniques on ground and in space; in: Behrend, D.; Baver, K.; Armstrong, K. (eds.) IVS 2014 General Meeting Proceedings - "VGOS: The New VLBI Network", pp 446-450, Science Press, ISBN (Print) 978-7-03-042974-2, ISBN (Online) 978-7-03-042974-2, 2014.

Tornatore, V., R. Haas, D. Deev, S. Pegrebenko, S. Casey, G. Molera-Calves, A. Keimpema, Single baseline GLONASS observations with VLBI: data processing and first results, In: 20th Meeting of the European VLBI Group for Geodesy and Astronomy, 162165, 2011.

Tornatore, V, R. Haas, S. Casey, D. Deev, S. Pegrebenko, G. Molera-Calvs, Direct VLBI Observations of Global Naviga- tion Satellite System Signals, In: International Association of Geodesy Symposia, Proc. IAG General Assembly, Melbourne - 2011, 247-252, 2014.

A. Hellerschmied, L. Plank, A. Neidhardt, R. Haas, J. Bhm, C. Pltz, J. Kodet, Observing satellites with VLBI radio telescopes a practical realization at Wettzell, this is- sue.

Jan Kodet and Petr Panek and Ivan Prochzka, Two-way time transfer via optical fiber providing subpicosecond precision and high temperature stability, Metrologia, Volume 53, Number 1, http://stacks.iop.org/0026-1394/53/i=1/a=18

Observing GNSS Satellites with VLBI on the Hobart-Ceduna Baseline

Plank L, McCallum J, Hellerschmied A, Böhm J, Lovell J

Abstract We have conducted a series of VLBI satellite tracking experiments using the Hobart (Tasmania) and Ceduna (South Australia) antennas. We give an overview of the newly developed process chain which spans everything from scheduling, observing, correlation and fringe fitting to a final geodetic analysis. The aim was to keep as close as possible to standard geodetic VLBI operations: we use VEX-files for the observations, DiFX and fourfit for the correlation and fringe fitting and VieVS for the analysis. Observations were made in the L1 and L2 band, with GPS satellites as the main targets as well as a few quasars for calibration. So far, only results of L1 are used, applying a simple ionospheric delay correction based on GPS TEC maps. The results are time series of up to six hours of total delays. The procedures we have developed now allow routine VLBI observations of GNSS satellites to be made. We hope this will trigger future observations and trigger further progress in this exciting area.

Keywords Space tie, Co-location in space, VLBI satellite tracking, VieVS

1 Introduction

While VLBI satellite tracking has been around for a few years now, observational data that can actually be used for analysis is sparse. The reasons for this are that the observations themselves are complex to realise and the standard processing chains are not yet ready to deal with this novel type of data.

In the literature one finds simulation studies about suitable satellite orbits for space tie satellites and a matching telescope network for tracking, as well as on the inclusion of such observations into standard geodetic experiments (Plank, 2014; Plank et al., 2014, 2016). Strategies to account for the effect of the ionosphere in L-band observations have also been developed (Männel and Rothacher, 2016). In terms of observations, great efforts have been undertaken by researchers at Onsala, Wettzell and Medicina (Tornatore et al., 2014; Haas et al., 2014; Hellerschmied et al., 2014), mainly observing a single GLONASS satellite over one hour duration. So far, the link between such test observations and a final geodetic analysis (which the simulation software is capable of doing) has been missing.

Using recent developments of a complete satellite scheduling tool (Hellerschmied et al., this volume) combined with the necessary experience in VLBI correlation as well as with near-field delay models, a series of test experiments were performed on the baseline between Ceduna and Hobart (approx. 1700 km). A number of new routines were developed in order to make the standard VLBI procedures applicable to the satellite observations. Once a working process chain had been established, observations could be repeated and modified to improve the data quality. Overall we would like to emphasize the importance of serious test observations, demonstrate how they allowed us to identify and resolve unforeseen issues, and comment on new problems which will have to be addressed in the future.

L. Plank, J. McCallum, J. Lovell
University of Tasmania, Private Bag 37, 7001, Hobart, Australia

A. Hellerschmied, J. Böhm
Technische Universität Wien, Gußhausstraße 27-29, 1040, Vienna, Austria

This manuscript is a brief summary of the experiments and findings that are also the topic of a journal paper that has been submitted to Journal of Geodesy. The interested reader is referred to Plank et al. (2016) for more details and background information.

2 Results

Starting and finishing with the Vienna VLBI Software (VieVS, Böhm et al., 2012), a complete process chain was developed (Figure 1): from the scheduling tool and the implementation in the field system for observing, to the correlation process using a near-field delay model and generating total delays which can then again be used in VieVS for a geodetic analysis. Wherever possible we use the standard procedures that are regularly applied in geodetic VLBI.

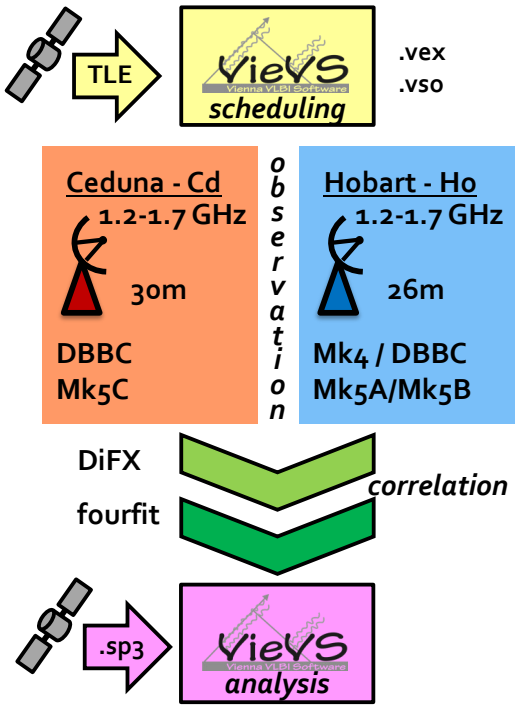

Fig. 1 The developed process chain in four steps: scheduling, observation, correlation, and analysis.

2.1 Scheduling

For the scheduling, the satellite scheduling module of VieVS has been used (Hellerschmied et al., 2015). It creates VEX files which can be loaded at the stations using the NASA Field System and automatically operate the telescopes and manage the recording during the observation. The target's position is input via publicly accessible two line element (TLE) orbit information. For the experiments discussed we use the telescopes in Hobart (26m, Tasmania) and Ceduna (30m, South Australia), both equipped with L-band receivers. In order to follow the satellites on their track through the sky, the topocentric right ascension and declination of the satellite was calculated with an update interval of 10 seconds. This means one gets a different VEX file for each of the tracking stations.

The scheduler further produces a combined VEX file, which is later used for correlation. A third format is the VSO file, which is the newly developed standard input for near-field targets in VieVS. It is used to create the a priori delay model as well as for the final geodetic analysis.

In the course of these experiments, an automated scheduling tool was developed and applied to schedule the whole session of six hours duration. At regular intervals (every 50 minutes) a block of quasar observations was scheduled, applying standard optimisation criteria for sky coverage etc. For each experiment a set of about five GPS satellites was selected, which were then re-observed regularly during the whole session of up to six hours. This has proven beneficial for assessing the quality of the a priori model. For the GNSS targets, fixed scan durations of five minutes were chosen.

2.2 Observations

The aim of the observations was to record the satellite signal both in the L1 and L2 band, as well as to add additional bands for the quasars in order to allow for bandwidth synthesis. Testing several setups in the initial experiments (also observing GLONASS satellites), the final mode was chosen to use eight intermediate frequency (IF) channels of 16 MHz bandwidth each. We used two-bit sampling and recorded in dual linear polarisations. This gives two channels each for L1 and

L2 and four channels for the quasar only, in total four frequency bands with dual polarisation.

For the tracking itself the station checks (e.g. *preob*) were held to a minimum in order to be able to keep up with the 10 second relocation interval. At the start of each scan, the telescope was put into position one minute before the satellite came in to the beam. This allowed the automatic gain control (AGC) to smoothly adjust the power levels and at first sight no additional attenuation was necessary. During a five minute scan data were recorded continuously. For a session of six hours duration about 1 TB of data was recorded per station.

The fact that the satellite signal is vastly stronger than a quasar signal turned out beneficial in checking and adjusting the tracking procedures. By connecting a spectrum analyser to the telescope back-end, the incoming signal can be monitored live during the observation (Figure 2).

Fig. 2 Live L1 GPS signal as seen on the spectrum analyser during the observation. The carrier signal with its peak at 1575 MHz as well as the side lobes are clearly visible.

2.3 Correlation

The data of the experiments were correlated using the DiFX software correlator (Deller et al., 2011). For configuration the combined VEX file was used. This is essentially the merger of the individual station-dependent VEX files, with the $SOURCE block having the information of the target position as seen from one telescope (topocentric right ascension and declination). Using this VEX file to run through DiFX's *vex2difx* and *calcif2* processes, first the input model (IM) files were created using the standard (quasar) model in Calc. In a next step, this erroneous delay model was replaced with a near-field model created in VieVS. There the satellite positions are read in from IGS orbit files in sp3-format. For correlation the rapid orbit product is sufficient.

Prior to correlation of the satellite scans the clock model was determined using the quasar data. The AIPS package (which is widely used in astronomical VLBI) was used for detailed studies of the auto- and cross correlation products and the residual fringe delays at high spectral and temporal resolution. In order to get the standard (geodetic) output we used *fourfit* of the HOPS package for fringe fitting in single-band mode. This has the advantage that we get total delays (a priori model plus residual delays) in the geodetic sense, referenced to reception at the first station at integer seconds.

As both stations recorded dual linear polarisation, we obtain four polarisation products for each frequency band. The generation of a combined polarisation product has not been successful so far (see McCallum et al., this volume). We also find worse results for the L2 band data, suggesting a combination of L1 and L2 data in order to account for ionospheric effects not feasible so far.

2.4 Analysis

The main product is a six-hour time series of total delays to a handful of GPS satellites. This data-set can then be used as input for the analysis software, in our case VieVS. While single-baseline observations are not sufficient yet to achieve geodetically useful results, the data are certainly well suited for testing and development of the analysis tools.

An initial check of the data can be done by comparing the observed with the computed delays, as for example done in Figure 3. For most of the five satellites the residuals show a systematic behavior, revealing insufficient modeling. It is also evident that there is good consistency between the individual ten-second results within a five minute scan for some of the satellites (red, pink, black), while others show rapid changes (green and blue). We think that this is due to the unresolved issues with the polarisation.

Overall one finds residuals within 8 ns or 2.5 m. On closer inspection, an elevation dependency can be identified, showing larger residuals for lower elevations. This is a strong indication that the residual delays are due to atmospheric propagation. When correcting for an ionospheric effect, which was calculated using global maps of the total electron content (TEC) provided by the IGS, the level of residuals decreases to about 4 ns or 1.2 m.

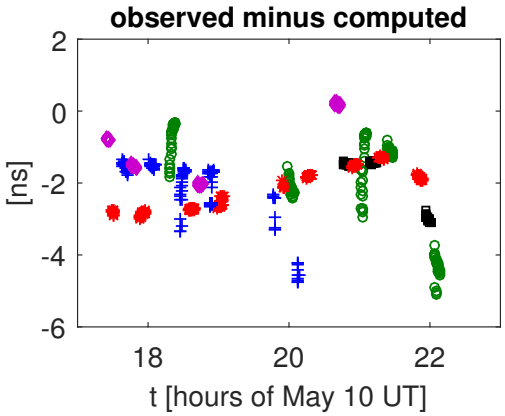

Fig. 3 Observed minus computed for a six-hour session in May 2016. Residuals for each satellite are color- and symbol coded.

These residual delays can subsequently be used in a least squares adjustment for the estimation of geodetic parameters. While the software (VieVS) would be ready to do so, the data does not have the quality yet (single baseline, only six hours, unresolved issues with the polarisation etc.) to give meaningful results.

3 Conclusions

The work described realises VLBI tracking of GNSS satellites from scheduling to analysis. The observations are unique in providing a time series of total delays over a session of six hours duration.

Performing this set of observing sessions showed that many more things need to be considered for this novel type of observations. Yet it also taught us which standard programs can be easily adjusted and which will need to be rewritten from scratch.

The authors hereby invite all interested colleagues to work with the data themselves and share their findings. Access to the data and information on comparisons is provided at `http://auscope.phys.utas.edu.au/opswiki/doku.php?id=wg7:home`.

Acknowledgements

This study made use of AuScope VLBI infrastructure. AuScope Ltd is funded under the National Collaborative Research Infrastructure Strategy (NCRIS), an Australian Commonwealth Government Programme. Parts of the correlation have been carried out on the Vienna Scientific Cluster (VSC).

The authors thank the Austrian Science Fund (FWF) for funding projects J 3699-N29 and SORTS I 2204. This work was supported by the Australian Research Council (FS1000100037 and FS110200045).

4 References

Böhm J, Böhm S, Nilsson T, Pany A, Plank L, Spicakova H, Teke K, Schuh H (2012) The new Vienna VLBI Software VieVS. In: Proceedings of the 2009 IAG Symposium, Buenos Aires, Argentina, International Association of Geodesy Symposia, vol 136, doi:10.1007/978-3-642-20338-1_126, 31 August - 4 September 2009

Deller A, Brisken W, Phillips C, Morgan J, Alef W, Capallo R, Middelberg E, Romney J, Rottmann H, Tingay S, Wayth R (2011) Difx-2: a more flexible, efficient, robust and powerful software correlator. PASP 123:275–287

Haas R, Neidhardt A, Kodet J, Plötz C, Schreiber U, Kronschnabl G, Pogrebenko S, Duev D, Casey S, Marti-Vidal I, Yang J, Plank L (2014) The Wettzell-Onsala G130128 Experiment - VLBI Observations of a GLONASS Satellite. In: Behrend D, Baver K, Armstrong K (eds) International VLBI Service for Geodesy and Astrometry 2014 General Meeting Proceedings, Science Press, pp 451–455, ISBN 978-7-03-042974-2

Hellerschmied A, Plank L, McCallum J, Sun J, Böhm J (this volume) Scheduling of VLBI Satellite Observations with VieVS.

Hellerschmied A, Plank L, Neidhardt A, Haas R, Böhm J, Plötz C, Kodet J (2014) Observing Satellites with VLBI radio telescopes - practical realization at Wettzell. In: Behrend D, Baver K, Armstrong K (eds) International VLBI Service for Geodesy and Astrometry 2014 General Meeting Proceedings, Science Press, pp 441–445, ISBN 978-7-03-042974-2

Hellerschmied A, Böhm J, Neidhardt A, Kodet J, Haas R, Plank L (2015) Scheduling VLBI Observations

to Satellites with VieVS. International Association of Geodesy Symposia, Springer Berlin Heidelberg, pp 1–6, doi:10.1007/1345_2015_183

Männel B, Rothacher M (2016) Ionospheric corrections for single-frequency tracking of GNSS satellites by VLBI based on co-located GNSS. J Geod 90(2):189–203, doi:10.1007/s00190-015-0865-6

McCallum J, Plank L, Hellerschmied A, Böhm J, Lovell J (this volume) Technical challenges in VLBI observations of GNSS sources.

Plank L (2014) VLBI satellite tracking for the realization of frame ties. Geowissenschaftliche Mitteilungen 95, http://geo.tuwien.ac.at/fileadmin/editors/GM/GM95_plank.pdf., Schriftenreihe der Studienrichtung Vermessung und Geoinformation, Technische Universität Wien, ISSN 1811-8380

Plank L, Böhm J, Schuh H (2014) Precise station positions from VLBI observations to satellites: a simulation study. J Geod 88:7:659–673

Plank L, Böhm J, Schuh H (2016) Simulated VLBI satellite tracking of the GNSS constellation: Observing strategies. In: Rizos C, Willis P (eds) IAG 150 Years: Proceedings of the IAG Scientific Assembly in Postdam, Germany, 2013, Springer International Publishing, Berlin, Heidelberg, pp 85–90, doi:10.1007/1345_2015_87

Plank L, Hellerschmied A, McCallum J, Böhm J, Lovell J (2016) VLBI observations of GNSS satellites: from scheduling to analysis. J Geod, submitted

Tornatore V, Haas R, Casey S, Duev D, Pogrebenko S, Molera Calvés G (2014) Direct VLBI Observations of the Global Navigation Satellite System Signals. In: Rizos C, Willis P (eds) IAG Symp. 139. Earth in the Edge: Science for a Sustainable Planet, pp 247–252

Near-Field VLBI Delay Models

Jaron F, Halsig S, Iddink A, Nothnagel A, Plank L

Abstract Reliable VLBI delay models are essential for geodetic applications. Near-field targets make it necessary for delay models to take curvature of the wavefronts into consideration. We have implemented two finite-distance delay models (Sekido & Fukushima, 2006; Duev et al., 2012) in the VLBI analysis software ivg::ASCOT. VLBI observations of GPS satellites allow us to compare computed delays with observed delays. We introduce the concepts behind these two delay models and present our results.

Keywords VLBI near-field models, geodetic VLBI, ivg::ASCOT

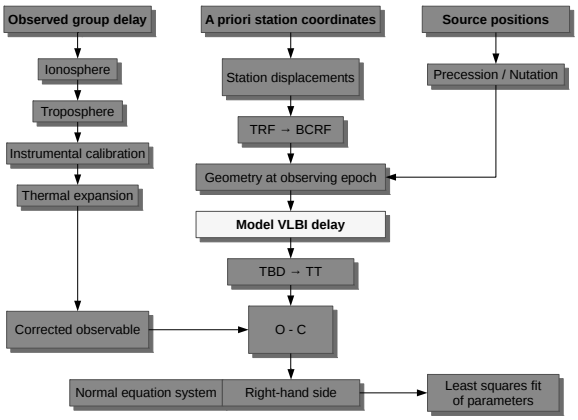

Fig. 1 Post-correlation VLBI analysis steps.

1 Introduction

VLBI observations of near-field targets make it necessary to take into consideration the curvature of the wavefronts. In particular, the assumption of planar wavefronts is no longer valid for the modeling of the VLBI delay.

Figure 1 gives a schematic overview of the post-correlation VLBI analysis steps. The fundamental observable is the group delay, which is the result of fringe fitting the correlator output and which has to be corrected for atmospheric and instrumental effects to obtain the corrected observable. A priori knowledge of station coordinates and source positions is combined to model the VLBI delay. The difference between the corrected observed (O) and the computed (C) delay, $O-C$, serves as the right-hand side of a normal equation system, which is finally used to determine the parameters of interest in a least squares fit.

The usual geodetic VLBI experiment consists in observing a quasar located at a distance so far away from the observer that the wavefronts can be considered planar upon their arrival at the telescopes (see Fig. 2, which appears as Fig. 1 in Sovers et al. 1998). The geometric delay τ is then proportional to first order to the scalar product between the source unit vector $\hat{\mathbf{k}}$ and the baseline vector $\mathbf{b}$,

$$\tau \propto \hat{\mathbf{k}} \cdot \mathbf{b}. \quad (1)$$

However, this assumption of planar wavefronts is not valid anymore in the case of near-field targets, which is why special near-field models are needed.

F. Jaron, S. Halsig, A. Iddink, A. Nothnagel
Institut für Geodäsie und Geoinformation – IGG Bonn, Nußallee 17, 53115 Bonn

L. Plank
University of Tasmania, School of Physical Sciences, Private Bag 37, Hobart, 7001, Australia

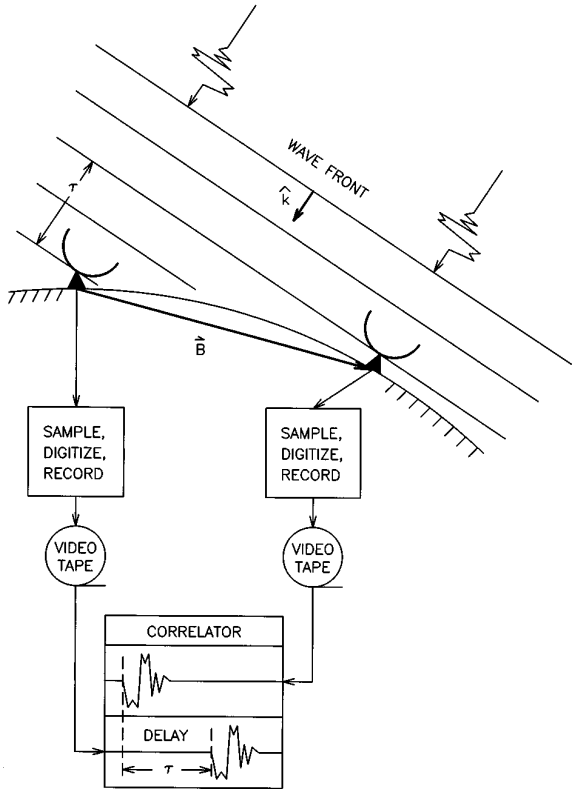

Fig. 2 Schematic diagram of a standard VLBI experiment. A distant quasar is observed, the wavefronts can be considered planar. Figure 1 in Sovers et al. (1998).

In Sect. 2 we present the concepts behind the two near-field VLBI delay models by Sekido & Fukushima (2006) (SF06 hereafter) and Duev et al. (2012) (D+12 hereafter). We implemented both of these algorithms into the VLBI analysis software ivg::ASCOT [1], and in Sect. 4 we present our results in comparison to observational data. We give our conclusions in Sect. 5.

2 Models

In this section we give a short explanation of the two near-field VLBI delay models by SF06 and D+12. For further details the reader is referred to the original papers.

[1] `http://ascot.geod.uni-bonn.de`

2.1 Sekido & Fukushima (2006)

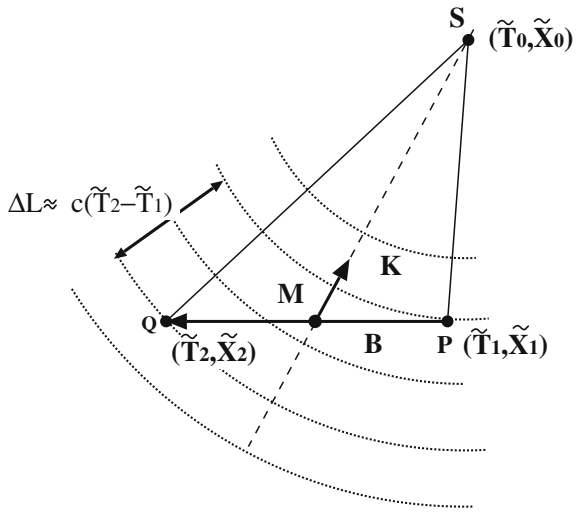

Fig. 3 Geometry of a VLBI observation of a near-field target. In the SF06 model, the pseudo source vector **K** points from the middle of the baseline into the direction of the source and plays a fundamental role in the computation of the VLBI delay. Figure 1 in SF06.

The geometry of a VLBI observation of a near-field target is shown in Fig. 3 (Fig. 1 in SF06), where all vectors are given in the barycentric celestial reference system (BCRS) and times are given in the barycentric dynamical time (TBD). A radio source in the near-field (denoted by **S** in Fig. 3) emits a radio signal at time $\tilde{T}_0$ and position $\tilde{\mathbf{X}}_0$. The signal is received at station 1 (**P** in the figure) at time $\tilde{T}_1$ and station coordinates $\tilde{\mathbf{X}}_1$. After a certain *delay* it arrives at station 2, i.e., at $\tilde{T}_2$ and $\tilde{\mathbf{X}}_2$.

The principle idea of SF06 is to construct a *pseudo source vector* **K**, which points from the middle of the baseline **B** into the direction of $\tilde{\mathbf{X}}_0$, i.e., the position of the source at time $\tilde{T}_0$. However, time and position of the emission of the signal are not known a priori and have to be determined first by solving the light-time equation,

$$\tilde{T}_0 = \tilde{T}_1 - \frac{\left|\tilde{\mathbf{X}}_0(\tilde{T}_0) - \tilde{\mathbf{X}}_\mathrm{E}(\tilde{T}_1) - \mathbf{R}_{1\mathrm{E}}(\tilde{T}_1)\right|}{c} - \Delta T_{\mathrm{g},01}, \tag{2}$$

$\tilde{T}_0$ signal emission time,
$\tilde{T}_1$ signal reception time at station 1,
$\tilde{\mathbf{X}}_0(\tilde{T}_0)$ source position at $\tilde{T}_0$,
$\tilde{\mathbf{X}}_\mathrm{E}(\tilde{T}_1)$ Earth barycenter,
$\mathbf{R}_{1\mathrm{E}}(\tilde{T}_1)$ vector from Earth barycenter to station 1,
c speed of light,
$\Delta T_{\mathrm{g},01}$ gravitational delay.

Equation (2) states that the time $\tilde{T}_0$, of emission of the signal, is obtained by subtracting from the time $\tilde{T}_1$, of reception of the signal at station 1, the time it takes the signal to travel from the source to receiver 1. This equation has to be solved numerically, and we use the Newton-Raphson method as proposed by SF06.

Once the light-time equation has been solved, the pseudo-source vector can be constructed,

$$\mathbf{K} \stackrel{\mathrm{def}}{=} \frac{\mathbf{R}_1(\tilde{T}_1)+\mathbf{R}_2(\tilde{T}_1)}{R_1(\tilde{T}_1)+R_2(\tilde{T}_1)} \tag{3}$$

with

$$\begin{aligned}\mathbf{R}_i(\tilde{T}_1) &= \tilde{\mathbf{X}}_0(\tilde{T}_0)-\tilde{\mathbf{X}}_i(\tilde{T}_1)\\ &= \tilde{\mathbf{X}}_0(\tilde{T}_0)-\tilde{\mathbf{X}}_\mathrm{E}(\tilde{T}_1)-\mathbf{R}_{i\mathrm{E}}(\tilde{T}_1).\end{aligned} \tag{4}$$

The delay is then given by

$$\tau = \frac{-\frac{\mathbf{K}\cdot\mathbf{b}}{c}\left(1-\frac{2W_\mathrm{E}}{c^2}-\frac{V_\mathrm{E}^2+2\mathbf{V}_\mathrm{E}\cdot\mathbf{v}_2}{2c^2}\right)-\frac{\mathbf{V}_\mathrm{E}\cdot\mathbf{b}}{c^2}\left(1+\frac{\hat{\mathbf{R}}_2\cdot\mathbf{V}_2}{c}-\frac{(\mathbf{V}_\mathrm{E}+2\mathbf{v}_2)\cdot\mathbf{K}}{2c}\right)+\Delta T_\mathrm{grav}}{\left(1+\frac{\hat{\mathbf{R}}_2\cdot\mathbf{v}_2}{c}\right)(1+H)}, \tag{5}$$

$\mathbf{K}$ pseudo source vector,
$\mathbf{b}$ baseline vector,
W_E gravitational potential,
$\mathbf{V}_i$ coordinate velocity of object i in the TDB frame,
$\mathbf{v}_2$ coordinate velocity of station 2 in GCRS,
ΔT_grav gravitational delay,
c speed of light,
$\hat{\mathbf{R}}_2 = \mathbf{R}_2/R_2$,
$H = \left|\frac{\mathbf{V}_2}{c}\times\hat{\mathbf{R}}_2\right|^2 \frac{\mathbf{K}\cdot\mathbf{b}}{2R_2}$ second order correction term.

The use of the pseudo source vector $\mathbf{K}$ makes the formula look similar to the conventional far-field delay model (IERS Conventions, 2010),

$$\tau = \frac{-\frac{\hat{\mathbf{k}}\cdot\mathbf{b}}{c}\left(1-\frac{2W_\mathrm{E}}{c^2}-\frac{V_\mathrm{E}^2+2\mathbf{V}_\mathrm{E}\cdot\mathbf{v}_2}{2c^2}\right)-\frac{\mathbf{V}_\mathrm{E}\cdot\mathbf{b}}{c^2}\left(1+\frac{\hat{\mathbf{k}}\cdot\mathbf{V}_\mathrm{E}}{2c}\right)+\Delta T_\mathrm{grav}}{1+\frac{\hat{\mathbf{k}}\cdot(\mathbf{V}_\mathrm{E}+\mathbf{v}_2)}{c}}. \tag{6}$$

2.2 Duev et al. (2012)

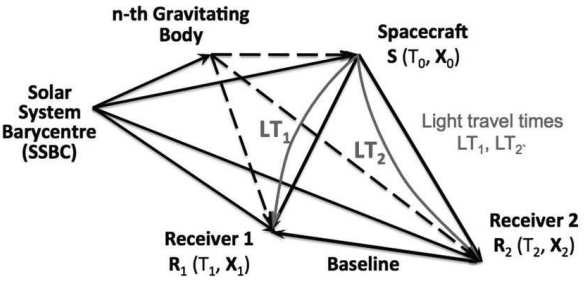

Fig. 4 Geometry of a VLBI observation of a near-field source. In case of the D+12 model the delay is obtained by solving the light-time equation twice, i.e., once for each signal propagation path (denoted by LT1 and LT2). Figure 2 in D+12.

Figure 4 (Fig. 2 in D+12) shows the geometry of a VLBI observation of a near-field source. The principle of the D+12 delay model is to solve the light-time equation (2) for each of the two signal propagation paths from the source to receiver 1 (denoted by LT1 in Fig. 4) and to receiver 2 (LT2).

The difference between the so obtained light travel times T_1 and T_2 has then to be transformed from TBD to TT, in order to obtain the VLBI delay,

$$\tau = \left(\frac{T2-T1}{1-L_C}\cdot\left[1-\frac{1}{c^2}\left(\frac{V_\mathrm{E}^2}{2}+U_\mathrm{E}\right)\right]-\frac{\mathbf{V}_\mathrm{E}\cdot\mathbf{b}}{c^2}\right)\cdot\left(1+\frac{\mathbf{V}_\mathrm{E}\cdot\dot{\mathbf{r}}_{2,\mathrm{gc}}}{c^2}\right)^{-1}, \tag{7}$$

$L_C = 1.4808268674\,1\,10^{-8}$, $1-L_C \stackrel{\mathrm{def}}{=} \left\langle\frac{\mathrm{dTCG}}{\mathrm{dTCB}}\right\rangle$,
c speed of light,
U_E gravitational potential,
$\mathbf{V}_\mathrm{E}$ velocity of the Earth,
$\dot{r}_{2,\mathrm{gc}}$ station 2 GCRS velocity,
$\mathbf{b}$ baseline vector.

3 Observations

On August 24, 2015, four GPS satellites (PRN02, 12, 24, 25) were observed on the baseline Hobart-Ceduna. Details about these observations can be found in Hellerschmied et al. (2016) and Plank et al. (submitted), and about GNSS observations on the baseline Hobart-Ceduna in general in Plank et al. (this volume)

4 Results

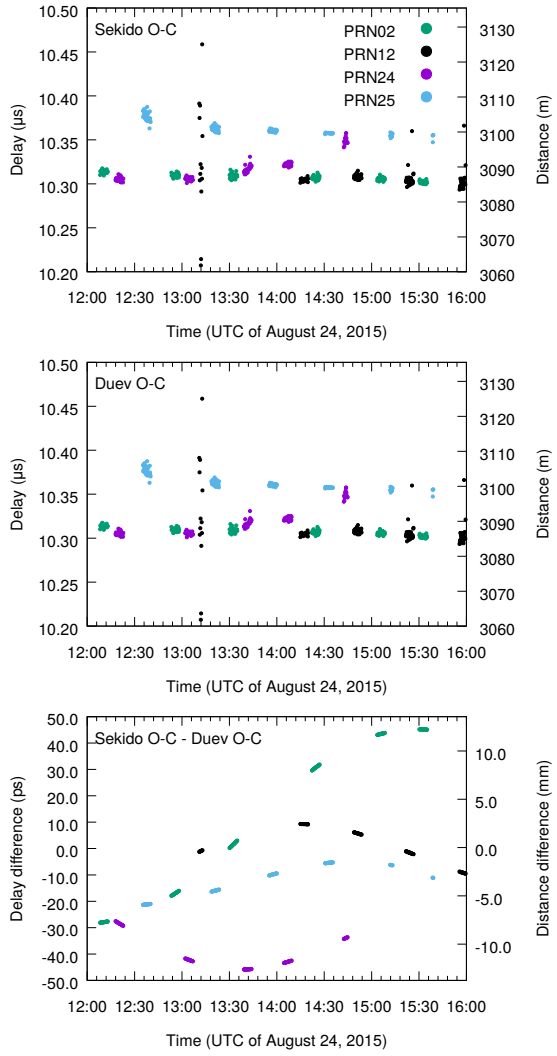

Fig. 5 Observed minus computed VLBI delays $(O-C)$ obtained with our implementations of the here presented near-field delay models. Top: SF06 model. Middle: D+12 model. Bottom: Difference between the results for the two models.

The results that we obtain for the observations of the four GPS satellites are presented in Fig. 5. The top panel shows the results for SF06, and the middle panel for D+12. The results are so similar that the plots look identical at first glance. In particular, both share the overall constant offset of $\sim 10.3\,\mu$s. In addition to that, every GPS satellite has its individual systematic trend. In particular, satellite PRN25 is offset to the other satellites by ~ 50 ns. PRN12 presents a large scatter at 13:12 UTC.

In order to investigate the differences between the results obtained with our implementation the models we plot the differences

$$\tau_{\text{Observed}} - \tau_{\text{Sekido}} - (\tau_{\text{Observed}} - \tau_{\text{Duev}}) = \tau_{\text{Duev}} - \tau_{\text{Sekido}}. \tag{8}$$

The bottom panel of Fig. 5 shows that the difference between the two models is varying between ± 50 ps. Again, these variations in difference present systematic trends for the individual satellites.

5 Conclusions

Near-field targets require near-field VLBI delay models, because the assumption of planar wavefronts is not applicable to these sources. Here is a summary of the features of the two models presented in Sect. 2.

The principle of the SF06 model is to construct a pseudo source vector in order to obtain a formula (Eq. 5) which resembles that of the conventional far-field delay (IERS Conventions, 2010). This feature may become useful in the context of delay-referencing by alternate observations of quasars and near-field targets (cf. Sect. 8 in Haas et al. this volume). For the SF06 model the light-time equation has to be solved only once, and abberational effects are taken into account in the final delay formula (Eq. 5).

The D+12 model solves the light-time equation twice and transforms the resulting signal travel time difference from barycentric dynamic time to terrestial time. By explicitely computing both signal propagation paths aberration is taken into account during this step. However, numerically solving the light-time equation twice also means approximatly twice the computation time when compared to the SF06 model. A future investigation could include a comparison of the two models with respect to computation time.

We have implemented in ivg::ASCOT both the SF06 and the D+12 model. Here we present our conclusions from our experience with the performance of our implementations of these models. We have tested these two algorithms by investigating the difference between the observed and computed VLBI delays $(O-C)$, a quantity which is essential for the final estimation of the parameters of interest.

In the case of the VLBI observations of four GPS satellites on the baseline Hobart-Ceduna (Hellerschmied et al., 2016; Plank et al., submitted), we find that there are well discernible systematic trends in the order of ~ 100 ns (top panel of Fig. 5). There are both systematics within each observed satellite, but also between the satellites, in particular PRN25 has a large offset compared to the other satellites. A search for a dependency of these observed sytematics on the elevation of the telescopes, the distance and velocity of the sources remained elusive. Further investigation is necessary in order to determine the origin of these systematic effects.

We find that the two models are consistent to about ± 50 ps in case of observations to GPS satellites, which have an altitude of $\sim 20\,000$ km. The differences between the two models are clearly systematic. Further investigation is needed to clarify under which conditions one model may be preferred over the other.

Acknowledgements

This research is supported by the Deutsche Forschungsgemeinschaft, DFG, project number No 318/14-1.

References

Duev, D. A., Molera Calvés, G., Pogrebenko, S. V., et al. 2012, Spacecraft VLBI and Doppler tracking: algorithms and implementation, A&A, 541, A43

Haas R, Halsig S, Han S, Iddink A, Jaron F, La Porta L, Lovell J, Neidhardt A, Nothnagel A, Tang G, Zhang Z, Observing the Chang'E-3 Lander with VLBI (OCEL), this volume

Hellerschmied, A., Böhm, J., Kwak, Y., McCallum, J., & Plank, L. 2016, VLBI observations of GNSS satellites on the baseline Hobart-Ceduna, EGU General Assembly Conference Abstracts, 18, 8895

IERS Conventions (2010). Gérard Petit and Brian Luzum (eds.). (IERS Technical Note ; 36) Frankfurt am Main: Verlag des Bundesamts für Kartographie und Geodäsie, 2010. 179 pp., ISBN 3-89888-989-6

Plank L, Hellerschmied A, McCallum J, Böhm J, Lovell J (2016) VLBI observations of GNSS satellites: from scheduling to analysis. J Geod, submitted

Plank L, McCallum J, Hellerschmied A, Böhm J, Lovell J (2017) Observing GNSS satellites with VLBI on the Hobart-Ceduna baseline (this volume)

Sekido, M., & Fukushima, T. 2006, A VLBI Delay Model for Radio Sources at a Finite Distance, Journal of Geodesy, 80, 137

Sovers, O. J., Fanselow, J. L., & Jacobs, C. S. 1998, Astrometry and geodesy with radio interferometry: experiments, models, results, Reviews of Modern Physics, 70, 1393

Implementation of VLBI Near-Field Delay Models in the c5++ Analysis Software

Klopotek G, Hobiger T, Haas R

Abstract We describe the implementation of two near-field delay models in the c5++ analysis software. The motivation for this work is to allow the calculation of a priori delay information for the correlation of VLBI raw observations of near-field targets and to prepare for the analysis of VLBI data of near-field objects. The software is tested by correlating VLBI observations of the Chinese Chang'E lunar lander on the Onsala–Wettzell baseline.

Keywords VLBI near-field models, geodetic VLBI, Chang'E-3, Moon, c5++

1 Introduction

During recent years, the geodetic VLBI community has become more and more interested in VLBI observations of objects located at a finite distance. One of the main drivers for an increasing interest in this topic are ideas of future co-location satellites that will be equipped with VLBI transmitters together with other space geodetic equipment, including GNSS receivers and Satellite Laser Ranging (SLR) reflectors. It is expected that such co-location satellites could be used to improve the International Terrestrial Reference Frame (ITRF). However, so far only a single prototype satellite exists and only a few experimental test sessions have been performed. Other near-field objects tracked with VLBI during the last years are GNSS satellites which were observed with regional VLBI networks in Europe, Australia and Asia on an experimental basis (Tornatore et al., 2014). Missions to other planets in the solar system and the Moon have been also areas of interest for utilization of VLBI observations (Lebreton et al., 2005; Kikuchi et al., 2009; Jones et al., 2015).

In late 2013 a robotic lander and a rover was deployed to the surface of the Moon within the Chang'E-3 (CE-3) mission of the Chinese Lunar Exploration Program (CLEP). The main scientific goal of this project was to examine the geological structure of the Moon and observe celestial bodies in the visible/near-infrared spectrum (Li et al., 2015). First European observations of the CE-3 signals with geodetic VLBI telescopes were performed in April 2014 on the Onsala–Wettzell baseline. Following these, an observational program was proposed to the IVS Program Committee to regularly observe the lunar lander with a global network of IVS stations (Behrend, 2013). Four OCEL-sessions (Observing the Chang'E Lander with VLBI) each year were granted by the IVS in 2014, 2015 and 2016.

An object is considered to be at a finite space ("near-field") if the distance between the source and a pair of telescopes creating a baseline is significantly smaller than the ratio of the squared baseline length divided by the observed wavelength (Born and Wolf, 1970). For these situations the commonly used plane-wave approximation is no longer valid and so-called "near-field models" have to be used for the data correlation as well as data analysis. Practical

Grzegorz Klopotek
Department of Earth and Space Sciences, Chalmers University of Technology, SE-412 96 Göteborg, Sweden

Thomas Hobiger
Department of Earth and Space Sciences, Chalmers University of Technology, Observatorievägen, SE-439 92 Onsala, Sweden

Rüdiger Haas
Department of Earth and Space Sciences, Chalmers University of Technology, Observatorievägen, SE-439 92 Onsala, Sweden

approaches for the computation of VLBI near-field delays can be found e.g. in Moyer (2000), Klioner (2003), Sekido and Fukushima (2006) or Duev et al. (2012). However, there is a lack of comprehensive comparison of these models, in particular the latter two approaches which are used in VLBI spacecraft tracking. Therefore, we present their brief comparison using delays from both approaches computed in the c5++ analysis software (Hobiger et al., 2010) for the target source located on the surface of the Moon. Moreover, we use the two aforementioned models for correlation of observations of the Chang'E-3 lander carried out in April 2014 during a test experiment at the Onsala Space Observatory and at the Geodetic Observatory Wettzell. In addition, we highlight the role of the c5++ analysis software in the processing pipeline of lunar VLBI data with the main aim of obtaining multi-band group delay observables. Finally, we formulate the outlook concerning observations to artificial radio sources on the Moon through the use of the VLBI technique.

2 Method & Data

First European test observations to the Chang'E-3 lander were carried out on April 8, 2014, at the Onsala Space Observatory and at the Geodetic Observatory Wettzell. The test session LUN04b consisted of 2 hours of lunar observations with scans of 15 second length when observing the lunar lander signal. Three blocks of observations to natural radio sources were included in the schedule, using a frequency setup with four S- and X-band channels each of 8 MHz bandwidth. For the lunar lander observations, the strong X-band signal of the Chang'E communication channel was observed, also with 8 MHz bandwidth. In this test session no DOR-tones were observed.

Data gathered during this experiment were correlated at the Onsala Space Observatory using the DiFX software (Deller et al., 2007). A simplified flowchart of the processing pipeline used in this study is depicted in Fig. 1. Manually created VLBI experiment (VEX) files were used to produce inputs to the mpifxcorr utility. After correlation, the resulting DiFX output files were converted to Mark4 format so that the Fourfit program could be used for fringe fitting.

Theoretical VLBI delays can be computed by default in the DiFX environment with the *calcif* tool that produces so-called "IM" (interferometer model) files containing VLBI delays expressed in polynomial form. However, *calcif* only includes a VLBI far-field models and thus is not suitable for lunar observations. Instead the *difxcalc* tool could be used, since it also includes VLBI near-field models. An alternative approach followed in this study is to use c5++ to replace the far-field model delays by near-field model delays.

For the LUN04b experiment data correlation was carried out using theoretical delays from the c5++ analysis software. This program is mainly utilized in the analysis of VLBI, SLR and GNSS data (Hobiger et al., 2014, 2015). However, a recently developed module was used to include a priori VLBI near-field delays into correlation process of this session. This was achieved by replacing the default delay polynomials in the IM files by those computed from the c5++ software which can provide near-field delays in accordance to the models described by Sekido and Fukushima (2006) and Duev et al. (2012). In c5++, VLBI delays or delay polynomials of a given degree can be computed using the spacecraft state vector in the body-fixed reference frame of a planet or the Moon (Archinal et al., 2011). The latter requires information from JPL's ephemeris files (Folkner et al., 2009). In case of satellites, NASA/NORAD Two-Line Elements (TLE) data or Multi-GNSS Experiment (MGEX) orbit products can be used to calculate position of objects either in ITRF or ICRF.

The aforementioned analysis software supports transformation of object's state vectors and reference points of telescopes to the Barycentric Celestial Reference System (BCRS) in which computed difference of reception times at both stations is expressed in the barycentric dynamical time (TDB) (Sekido and Fukushima, 2006). The conversion of the computed delays to the time-scale at observing stations is also supported in the c5++ software.

Delay differences between the near-field models described in Sekido and Fukushima (2006) and Duev et al. (2012) during a period of 30 days for an object located on the lunar surface are presented in Fig. 2.

For short baselines such as ONSALA60–WETTZELL, the delay differences show a variation on the level of tens of picoseconds, see Fig. 2 . This level of disagreement tends to scale with the increasing distance between VLBI stations.

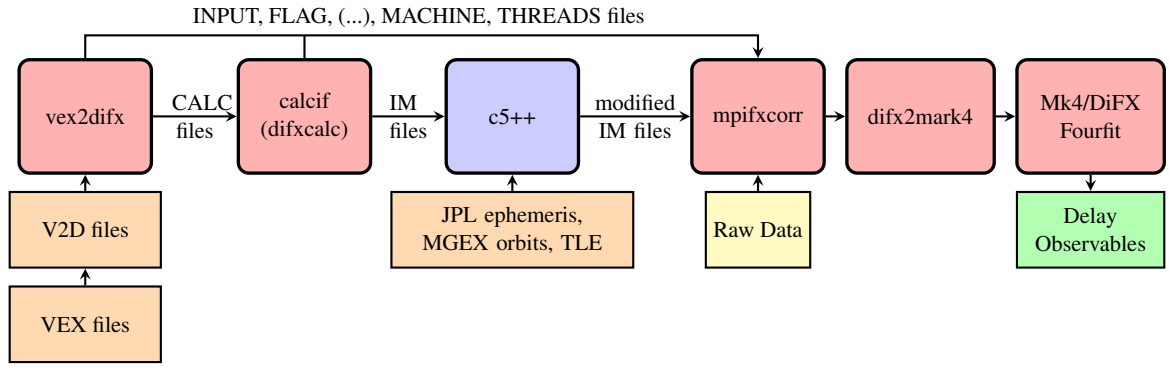

Fig. 1 Simplified schematics of the VLBI data correlation with DiFX using the common processing chain supplemented by the c5++ analysis software. After the DiFX processing is finished, the program Fourfit program can be used for fringe-fitting.

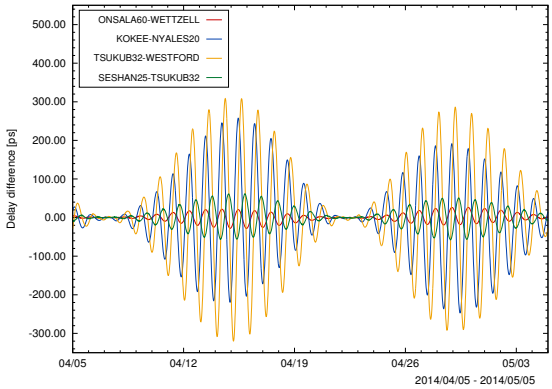

Fig. 2 Delay differences for a period of 30 days computed with the c5++ analysis software for a stationary object located on the Moon (44.12 N, 19.51 W) using the models of Sekido and Fukushima (2006) and Duev et al. (2012). No technique-specific, atmospheric nor tidal effects contributing to the VLBI delays have been considered here.

For intercontinental baselines such as KOKEE–NYALES20 the delay differences reach up to hundreds of picoseconds at several epochs during the considered period. Conclusions on the origin of such large discrepancies and pattern cannot be made at this stage and further investigations are needed, both in terms of baseline length and configuration as well as distance and type of the tracked source.

3 Results

Correlation of VLBI observations of the communication channel of the Chang'E lunar lander using the processing chain presented in Fig. 1 was carried out for session LUN04b twice, each time applying a different near-field delay model. Results from the fringe-fitting with Mk4/DiFX Fourfit for a single scan on the ONSALA60–WETTZELL baseline are shown in Fig. 3

Almost identical single band delay values were obtained in the two runs. The difference between the estimated single band delays is a few ps. The signal to noise (SNR) as well as the mean amplitude values of the cross-correlated signal are almost identical. A slope of the correlator phase and amplitude w.r.t. time for a single reference frequency of 8491.98 MHz is not seen on the plot.

4 Conclusions and Outlook

In this study we compare a priori VLBI delays for the target source on the Moon that were computed using two near-field models commonly used in VLBI spacecraft tracking. In addition, we present results of data correlation from the test observations of the Chang'E-3 lander located on the surface of the Moon. We also describe the role of the c5++ analysis software in correlation of VLBI data. Near-field delays calculated in c5++ for the source on the Moon using approaches described in Duev et al. (2012) and Sekido and Fukushima (2006) differ at the level of tens of picoseconds for the shorter baselines ($<$ 2000 km). However, this fact did not affect the obtained delays on the ONSALA60–WETTZELL baseline in a significant manner. Differences between delays

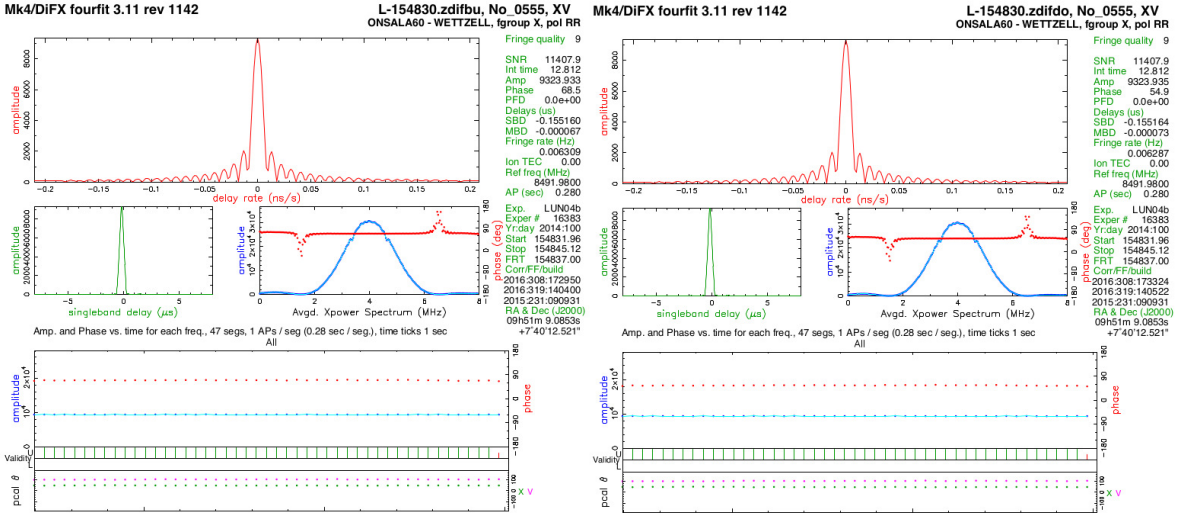

Fig. 3 Fringe-fitting results for the X-band carried out in the Mk4/DiFX Fourfit ver. 3.11 using VLBI near-field models described in Duev et al. (2012) (left) and Sekido and Fukushima (2006) (right) on the ONSALA60–WETTZELL baseline. A priori delay polynomials for the DiFX correlation were determined with the c5++ analysis software and then fed into IM files for DiFX.

from both models tend to scale with the distance between stations and they can reach up to 300 ps at some epochs on intercontinental baselines such as TSUKUB32–WESTFORD. This needs to be investigated in the future. Moreover, the correlation of lunar observations on intercontinental baselines using these two theoretical models could also be beneficial for such a comparison.

No major problems related to the correlation and fringe-fitting processes have been identified. The high SNR and amplitude values obtained on the ONSALA60–WETTZELL baseline indicate that the observation time of the Chang'E-3 lander could be decreased in this case in order to schedule more lunar observations within the same session.

Incorporation of the c5++ analysis software into the data correlation chain described here allowed us to identify numerical issues, correct bugs concerning calculation of VLBI delays in a finite space and develop a module capable of processing of IM files used in the DiFX software.

Our results can provide new insights into the correlation of lunar observations from previous, recent and future lunar exploration missions. Further work related to the observation of radio transmitters on the Moon is considered in order to validate the two VLBI near-field models within the c5++ environment. It is also planned to carry out simulations concerning determination of the position of an object on the lunar surface through the use of geodetic VLBI. Furthermore, we will also study optimized observation schedules dedicated for lunar observations and the potential impact of those observations on estimation of Moon and Earth-based parameters. This is thought to enable geodetic VLBI to observe and monitor artificial radio sources on the surface of the Moon.

5 Acknowledgments

The authors would like to thank Dmitry Duev for his feedback concerning VLBI near-field model, as well as Alexander Neidhardt from the Technical University of Munich for providing data from lunar observations carried out at the Geodetic Observatory Wettzell.

References

Archinal, B.A., A'Hearn, M.F., Bowell, E., Conrad, A., Consolmagno, G.J., Courtin, R., Fukushima, T., Hestroffer, D., Hilton, J.L., Krasinsky, G.A., Neumann, G., Oberst, J., Seidelmann, P.K., Stooke, P., Tholen, D.J., Thomas, P.C., Williams, I.P., 2011. Report of the IAU Working Group on Cartographic Coordinates and Rotational Elements: 2009.

Celestial Mechanics and Dynamical Astronomy 109, 101–135. doi:10.1007/s10569-010-9320-4.

Behrend, D., 2013. Data Handling within the International VLBI Service. *Data Science Journal* 12, WDS81–WDS84. doi:10.2481/dsj.WDS-011.

Born, M., Wolf, E., 1970. Principles of Optics. Fourth ed., Pergamon Press Inc., Bath, Great Britain.

Deller, A.T., Tingay, S., Bailes, M., West, C., 2007. DiFX: A Software Correlator for Very Long Baseline Interferometry Using Multi-processor Computing Environments. *Publications of the Astronomical Society of the Pacific* 119, 318–336. doi:dx.doi.org/10.1086/513572.

Duev, D.A., Calves, Molera, G., Pogrebenko, S.V., Gurvits, L.I., Cimo, G., Bahamon, T.B., 2012. Spacecraft VLBI and doppler tracking: algorithms and implementation. *Astronomy & Astrophysics* 541, A43. doi:10.1051/0004-6361/201218885.

Folkner, W.M., Williams, J.G., Boggs, D.H., 2009. The Planetary and Lunar Ephemeris DE 421. IPN Progress Report 42-178.

Hobiger, T., Otsubo, T., Sekido, M., 2014. Observation level combination of SLR and VLBI with c5++: A case study for TIGO. *Advances in Space Research* 53, 119 – 129. doi:http://dx.doi.org/10.1016/j.asr.2013.10.004.

Hobiger, T., Otsubo, T., Sekido, M., Gotoh, T., Kubooka, T., Takiguchi, H., 2010. Fully automated VLBI analysis with c5++ for ultra rapid determination of UT1. *Earth Planets Space* 62, 933–937. doi:10.5047/eps.2010.11.008.

Hobiger, T., Rieck, C., Haas, R., Koyama, Y., 2015. Combining GPS and VLBI for inter-continental frequency transfer. *Metrologia* 52, 251. doi:10.1088/0026-1394/52/2/251.

Jones, D.L., Folkner, W.M., Jacobson, R.A., Jacobs, C.S., Dhawan, V., Romney, J., Fomalont, E., 2015. Astrometry of Cassini With the VLBA to Improve the Saturn Ephemeris. *Astronomical Journal* 149, 28. doi:10.1088/0004-6256/149/1/28.

Kikuchi, F., Liu, Q., Hanada, H., Kawano, N., Matsumoto, K., Iwata, T., Goossens, S.J., Asari, K., Ishihara, Y., Tsuruta, S., Ishikawa, T., Noda, H., Namiki, N., Petrova, N., Harada, Y., Ping, J., Sasaki, S., 2009. Picosecond accuracy VLBI of the two subsatellites of SELENE (KAGUYA) using multifrequency and same beam methods. *Radio Science* 44. doi:10.1029/2008RS003997.

Klioner, S.A., 2003. A Practical Relativistic Model for Microarcsecond Astrometry in Space. *The Astronomical Journal* 125, 1580. doi:10.1086/367593.

Lebreton, J.P., Witasse, O., Sollazzo, C., Blancquaert, T., Couzin, P., Schipper, A.M., Jones, J.B., Matson, D.L., Gurvits, L.I., Atkinson, D.H., Kazeminejad, B., Perez-Ayucar, M., 2005. An overview of the descent and landing of the Huygens probe on Titan. *Nature* 438, 758–764. doi:10.1038/nature04347.

Li, C., Liu, J., Ren, X., Zuo, W., Tan, X., Wen, W., Li, H., Mu, L., Su, Y., Zhang, H., Yan, J., Ouyang, Z., 2015. The Chang'e 3 Mission Overview. *Space Science Reviews* 190, 85–101. doi:10.1007/s11214-014-0134-7.

Moyer, T.D., 2000. Formulation for Observed and Computed Values of Deep Space Network Data Types for Navigation. JPL Deep-Space Communications and Navigation Series.

Sekido, M., Fukushima, T., 2006. A VLBI Delay Model for Radio Sources at a Finite Distance. *Journal of Geodesy* 80, 137–149. doi:10.1007/s00190-006-0035-y.

Tornatore, V., Haas, R., Casey, S., Duev, D., Pogrebenko, S.V., Calvés, G.M., 2014. Direct VLBI Observations of Global Navigation Satellite System Signals, in: Rizos, C., Willis, P. (Eds.), *Earth on the Edge: Science for a Sustainable Planet: Proceedings of the IAG General Assembly*, Springer Berlin Heidelberg, Berlin, Heidelberg. pp. 247–252. doi:10.1007/978-3-642-37222-3_32.

Research and Analysis of Lunar Radio Measurements of the Chang'E-3 Lander

Tang G, Nothnagel A, Haas R, Neidhardt A, Schüler T, Zhang Q, Cao J, Han S, Ren T, Chen L, Sun J, Wang M, Lu W, Zhang Z, La Porta L

Abstract The China Chang'E-3 successfully landed softly on the lunar surface on December 14, 2013, the lander was equipped with X-band DOR transponder, which could be an ideal VLBI beacon on the moon. The Lunar Radio Measurements (LRM), including the ranging, Doppler, carrier phase, VLBI delay and delay rate can be acquired from ground TT&C antennas and VLBI antennas, which will greatly contribute to space geodesy than LLR that only provides the ranging observation. Since 2014, OCEL(Observing the Chang'E-3 Lander with VLBI) project has been conducting jointly by IVS and BACC(Beijing Aerospace Control Center), a global IVS R&D network augmented with two China Deep Space Stations was configured for Chang'E-3 lander observation. In this paper, the progress and preliminary analysis results based on the experimental data with MEKAS (Moon Earth Kinematical Analysis Software) is presented.

G.S. Tang, Q. Zhang, J.F. Cao, S.T. Han, T.P. Ren, L. Chen, J. Sun, M. Wang, W.T. Lu
National Key Laboratory of Science and Technology on Aerospace Flight Dynamics, Beijing Aerospace Control Center, Beiqing Road 26, 100094, Beijing, China

A. Nothnagel, Z.K. Zhang, L. La Porta
Institute of Geodesy and Geoinformation, University of Bonn, Nussallee 17, 53115, Bonn, Germany

R. Hass
Chalmers University of Technology, Onsala Space Observatory, SE-412 96, Onsala, Sweden

A. Neidhardt
Munich University of Technology, Geodetic Observatory Wettzell, Arcisstrae 21, 80333, Munich, Germany

T. Schüler
Federal Agency for Cartography and Geodesy, Richard-Strauss-Allee 11, 60598, Frankfurt am Main, Germany

Keywords Chang'E-3 lander; Yutu Rover; X-band transponder; DOR; Lunar Radio Measurement

1 Introduction

In the 1970s, the Apollo era, a program of ALSEP-Quasar VLBI has been carried out for the first time (Slade et al, 1977). Nearly 40 years later, the successful deployment of the Chang'E-3 lander on the moon with its X-band transponder has opened a new window for VLBI observations of the moon(Tang et al, 2014). The VLBI observations of the moon provide a direct opportunity to tie the Extragalactic-planetary frame and wide distribution of IVS station provides a new chance to break through the limitations that Lunar Laser Ranging (LLR) confronted. As LLR in some sense is independent of International Celestial Reference Frame (ICRF) which limit LLR increasing its impact in earth and lunar science (Williams et al, 2004).
In this paper, a brief introduction about the LRM technical system mainly focusing on the radio transponder on the lander is given on section 2, then we talk about OCEL project in section 3, and experimental data preliminary results are discussed in section 4, conclusions and prospect of future work are given in section 5.

2 Chang'E-3 lander

Launched on December 2, 2013. ChangE'3 made a soft landing at the plains of Sinus Iridum (Rainbow Bay) on lunar surface on 14 December 2013 successfully. Since

then, the lander has been serving as an ideal VLBI beacon on the moon for many scientific observations.

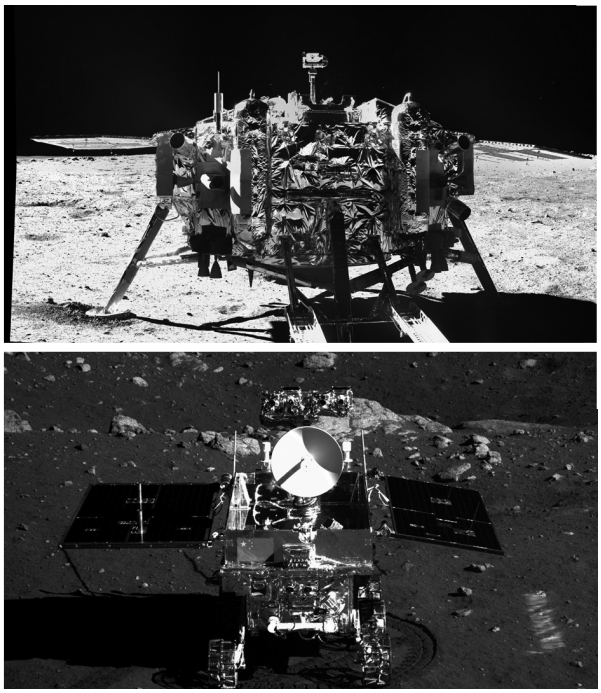

Fig. 1 Chang'E-3 lander and Yutu rover.

The lander is equipped with X-band DOR transponder, which can transmit X-band signal to the ground when it is tracked by China Deep Space Network (CDSN). This signal not only can be utilized to provide range and Doppler observations by CDSN, but can also be received by wide distributed IVS antennas to provide VLBI observations. Three years after its landing, the lander transponder still works well.

Besides the standard coherence-transmitting mode, the DOR transponder could also be worked as One-Way mode, which means the transponder produces the signal with the USO onboard and transmits it. The advantage of the second mode is that the transponder could be still active out of the view of CDSN, which makes the observation arc much longer for the observation of IVS stations. Fig. 3 shows the downlink signal of the lander.

Two groups of DOR tones are coherent with the carrier, with the re-transmit ratio 1/2200 and 1/440 respectively. Usually two DOR tones with smallest spanned bandwidth is used for resolving ambiguity, and the DOR tones with widest spanned bandwidth is used

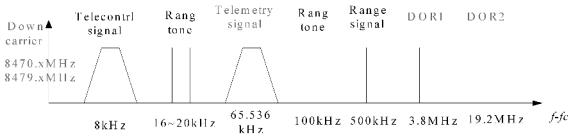

Fig. 2 Downlink signal of X frequency band in Change 3 lander.

to acquire the residual delay observable(Kikuchi et al, 2004; Tang 2012) .

3 OCEL Progess

Following proposals to the IVS Observing Program Committee, a global IVS R&D network augmented with two China Deep Space Stations was configured for joint observations of the lander in a project called OCEL (Observing the Chang'E-3 lander with VLBI). From July 2014 to the end of 2016, the Chang'E-3 lander was observed successfully during twelve sessions, eight of which is 24-hour sessions. More than 10 stations distributed all around the world participated in each observing session.

For the OCEL observations, the DeltaDOR mode was adopted, which means a sequence of "Quasar - Chang'E-3 - Quasar". Here, quasars with small separation angles are preferred to eliminate common errors as much as possible. As discussed above, the Chang'E-3 Lander is equipped with an X-band transponder which transfers an X-band carrier and four DOR tones at +/-19.25 MHz and +/-3.85 MHz, DOR tones are recorded in five different channels. Phase calibration (PCAL) is used to remove any offset in phase due to the BBC electronics of different channels. When the phases of the PCAL tones are too noisy, a strong calibrator is used to mannually specify the phase of each channel.

4 Preliminary Results

4.1 Correlator BSCS

BSCS(BACC Software Correlator System) is designed to run on Beowulf clusters consisting of commodity machines with parallel processing algorithms adopted

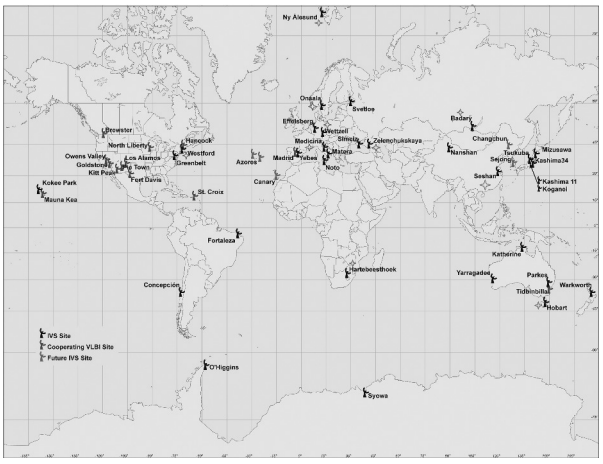

Fig. 3 Tracking stations in OCEL01(4-angle star)

in the software(Han et al, 2014). The control terminal and processing cluster are connected via a LAN, an operator logins into the manager node, runs the software via shell script. The basic steps include: raw data and parameter file preparation, core processing, error elimination.

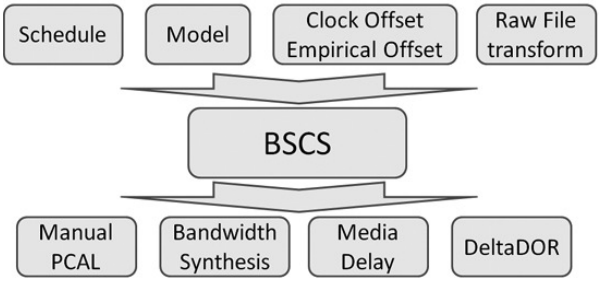

Fig. 4 Flow Chart of data processing

OCEL experiment data is transferred to BACC through shipment, Fig. 5 shows the interferometric fringe of the X-band channels of a lander scan. Besides DOR tones, wide band data communication signal could be identified.

4.2 analysis

MEKAS (Moon-Earth Kinetics Analysis Software) is developed at BACC. The main component of the software is a collection of modules, which are coded in FORTRAN. MEKAS has the four main basic functions: observation simulation, partial derivatives generation, estimation of uncertain parameters and covariance analysis. The observations that can be processed in MEKAS include Ranging and Doppler, VLBI delay and rate, DOR and DOD, Lunar laser Ranging, et. al. The parameters that can be estimated or considered includes locations of lunar landers or reflectors, station coordinates, Earth rotation parameters, observation bias, and lunar love numbers.

We analysis the experiment data in 2014, the whole observable consists of data obtained in eight days. There are about eleven IVS stations involved in the observation. All of the observables in 2014 are used to solve the position of the lander. In our algorithm, we solve the position of the lander by iteration. When we use all the IVS delay data to solve the position of the lander, the result is convergent, and the position solved is (1172753.438 -416374.684 1208176.687)(m) in the principal inertia axis of Moon, which deviate (-422.992 -80.258 64.954)(m) from our initial position. In our calculation, the largest number of the data points we used is given by the baseline NY-WZ; the smallest root mean square of the residual is given by the baseline SH-ZC, it is about 0.2 m. The residuals of baseline SH-ZC is shown in the following picture.All the units of the vertical axes is meter.

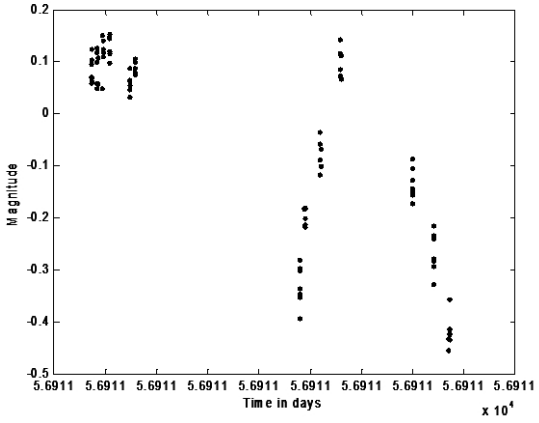

Fig. 6 The residual given by the baseline SH–ZC(IMJD = 56911).

Biases or secular terms could be identified in the residuals. If we fitted out these secular terms, we believe that the root mean of squares are all small to the level 0.1 m. The reasons which lead to the secular terms in the residuals include residual uncalibrated wet atmosphere delay and larger separated angle between the lunar and

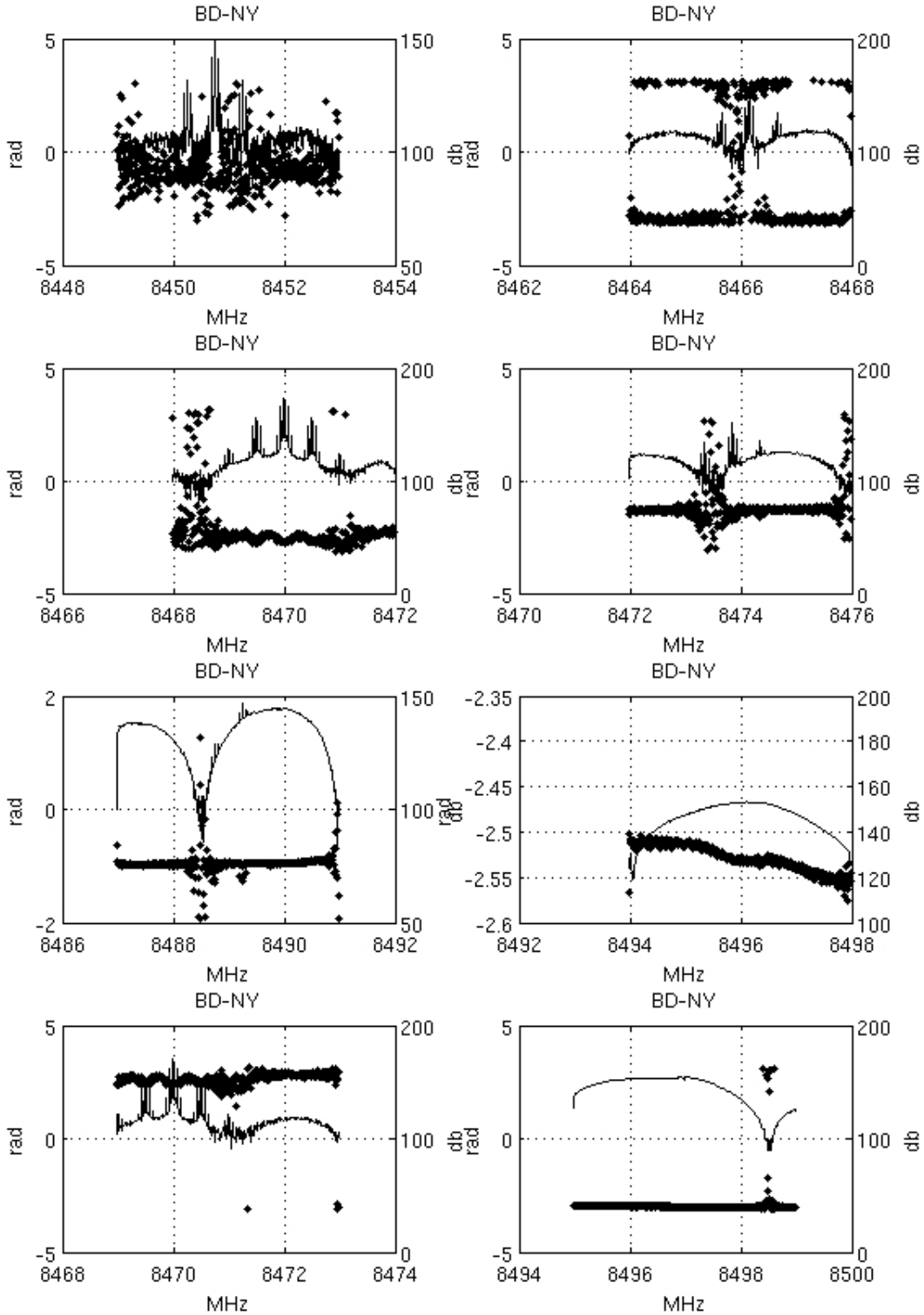

Fig. 5 Interferometric fringe

calibration quasar, which has a serious bad effect on the low elevation angle case.

5 discussion

After the high accuracy position determination, the lander could be utilized as a very good radio beacon to contribute to lunar and earth science as LLR reflectors. OCEL projects has been conducting since 2014, with global distributed IVS antenna tracking the lander, it is convenient and cheap to expand the ground observe distribution which is the target that LLR technique always be eager to pursuit, this is expected to contribute more to earth and lunar science.

In the following work, with the improvement of the measurement accuracy and the increasement of the arcs of observation, a more accurate position of the lander will be expected by making use of the IVS observables .

6 References

M. A. Slade, R. A. Preston, A. W. Harris, L. J. Skjerve, and D. J. Spitzmesser. ALSEP-quasar differential VLBI. The moon, 1997,17(2), 133-147.

G. Tang, J. Cao, S. Han, S. Hu, T. Ren, L. Chen, J. Sun, M. Wang, Y. Li, L. Li. Research on Lunar Radio Measurements by Chang'E-3. IVS General Meeting Proceedings, 2014, 473-477.

J. G. Williams, D.H. Boggs, S.G. Turyshev, and J. T. Ratcliff. Lunar Laser Ranging Science. 14th International Workshop on Laser Ranging, San Fernando, Spain, 2004, 7-11.

F. Kikuchi, Y. Kono, M. Yoshikawa, M. Sekido, M. Ohnishi, Y. Murata, J.S. Ping, Q.H. Liu, K. Matsumoto, K. Asari, S. Tsuruta, H. Hanada, N. Kawan. VLBI observation of narrow bandwidth signals from the spacecraft. Earth, planets and space, 2004, 56.11: 1041-1047.

G.S. Tang, Radiometric Measurement Technique for Deep Space Navigation. China, Beijing: National Defense Industry Press, 2012.

S. Han, G. Tang, L. Chen, J. Cao, T. Ren, M. Wang. VLBI Software Correlator in Interferometric Tracking Center of China DSN. IVS General Meeting Proceedings, 2014, 482-484.

Observing the Chang'E-3 Lander with VLBI (OCEL)

Technical Setups and First Results

Haas R, Halsig S, Han S, Iddink A, Jaron F, La Porta L, Lovell J, Neidhardt A, Nothnagel A, Plötz C, Tang G, Zhang Z

Abstract We present the current status of a research and development (R&D) project to observe the Chang'E-3 lander with VLBI. During 2014 to 2016 twelve so-called OCEL (Observing of the Chang'E-3 Lander) sessions were conduced. The purpose of these sessions is to integrate the lunar observations into VLBI sessions with a standard geodetic approach to benefit from relative observations of nearby quasars and from directly observed auxiliary information such as observed UT1–UTC and nutation offsets of date. The scheduling strategy and frequency setup were continually refined during the project. The observed data were correlated with the standard geodetic software correlator DiFX. Several strategies were tested to fringe-fit the correlator output but so far no conclusive results were achieved. More investigations on this topic are needed before the final VLBI observables can be produced and analyzed. Meanwhile, two VLBI data analysis software packages have been extended to allow the analysis of the lunar lander observations.

Keywords VLBI, Chang'E-3 lunar lander, DOR signals, Scheduling, Correlation and fringe fitting, Technical realization

R. Haas
Chalmers University of Technology, Department for Earth and Space Sciences, Onsala Space Observatory, SE-439 92 Onsala, Sweden, e-mail: rudiger.haas@chalmers.se

A. Nothnagel · S. Halsig · A. Iddink · F. Jaron · L. La Porta · Z. Zhang
Institute of Geodesy and Geoinformation, University of Bonn, Nussallee 17, DE-53115 Bonn, Germany, e-mail: nothnagel@uni-bonn.de

J. Lovell
School of Mathematics and Physics, University of Tasmania, Private Bag 37, Hobart 7001, Australia, e-mail: Jim.Lovell@utas.edu.au

A. Neidhardt
Technische Universität München, Forschungseinrichtung Satellitengeodäsie, Geodetic Observatory Wettzell, Sackenrieder Str. 25, DE-93444 Bad Kötzting, Germany, e-mail: neidhardt@fs.wettzell.de

C. Plötz
Federal Agency for Cartography and Geodesy, Geodetic Observatory Wettzell, Sackenrieder Str. 25, DE-93444 Bad Kötzting, Germany, e-mail: christian.ploetz@bkg.bund.de

G. Tang · Z. Zhang · S. Han
Beijing Aerospace Control Center, National Key Laboratory of Science and Technology on Aerospace Flight Dynamics, No. 120, Box 5130, Beijing, China, 100094, e-mail: tanggeshi@bacc.org.cn

1 Introduction

The successful deployment of the Chang'E-3 landing module (Fig. 1) on the Moon in 2013 (Barbosa, 2013; Tang et al., 2014; Zheng et al., 2014) is not only a success for modern lunar surface exploration but also for the first steps of Earth-Moon system geodesy beyond Lunar Laser Ranging (LLR) and lunar orbiters like previous Chang'E and SELENE or the Lunar Reconnaissance Orbiter (LRO). The reason is that the lander is equipped with a radio frequency transmitter at X-band which emits a faint modulated signal which is detectable on Earth by geodetic radio telescopes. With geodetic and astrometric very long baseline interferometry (VLBI) being predominantly sensitive to angular variations of the transmitting radio source, VLBI observations of the lander provide invaluable complementary information on the kinematics of the Moon

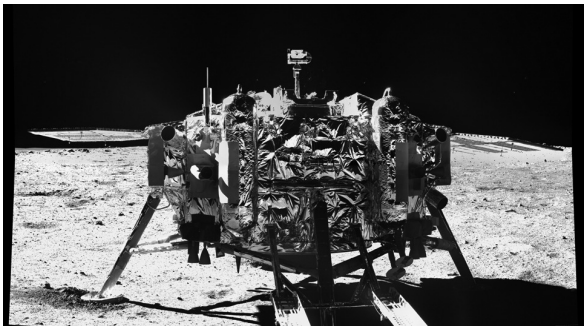

Fig. 1 Chang'E-3 lander.

represented through the fixed position of the lander on the Moon.

Observations of the lander alone would certainly provide some benefits in their own right. However, referring the lander observations to those of the extremely accurate positions of quasars and other compact extra-galactic radio sources tabulated, e.g., in the Second Realization of the International Celestial Reference Frame (ICRF-2) (Fey et al., 2015) produces a much better accuracy in an absolute sense. In our analysis approach we use the group delay observables of quasars in the vicinity of the direction to the Moon to compute corrections for the lander observations (Sec. 8). The main reason for the necessity of these calibrations is the lack of S band observations needed for ionosphere corrections. The second is that the estimates of the clock behavior and of the wet atmosphere contribution can thus be carried out only with the quasar observations leading to a clear separation of these estimates from the lunar observations and any unwanted side effects.

In order to exploit these favorable circumstances, a project called *Observing the Chang'E-3 Lander with VLBI* (OCEL) was initiated preparing for joint VLBI observations of the Lander and natural compact extra-galactic radio sources (mostly quasars). Following observing proposals to the Observing Program Committee (OPC) of the International VLBI Service for Geodesy and Astrometry (IVS) (Nothnagel et al., 2016), we were able to schedule four 24 h observing sessions each in the three years of 2014 to 2016 with subsets of the IVS observing network (Table 1).

It should be noted here that space agencies such as NASA, ESA, or CSA have long experience with VLBI and DOR observations (differential one-way ranging) of spacecraft emitting modulated signals. They predominantly observe frequency channels with very narrow bandwidths and employ up to 8-bit digitization. The difference of the OCEL project, however, is that we use radio telescopes of the IVS which are set up almost exclusively for observations of faint signals of natural radio sources such as quasars with 2-bit digitization at maximum. Here, we avoid system and setup changes as much as possible keeping the high sensitivity for the quasar observations because we want to determine the position of the Lander with respect to the quasi-inertial celestial reference frame. At the same time, we want to observe the lander and the quasars with the same setups to avoid unwanted group delay biases. This of course leads to some necessary compromises.

2 Previous Moon observations and expected results of the OCEL project

The Moon as the Earth's only permanent natural satellite has always been a prime object of study and exploration. Numerous space missions have been undertaken to study the Moon. The current main type of observations of the Moon is lunar laser ranging (LLR). It links the Moon and the Earth directly and helps to determine a number of parameters of the lunar orbit, librations, and the Moon's interior structure (Mueller et al., 2013; Munghemezulu et al., 2016). Considering the long history of LLR observations, the yield is rather sparse. There are only 22 361 LLR observations from 1969 to 2015, and more than 85 % of the observations are concentrated on two sites, McDonald, USA and Grasse, France (Bouquillon et al., 2013; Barache et al., 2015).

Using a radio frequency transmitter on the Moon was already employed almost 50 years ago. From 1969 to 1972 the Apollo program was carried out by the US National Aeronautics and Space Administration (NASA) which accomplished landing the first humans on the Moon. With the Apollo program, the Apollo Lunar Surface Experiments Package (ALSEP) was carried to the Moon which comprised a set of scientific instruments placed at the landing sites including S band (2.3 GHz) transmitters for each of the 5 ALSEP sites (King, 1975; King et al., 1976; Bates et al., 1979).

The analysis of observations of the differential ALSEP phases by the Massachusetts Institute of Tech-

nology (MIT) group estimated the relative ALSEP positions and physical librations with over 16 month of observations making use of 6 radio telescopes. The technique of differential VLBI was used to measure the relative positions of the ALSEP transmitters with quoted uncertainties of less than 0.005" of geocentric arc (King, 1975; King et al., 1976) which is about 9.2 m on the surface of the Moon. Combined with LLR data, the uncertainties in the relative coordinates of the 5 ALSEP transmitters were 30 meters in the radial coordinates and 10 meters in the two transverse coordinates (King, 1975; King et al., 1976). Values determined for the libration parameters have uncertainties smaller than the uncertainties obtained only with LLR (King, 1975; King et al., 1976).

A program of differential ALSEP-Quasar VLBI observations was planned and carried out around 1977 at the NASA Jet Propulsion Laboratory (Slade et al., 1977). However, soon afterwards on September 30, 1977 the ALSEP operations ended with the termination of support operations (Bates et al., 1979). The general scientific goals of ALSEP-Quasar program were to obtain high accuracy observations of value to tie the lunar ephemeris to the inertial reference frame of extra-galactic radio sources, to test gravitational theories, and to measure the Earth-Moon tidal friction interaction (Slade et al., 1977).

The deployment of the Chang'E-3 lander on the Moon in November 2013 and its capability to transmit weak modulated signals opened up the window for a new era of lunar observations from Earth. With an initial VLBI observing session of one hour duration on December 14, 2013 with 4 radio telescopes carrying out unified X-band (UXB) observations (including range and range rate from Doppler measurements) and with two-hour UXB observations of 3 telescopes on December 17, 2013, the position of the Chang'E-3 lander was estimated at the Beijing Aerospace Control Center (BACC) (Cao et al., 2016). Compared with positioning results of NASA Goddard Space Flight Center (GSFC) employing observations of the Lunar Reconnaissance Orbiter (LRO), the differences in a Mean Earth System are about 2.4 meters in altitude, and 0.002° (7.2 arcseconds) in latitude and longitude which is about 85 meters on the Moon (Cao et al., 2016).

Compared with all these observations, VLBI in the OCEL project can be undertaken by a number of sites distributed over the globe with more than a hundred observations within one observing session of 24 h duration. At the onset of the OCEL project a few scientific goals and possible results were identified.

Firstly, the accuracy of the determinations of the Chang'E-3 lander positions in the inertial frame is expected to be superior to any previous determinations. Assuming a conservative angular sensitivity of the long baselines employed in the IVS network observations of 5 mas (milliarcseconds) results in a tangential uncertainty of 9.2 m in each component. This precision is about a factor of three better than that of LRO which is about 30 m in the horizontal components and 5 m in the vertical direction.

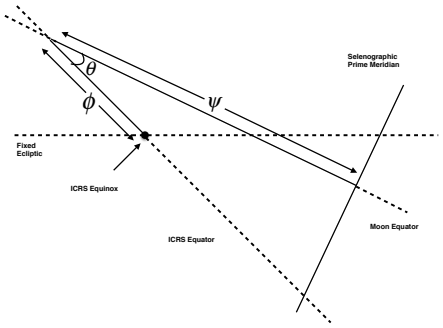

Fig. 2 Equatorial reference frame showing the Euler angles (Ψ, Θ, Φ) used to describe the lunar principal axis (PA) system (Taylor et al., 2010).

Secondly, the lunar librations are currently mainly calculated with LLR observations and published in lunar ephemeris. For instance, LLR observations from 1970 to 2007 were used for the computation of the JPL ephemeris DE421, and likewise from 1970 to 2012 for DE430 (Folkner et al., 2008, 2014). The libration part of the JPL lunar ephemeris after DE430 are all based on DE430. Therefore, the librations after 2012 can only be obtained by extrapolations which cause a loss in accuracy. Comparing the Euler angles from the DE421 and DE430 JPL ephemeris files, shifts of about 2 microradians (0.41") occur.

VLBI has a high sensitivity in the transverse direction. For this reason, corrections to the three Euler angles which describe the rotation of the Moon (Taylor et al. 2010, as shown in Fig. 2) can be estimated, especially the angle between the direction of the intersection of the Moon's and ICRS's equator to the Equinox (Φ).

Besides the Euler angles, the free libration parameters can be estimated. Combining the OCEL observations with LLR data will help to improve the estimates of all libration parameters. With better libration modeling, all other parameters of interest such as the positions of the Chang'E-3 lander or lunar orbital parameters will also benefit.

Thirdly, the effects, which cause the Moon's mean longitude to depart quadratically with time from the predictions of the Newtonian or general relativistic gravitational theory, are a time variation of the gravitational constant G and tidal friction (Slade et al., 1977). The mean motion is commonly used to characterize these effects in mean longitude. We will combine our results with LLR data to increase the sensitivity of the OCEL observations for the mean motion of the Moon if longer observing time will be available. Then we may learn more of the effect on the lunar mean longitude as a consequence of the slow time variation of G or even to estimate some parameters of the Parametrized Post-Newtonian (PPN) formalism (Will, 2014). Potential parameters include the parameters which cause the light deflection effect, the orbital polarization effect and/or the Nordtvedt effect.

3 Signal Characteristics

The Chang'E-3 lander is equipped with a DOR transponder with an on-board power of about 0 dBW. Two kinds of working modes are supported (Han et al., 2015). One is coherent transmission which means that the lander receives an up-link signal and transmits a signal with the frequency multiplied by a fixed ratio. The other one is a one-way mode where the lander produces the transmission signal with its onboard USO (Ultra Stable Oscillator). The Chang'E-3 DOR module is only operating if activated by the ground control station.

Two groups of DOR tones are coherent with the main carrier of 8470 MHz with ratios of 1/440 ($\pm$ 19.25 MHz) and 1/2200 ($\pm$ 3.85 MHz), respectively. Consequently, the lander transmits 5 DOR-tones at 8450.75, 8466.15, 8470.00, 8673.85, and 8489.25 MHz (located in X band). Figure 3 depicts the spectrum of the DOR tones with the main carrier. In the Chang'E-3 case, the DOR tones are modulated with additional signals which can be identified next

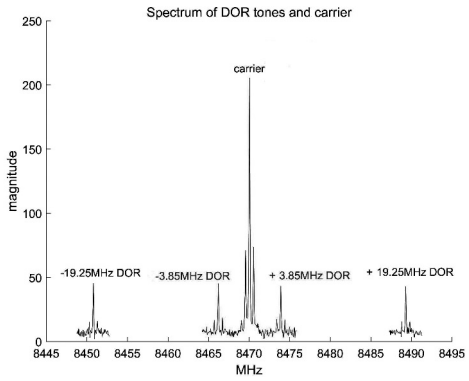

Fig. 3 Signal spectrum of Chang'E-3 transmitter.

to the main peaks in the picture. The output power of the transmitter for these DOR-tones is on the order of 1 W over the bandwidth of the five DOR tones. In the vicinity of the DOR tones, communication with the lander is realized at 8496 MHz, and/or 8497 MHz with much higher output power (12/25 dBW). S band signals are not transmitted by the lunar lander.

4 Preparation of Observing Sessions

Observations of an artificial radio source on the Moon are different in several aspects compared to usual geodetic VLBI observations. As seen from a pair of radio telescopes on Earth, the Chang'E-3 lunar lander has to be considered as a near-field target. This means that the right ascencion (RA) and declination (DEC) that are usually used to steer radio telescopes for the observation of radio sources, are station-dependent. The artificial radio source is also much stronger than the usually observed natural radio sources (see Sec. 3). Thus, we carried out several test observations and developed a suitable strategy to plan observing schedules for networks of globally distributed IVS stations.

4.1 First test observations

As a preparation for the OCEL project, first test observations with IVS stations were performed in April 2014

using the Onsala 20 m, Wettzell 20 m and Tianama 65 m radio telescopes. The goal was to test whether the way to prepare the necessary vex-files (see Sec. 4.2) worked and what attenuation was necessary at the radio telescopes in order to receive the rather strong lunar lander signals.

The communications channels at 8496 MHz and 8497 MHz were specified with an output signal level of 12 dBW and 25 dBW at the lunar lander (see Sec. 3). Calculations based on these a priori information indicated that we had to expect reception of signals, which are stronger by 27 dB and 40 dB, respectively, than the rather strong natural radio source 4C39.25 at X-band. Correspondingly, the DOR signals were expected to be stronger by at least 15 dB.

The pictures presented in the upper row in Fig. 4 show the signal spectrum observed with the Onsala VLBI system for the test experiment on April 10, 2014. At this date only the communication channel at 8496 MHz was active, but no DOR signals were transmitted. The upper left photo clearly shows that the communication signal is prominent in the spectrum, and the zoom-in on the upper right photo shows that the signal is at least 15 dB stronger than the background. The lower left photo shows the signal spectrum observed at Wettzell, while the lower right photo shows the corresponding signal observed at Tianma.

Based on these test observations, we drew the conclusion that the lunar lander signals would not saturate the VLBI systems and that modern digital backends would be able to adjust attenuation with automatic gain control (AGC) when observing natural radio sources and lunar lander signals in an alternating mode. Nevertheless, in order to build in a further level of protection for the VLBI systems, we concluded to prepare the vex files for the real OCEL-sessions by adding a special lunar lander setup (see Sec. 4.3) that allow stations that are not yet equipped with modern digital backends, to adjust attenuation levels accordingly.

Test observations were also planned and performed at other international IVS stations. Figure 5 depicts spectra obtained from autocorrelation of observations done with the Hobart 26 m radio telescope on June 10, 2014. At this date, both the communication channel (left) and the central DOR tone (right) were transmitted and could be observed.

The data observed on April 10, 2014 were used to test the data correlation, too. This was done with the

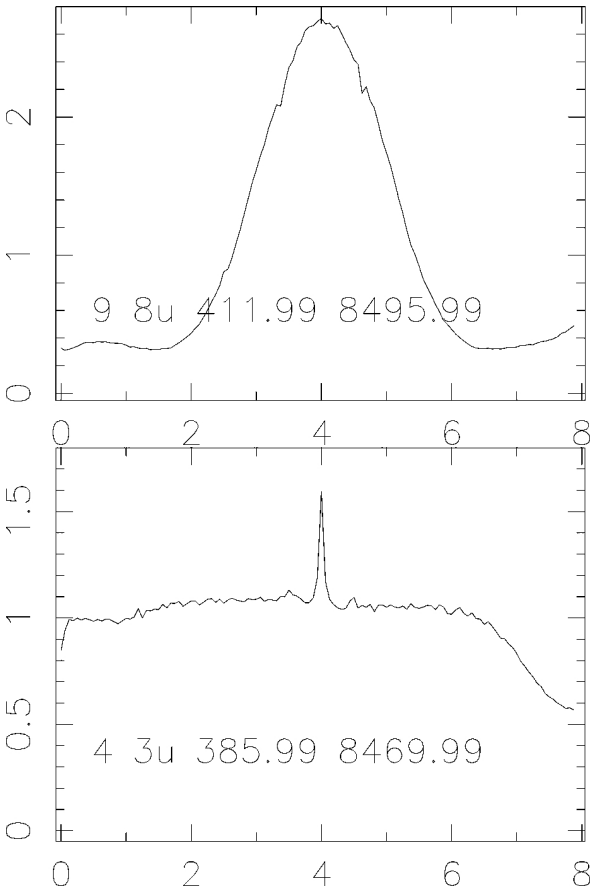

Fig. 5 Spectra of the lunar lander communication channel (left) and the central DOR-tone (right) observed during a test experiment on June 10, 2014 using the Hobart 26 m radio telescope. These graphs are autocorrelation results of observations done with several channels of 8 MHz bandwidth.

DiFX software correlator (Deller et al., 2007b) which is installed on a server at the Onsala Space Observatory. The a priori delay values needed in the .im-files were calculated with a special version of the c5++ software (Hobiger et al., 2010) that was extended by Klopotek et al. (this volume) by the near-field VLBI models following (Duev et al., 2012) and (Sekido and Fukushima, 2006). Correlation with DiFX and fringe-fitting with *fourfit* (Sec. 7) seem to have been successful (Klopotek et al., this volume).

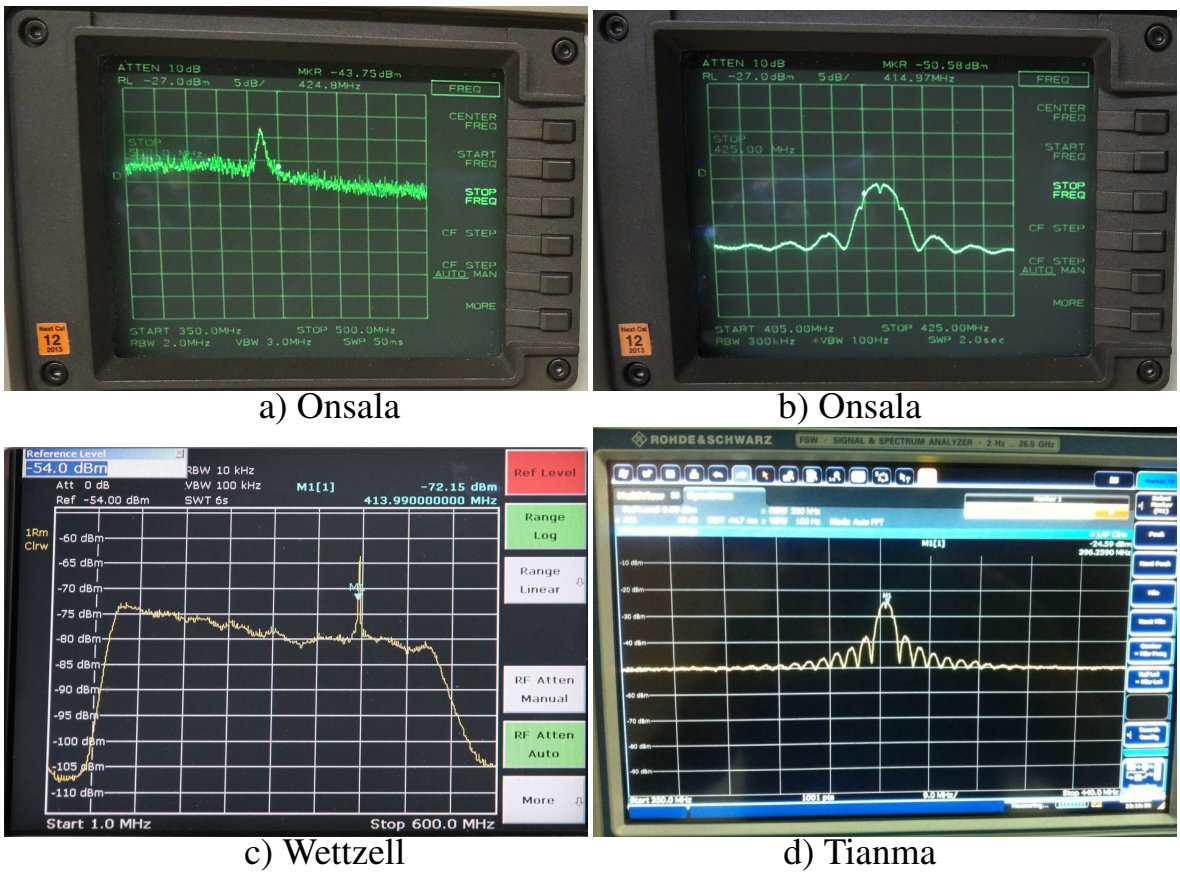

Fig. 4 Spectra of the lunar lander communication channel observed during a test experiment on April 10, 2014 using the Onsala 20 m (a, b), Wettzell 20 m (c) and Tianma 65 m (d) radio telescopes. The upper left photo (a) is taken at Onsala and covers 150 MHz bandwidth, while the upper right photo (b) is a zoom-in to 20 MHz bandwidth only and uses the max-hold option of the spectrum analyzer. The signal peak is at 416 MHz, corresponding the to communication channel at 8496 MHz that is down-converted with the LO-frequency of 8080 MHz.

4.2 Scheduling the OCEL-sessions

Table 1 lists the world-wide IVS stations participating in the 12 OCEL sessions in 2014 through 2016. The site distribution is rather dense in Asia and Europe, however there are also a few stations in the American-Pacific region.

So far, scheduling of near-field sources is not standard in the geodetic VLBI scheduling software *sked* (Sked, 2016) and skd-files with near-field radio sources are not possible. Also, VEX2 (VEX2, 2016) is not available yet, meaning that it is not possible to have a station-specific RA/DEC in a common vex-file for all stations that are involved in a session. Instead, for a session with n stations observing a near-field radio source a total number of n individual vex-files need to be prepared. The software *sked* was used for the scheduling process and included a combination of automated scheduling and manual scheduling. The following scheduling strategy was applied:

Step 1: Chang'E-3 visibility
Time series of RA/DEC, azimuth (AZ) and elevation (EL) of the Chang'E-3 lunar lander were calculated for all stations participating in the session to be planned. This was done using the JPL Horizons system (JPL HORIZONS, 2016). Average values of the lunar lander RA/DEC for hourly temporal resolution as well for the whole 24 h session were determined. The mean RA/DEC with hourly temporal resolution were plotted together with the ICRF radio sources allowing to identify sources within close distance ($<$ 3 degrees)

Table 1 Overview of the stations participating in the 12 OCEL sessions observed in 2014 through 2016. The IVS 2-character station abbreviations are used to indicate the individual stations: Bd – (Badary 32 m), Ft – (Fortaleza 14.2 m), Hh – (HartRAO 26 m), Ho – (Hobart 26 m), Ht – (HartRAO 15 m), Kk – (Kokee Park 20 m), Km – (Kunming 40 m), Ma – (Matera 20 m), Mc – (Medicina 32 m), Ny – (Ny-Ålesund 20 m), On – (Onsala 20 m), Sh – (Shanghai 25 m), Ur – (Urumqi 25 m), Wz – (Wettzell 20 m), Zc – (Zelenchukskaya 32 m).

OCEL											
#01	#02	#03	#04	#05	#06	#07	#08	#09	#10	#11	#12
Bd	Bd	Bd	-	Bd	Bd	Bd	Bd	Bd	Bd	Bd	Bd
-	-	-	-	Ft	Ft	-	Ft	Ft	Ft	Ft	Ft
Hh	Hh	-	-	Hh	Hh	Hh	-	Hh	Hh	Hh	Hh
Ho	-	Ho	Ho	Ho	Ho	Ho	Ho	Ho	Ho	Ho	Ho
-	-	Ht	Ht	-	-	-	Ht	-	-	-	-
-	-	-	Kk	Kk	Kk	Kk	Kk	Kk	-	Kk	Kk
-	-	-	-	-	-	-	-	-	-	Km	-
-	Ma	Ma	Ma	Ma	Ma	Ma	Ma	Ma	-	-	Ma
-	-	-	-	-	-	-	-	-	Mc	Mc	-
Ny	Ny	Ny	Ny	Ny	Ny	Ny	Ny	Ny	Ny	Ny	Ny
On	-	-	-	On	On	On	On	On	-	On	On
Sh	Sh	Sh	-	Sh	Sh	-	-	-	Sh	-	-
-	Ur	Ur	Ur	-	-	-	-	-	Ur	Ur	Ur
Wz	Wz	Wz	Wz	Wz	Wz	Wz	Wz	Wz	Wz	Wz	Wz
Zc	Zc	Zc		Zc	Zc	Zc	Zc	Zc	Zc	Zc	Zc
number of participating stations											
8	8	9	7	11	11	9	10	10	10	12	11

(Fig. 6). Additionally, elevation plots for all stations were produced in order to see which stations would be able to observe the lunar lander at what time, and whether common visibility existed. An example of such a visibility plot is presented in Figure 7 for the session OCEL-11 (RD1609). The inhomogeneity of the network becomes clear, with many Asian and European stations, but few in the American-Pacific region.

Step 2: Adjustment of radio source catalogue in *sked*
If not available already in the standard radio source catalogue used in the *sked* program (*source.cat.geodetic.good*), the near-by radio sources identified in the previous step were added to the catalogue. The necessary position and flux information was adopted from the Radio Fundamental Catalog RFC (2016). The lunar lander was also added to the source and flux catalogues, using the average RA/DEC over 24 hours for the position and a strong flux of 99 Jy as the flux. The actual transmission power of the lunar lander corresponds to even larger flux values, so this flux can be regarded as a very conservative assumption.

Step 3: Automatic and manual scheduling
The general overall scheduling strategy was to use alternating observing blocks of primarily 30 minutes length, where the observations were scheduled either a) using the standard automated approach in *sked*, i.e. optimizing for local sky coverage for all stations, or b) using a manual scheduling approach to observed the lunar lander alternated with near-by radio sources. The first type of scheduling can be called "geodetic", while the second type can be called "delay-referencing" (Sec. 8), though the arc length between the lunar lander and the near-by radio source sometimes were much larger than just a few degrees. The delay-referencing intervals were of course only scheduled for the stations that could see the Moon and during times when the lunar lander was actively sending. While the lunar lander was not sending for about 9 hours every night during the first four OCELs, it was just interrupting the signal transmission every 5.5 h for a duration of 30 minutes for the other OCELs. These outages were necessary to avoid overheating of the lunar lander.

For the geodetic intervals, the standard SNR goals of 25 and 15 in X- and S-band, respectively, were used. However, for the delay-referencing intervals, the X band SNR goal was increased to 35 in order to compensate for that only 5 DOR tones instead of 8 channels could be observed (Sec. 4.3, Tab. 2). The stations that could not see the Moon were scheduled during these intervals with the standard geodetic approach. The reason for this strategy, i.e., alternating between geodetic and delay-referencing blocks, was to assure that there were observations in all directions for each station, in order to be able to determine the standard geodetic parameters especially atmospheric and clock parameters for the lunar observations in these sessions, too. As an example, Figure 8 depicts sky plots of all stations participating in OCEL-11 (RD1609). Bands of lunar lander observations and close-by radio sources are visible in all sky plots, except for Ny-Ålesund that could not see the Moon during this session at all.

Step 4: Creation of a template vex-file for the session
Once the 24 h schedule was completed, the information was saved directly from the *sked*-program as skd- and vex-file. The resulting vex-file was sent through a small program to replace in the *m* scans observing

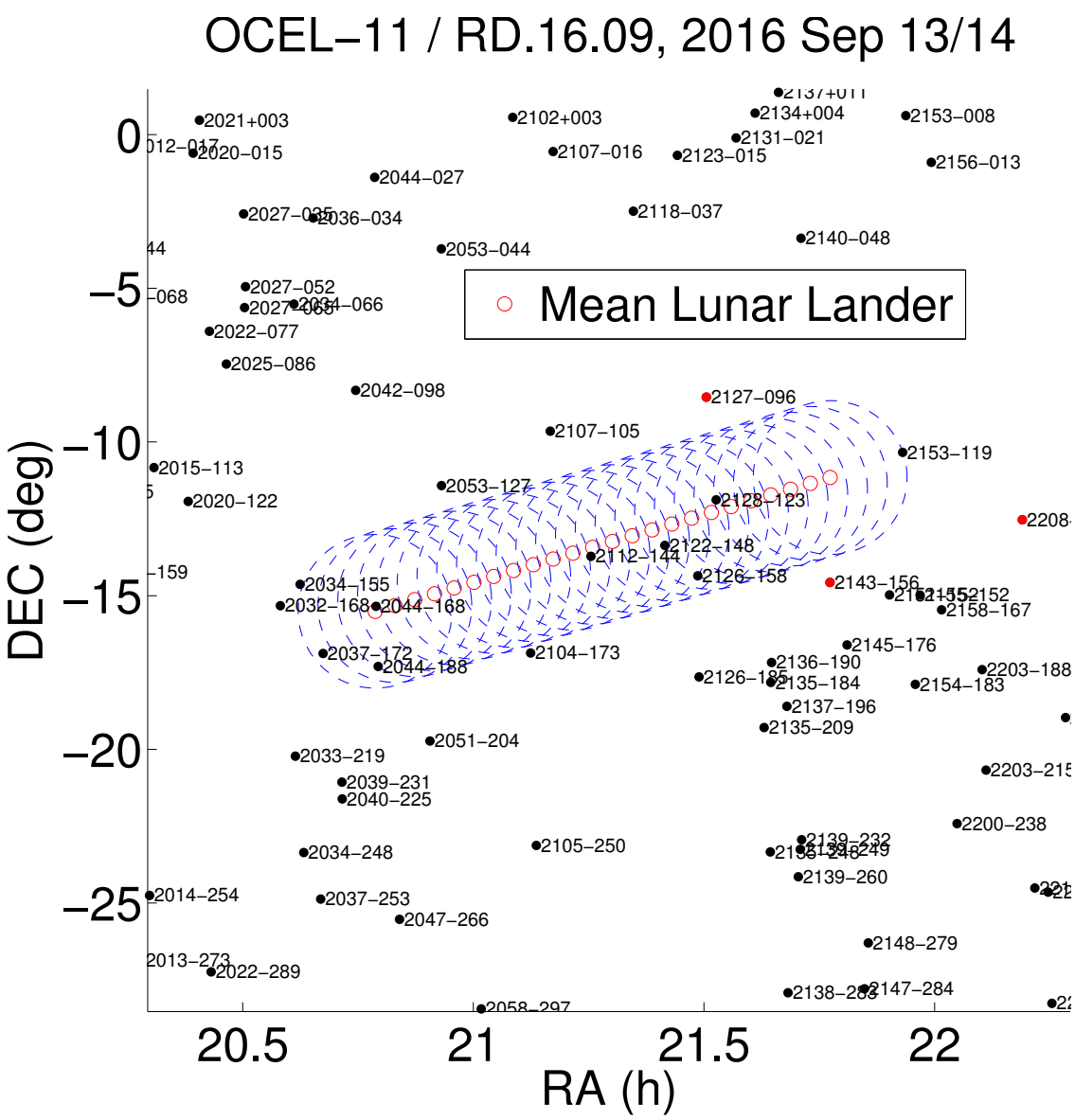

Fig. 6 Chang'E-3 lunar lander right ascencion (RA) and declination (DEC) during OCEL11 (RD1609, 2016-09-13/14). Shown are hourly values of the mean RA, DEC (small red circles) as seen for the 12 stations network for OCEL-11, and areas with 3 degree radius around (dashed blue lines). Also shown are the ICRF radio sources in this area of the sky. Defining sources of the ICRF2 are shown with red dots.

the lunar lander the radio source name OCEL-xx by a radio source name consisting of "L-HHMMSS" and the start time of the scan in hour (HH), minute (MM) and second (SS). Thus, *m* different radio source names such as, e.g., "L-173015" were included in the vex-file. The sections $MODE, $BBC, $FREQ, $IF in the vex-file were edited and corresponding information for the lunar lander observations were added. For example, for the first 10 OCEL sessions, there were different frequency setups for the "geodetic" and the "delay-referencing" observations. The "geodetic" observations used standard frequency setups, e.g., as in the IVS R1 or T2 sessions, while the frequency setup for the lunar lander observations, and the corresponding delay-referencing sources, were adapted to fit to the DOR-frequency setup of the lunar

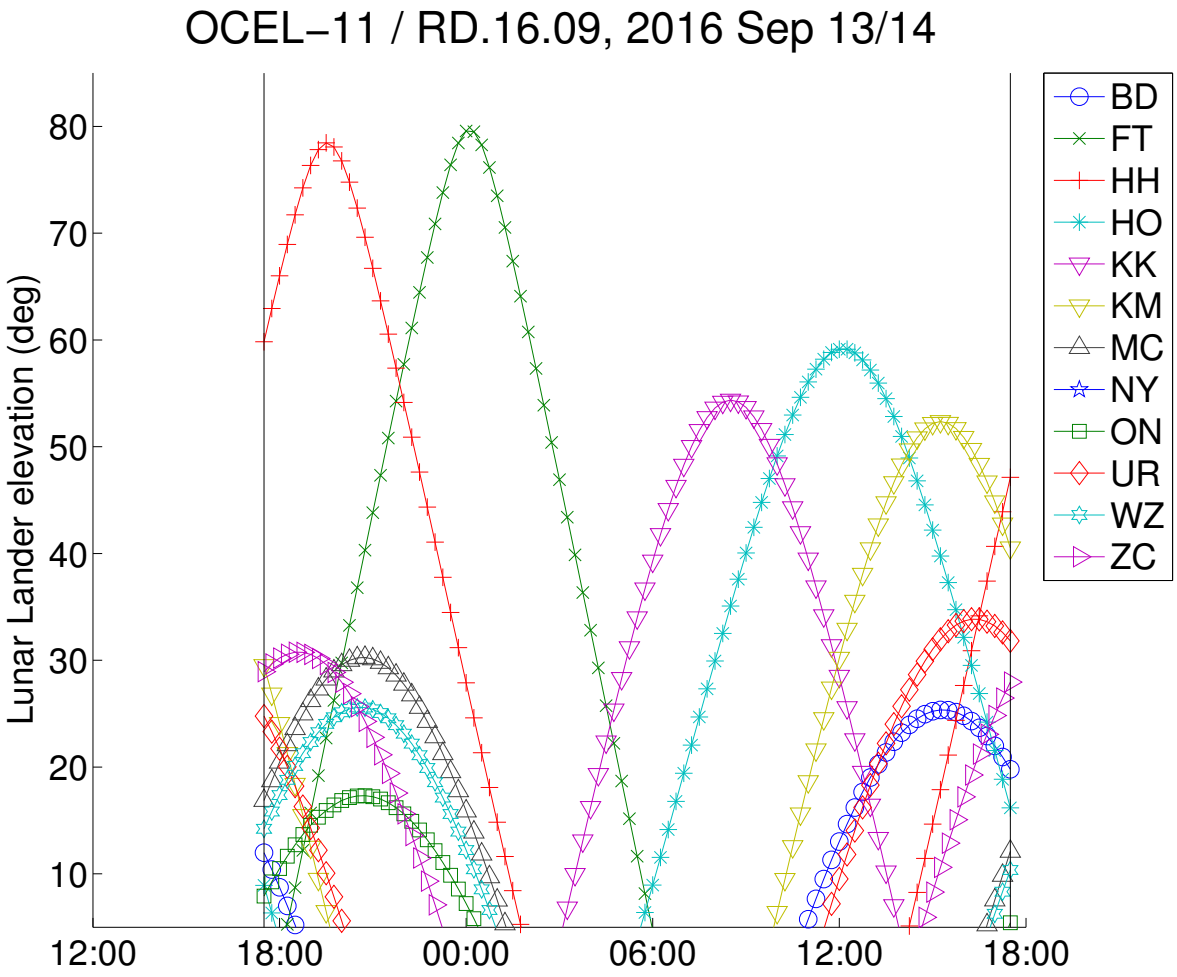

Fig. 7 Time series of lunar lander elevation for all stations participating in OCEL-11 (RD1609, 2016-09-13/14). The "American-Pacific-gap" in the network becomes clear. For about 2 hours after about 2.00 UT on September 14, the Moon is only visible for one single station in the network, Fortaleza.

lander. Only for the last two sessions, (OCEL-11 and OCEL-12), a special frequency setup was used that avoids the necessity to change frequencies between the geodetic and the lunar lander (and delay-referencing) observations. More details on this issue see Sec. 4.3.

Step 5: Creation of station-specific vex-files
The result of the vex file adjustment in the previous step was a template vex-file for the whole session. This template vex file still contained just a single common RA/DEC position of the lunar lander, for all times and all stations. Thus, the template vex file was then copied n times to create n station-specific vex files, one for each of the $n$stations participating in the session. Finally, the station-specific right RA/DEC information was added in the $SOURCES section of the vex file. This was provided by BACC as time series of RA/DEC for each station with 1 minute temporal resolution. Using these, RA/DEC for the particular scan start times were interpolated and added to $SOURCES sections in the individual vex files.

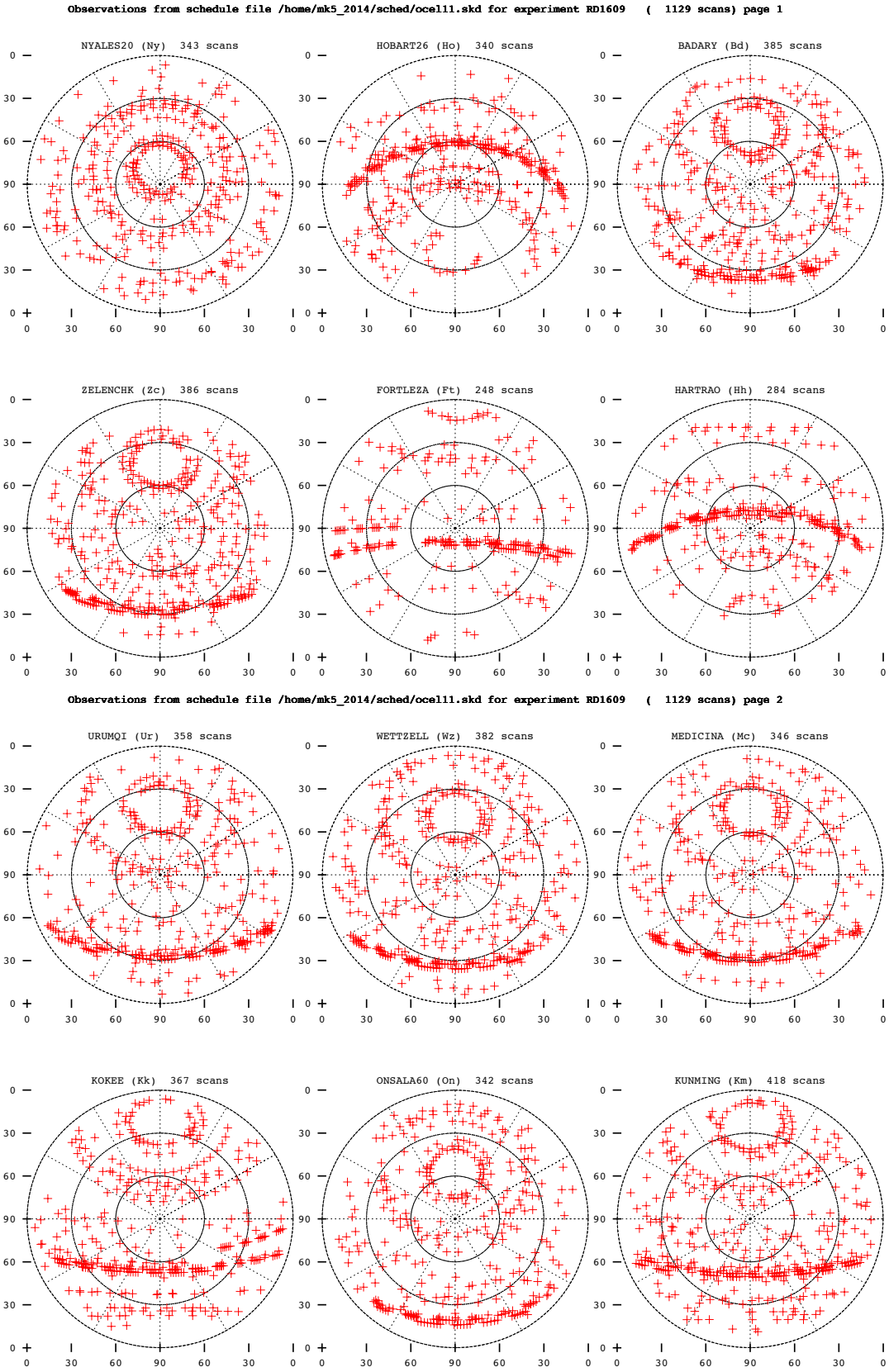

Fig. 8 Sky plots for OCEL11 (RD.16.09, 2016-09-13/14).

4.3 Frequency Setups for OCEL Sessions

Considering the frequency allocations described in Sec. 3, the initial plan for the OCEL sessions was to observe in different modes for different purposes:

- quasar observations with a wide coverage of right ascensions and declinations for precise clock, atmosphere and Earth orientation parameter determinations using standard geodetic frequency bands
- intensive observations of one or two quasars close to the lander direction for delay referencing in a frequency mode which matches the frequency allocation of the DOR tones
- lunar lander observations covering the five frequencies listed above

For these sub-sessions, suitable frequency setups needed to be found. Several challenges occurred:

- The purely geodetic observations were supposed to be done with an as good as possible wide-band frequency setup, e.g., as for the IVS R1 sessions
- The lunar lander DOR tones require a narrow-band frequency setup and the minimum separation between the DOR tones is less than 4 MHz
- Alternating between wide-band and narrow-band is not possible for some IVS stations without hardware changes, i.e., not possible during a running session
- For some IVS stations the contrast in signal strength between natural radio sources and the lunar lander signals might challenge the receiving system

The approach to address the issue of frequency setup was to test a number of different setups. The goal was to learn from experience gained and to adapt the frequency setup accordingly for the planning of the further sessions. In the end, this plan did not work out completely, since difficulties in correlating and analyzing the data occurred, and thus the experience gained sometimes came too late to be used for the planning of the next sessions.

The first OCEL-session was planned with a standard wide-band R1-setup with 8 MHz channel bandwidth for the geodetic observations, and to a special narrow-band frequency setup with 8 MHz bandwidth, aiming at the DOR-tones for the delay-referencing observations (Tab. 2) . In order to allow for potentially necessary changes in signal attenuation during the delay-referencing observations due to the strong contrast in signal strength between the lunar lander and natural radio sources, a third setup was introduced, too. However, this approach turned out to be unfavorable since several DOR-tones fell in the same 8 MHz wide channel, a situation which could not be handled by *fourfit*.

Thus, for OCEL-02 the frequency setup was changed to use only 4 MHz bandwidth per channel. The frequency setup for the EURO sessions was used for the geodetic parts of the session, and a corresponding frequency setup for the lunar lander. This approach was also used for OCEL-03. However, for OCEL-04 the wide-band frequency setup similar to OCEL-01 was used again.

During the first four OCEL sessions, phase-cal was active and the frequencies used ended on .99 to allow the stations to monitor the pcal-signal locally with an oscilloscope. This was also the case for the lunar lander observations, i.e., the lunar lander DOR tones were not in the middle of the channel bandwidth. For OCEL-05 through -12 instead the frequencies aiming at the lunar lander were set to really get the DOR-tones in the center of the channels.

The geodetic parts of OCEL-05 to OCEL-09 were using the wide-band R1-setup with 8 MHz bandwidth channels, while the delay-referencing parts used a narrow-band lunar lander setup with 4 MHz bandwidth channels. It was realized that the change in channel bandwidth caused delay offsets. Thus, for OCEL-10 the frequency setup was modified to use also 4 MHz for the geodetic parts. For OCEL-05 to -07, phase-cal was switched off everywhere deliberately because it was thought at that time that it would interfere with the DOR tones.

Finally, starting with OCEL-11 a special narrow-band frequency setup was used that avoids any frequency and/or bandwidth changes when switching from geodetic to delay-referencing observations. Keeping the DOR frequencies with their 3.85 MHz smallest common denominators, the outer frequencies were chosen to match the 360 MHz spanned bandwidths of the IVS narrow band setups and, at the same time, to produce a reasonable delay resolution function. This allows 8-channel geodetic observations and 5-channel delay-referencing observations without a need for channel re-allocations.

Table 2 Frequency allocations for delay-referencing and lunar lander observations with bandwidths (BW), upper sideband, shaded if channels do not match the DOR tone sequence. BW (x/y/z) with x for quasar observations, y for nearby quasars (for delay referencing), z for lunar observations. DOR tone frequencies at the bottom

Channel number, frequency, and bandwidth (MHz)									
OCEL	CH01	CH02	CH03	CH04	CH05	CH06	CH07	CH08	BW
#01	8212.99	8252.99	8465.99	8491.99	8446.99	8461.99	8465.99	8485.99	8/8/8
#02	8448.99	8463.99	8467.99	8471.99	8486.99	8493.99	8468.99	8494.99	4/4/4
#03	8466.99	8492.99	8448.99	8463.99	8467.99	8471.99	8486.99	8497.99	4/4/4
#04	8212.99	8252.99	8446.99	8461.99	8465.99	8469.99	8484.99	8491.99	8/8/8
#05	8212.99	8252.99	8448.75	8464.15	8468.00	8471.85	8487.25	8492.00	8/4/4
#06	8212.99	8252.99	8448.75	8464.15	8468.00	8471.85	8487.25	8492.00	8/4/4
#07	8212.99	8252.99	8448.75	8464.15	8468.00	8471.85	8487.25	8492.00	8/4/4
#08	8212.99	8252.99	8448.75	8464.15	8468.00	8471.85	8487.25	8492.00	8/4/4
#09	8212.99	8252.99	8448.75	8464.15	8468.00	8471.85	8487.25	8491.10	8/4/4
#10	8212.99	8252.99	8448.75	8464.15	8468.00	8471.85	8487.25	8491.10	4/4/4
#11	8210.05	8221.60	8448.75	8464.15	8468.00	8471.85	8487.25	8568.10	4/4/4
#12	8210.05	8221.60	8448.75	8464.15	8468.00	8471.85	8487.25	8568.10	4/4/4
DOR tone frequencies (MHz)									
			DOR 1	DOR 2	DOR 3	DOR 4	DOR 5		
			8450.75	8466.15	8470.00	8473.85	8489.25		

5 Near-field VLBI Delay Models

VLBI observations of near-field targets require special delay models which take into consideration the curvature of the wavefronts. Two such models are described in Sekido and Fukushima (2006) and Duev et al. (2012). Both exist in the CALC11 module employed for computing the a priori delays in the correlation process (Sec. 6). We have also implemented both of these algorithms in the VLBI analysis software ivg::ASCOT[1]. The algorithms were also included by Klopotek et al. (this volume) in the c5++ software (Hobiger et al., 2010) to both produce a priori delay values for the DiFX correlator and to allow the data analysis of VLBI observations of near-field targets. The two models differ in concept but are consistent to about $\pm$50 ps for observations of GPS satellites, which have an altitude of $\sim$20 000 km. However, the differences between the two models are clearly systematic. A further discussion about the implementation and comparison of the two models is presented in Jaron et al. (this volume). Since the differences are rather small, it does not matter which model is used for computing the a prioris for the correlation.

For the subsequent data analysis, a model of choice does not exist yet. Solving the light-time equation explicitly for the two signal propagation paths should in principle allow the Duev et al. (2012) model to yield better results than the Sekido and Fukushima (2006) model. The reason is that the latter model employs a pseudo source vector which uses some approximation.

[1] `http://ascot.geod.uni-bonn.de`

6 Correlation

The correlation of the OCEL sessions is being carried out in Bonn where the Distributed FX Correlator (DiFX) (Deller et al., 2007a) is installed on a high performance computing cluster with 2 Gbps internet connection. Most of the data have therefore been transferred via Internet and only a few modules were shipped to Bonn. The files required for the correlation in DiFX are a .vex file, such as one produced by the programs SKED or SCHED, and a .v2d configuration file. The .vex file contains all information about the settings of the base band converters (BBCs) and their allocations, the station locations, the technical details of the radio telescopes (in particular type of mounting, e.g., equatorial, azimuth-elevation), the a priori station clock models, the planned observations (scan start and stop time for each participating station, selected target), the coordinates of the target source and the Earth orientation parameters. The .v2d file is used to specify cor-

relation options, e.g., the number of spectral channels to be used for the FFTs, the integration time, and the media types for each station.

The OCEL sessions include three different kinds of observations. In the frame of each 24-hr session, a large number of quasar observations was carried out with a frequency set-up used in routine IVS sessions, mainly to determine the clock parameters of the observatories. In between, blocks of Chang'E-3 observations were carried out having special X band setups to match the frequencies of the tones emitted by the lander (Sec.4.2). Finally, quasars which are located at close angular distance from the Moon have been observed with that same frequency setup before and after each lunar scan block in order to calibrate the lander observations. For various reasons, it is convenient to use slightly different options for correlation in the three cases which in turns means to deal with three different passes of correlation per session.

Following the scheduling process (Sec. 4.2), each station used a station-specific .vex file to run the observations which is a consequence of the apparent celestial coordinates of the target depending on the observer's position on Earth. Quite some editing work is therefore needed to prepare the .vex file for the correlation of the lunar lander scans. In particular, we had to modify the $SOURCE section, where DiFX expects to find the geocentric celestial coordinates of the target and not station based coordinates. The program Vex2difx reads the .vex and the .v2d file and produces .input and .calc file pairs for each job (scan). The .input file is used by mpifxcorr to drive the correlation proper whilst the .calc file manages the geometric model calculation. In the standard DiFX pipeline it is then enough to run the program startdifx to produce the visibilities (amplitude and phase) for each accumulation period.

The apriori model delays, which are used to align the data streams before correlation, are produced by using the Goddard CALC package. The version of CALC (CALC09) included in the DiFX installation as of June 2016 did not include a near-field model. Only at the beginning of 2016, a newer version of CALC (CALC11) has been released, which includes a near-field option. When working with the lunar lander scans we therefore abandoned the standard processing pipeline and used the program difxcalc, which calls CALC11 for computing the correlator model. Another difference w.r.t. the standard processing data flow is that after running vex2difx, we must also edit the .calc files. In the standard case the target is a fixed object in the sky, i.e., its coordinates are the same for each station, whereas for a near-field object we need to feed DiFX the position of the target as a function of time. We wrote a standalone C++ based package which uses the JPL SPICE libraries to compute the ephemeris of the lunar lander for each scan. Finally, by running the program difxcalc on all .calc files we produced the .im file for each scan and startdifx to run the correlation.

7 Fringe Fitting

The fringe fitting process follows correlation and is applied to determine group delays, phase delays and (phase) delay rates from the arrays of visibilities. The standard fringe fitting program used in connection with geodetic correlators is the Haystack Observatory Processing Software (HOPS) component *fourfit*[2]. Another option is program PIMA (Petrov et al., 2011).

7.1 Fourfit-DOR

The program *fourfit* is being used at the Bonn Correlator Center for processing geodetic correlation output of observations of natural extra-galactic radio sources such as quasars (Bertarini, 2013; Cappallo, 2016). When observing quasars for geodetic applications, normally flat-spectrum candidates in the radio frequency domain (mostly at S and X band) are chosen and finite bandwidth channels are digitized and recorded. Based on the theory of Fourier transform, a rectangular function in one domain corresponds to a SINC function in the other. Its main lobe width is inversely proportional to the rectangular width. So, for a rectangular bandpass the peak in the delay domain is as sharp as the spanned bandwidth permits (Fig. 9).

In contrast to this, the Chang'E-3 DOR tones produce rather narrow peaks in the frequency spectrum and, thus, the signals in the delay domain are different from quasar continuum spectra (Fig. 10).

Apparently, *fourfit* does not seem to be capable of DOR tone processing for some hard-coded limitations related to the flat spectrum of the assumed natural radio

[2] http://www.haystack.mit.edu/tech/vlbi/hops.html

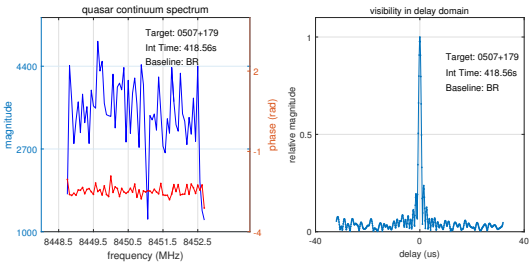

Fig. 9 Quasar continuum cross-power spectrum and delay resolution.

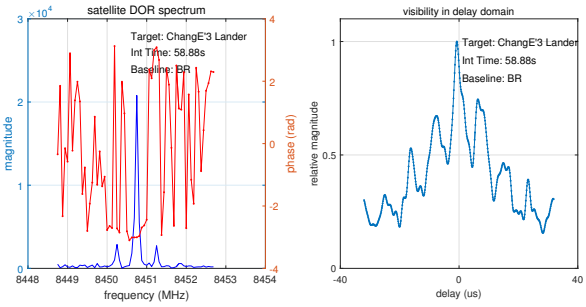

Fig. 10 Cross-power spectrum of DOR tones and delay resolution.

sources. In contrast to this, the bandpass of a standard observing channel contains the man-made DOR tone, normally appearing as a sharp peak, plus some more or less pronounced noise contribution (see, e.g., Fig. 14, middle panel). The latter one needs to be filtered out for the group delay determination to provide the correct result. For this reason, we extended the fringe fitting algorithm of *fourfit* to allow for processing of DiFX correlation output of DOR tones. The extended program is called *fourfit-DOR* below.

The idea behind *fourfit-DOR* is that the correlator output is pre-processed in the frequency domain first to identify the frequency of the DOR tone in the cross-power spectrum. Normally, this is identical to the nominal transmission frequency but may have been corrupted easily by noise contributions. The time series of amplitudes and phases per accumulation period for each channel are then used for a 2-dimensional search of the residual multi-band delay and residual delay rate. More details about the background of *fourfit-DOR* can be found in Han et al. (in prep.).

Here, the new algorithm is validated with data of the OCEL project. After correlation with the DiFX correlator, the visibilities are used to first compute the observables with *fourfit* (Version 3.12, Opensuse Leap

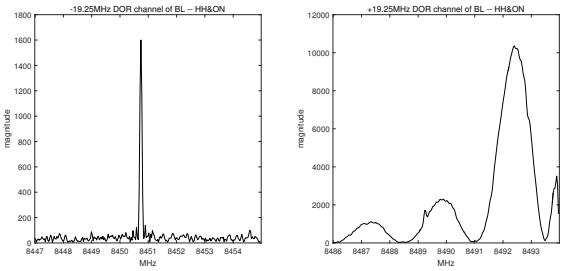

Fig. 11 Original cross-power spectrum of DOR tone channel #1 and #5. In the right panel the DOR tone is masked almost completely by RFI just sticking out of the second rise as a small peak.

42.1 Operation System) and then with *fourfit-DOR*, in which the new algorithm is implemented.

Test 1

In OCEL sessions -01/-02/-03/-04, the scheduled observing channel frequency spacing is different from that of the DOR tone frequencies. In the first test, we study the effect of the inconsistent frequency spacing. For example, in OCEL-01 the observed channel bandwidth is 8 MHz with the frequencies of the two outer channels being 8446.99 MHz and 8485.99 MHz. They cover the two outer DOR tone frequencies 8450.75 MHz and 8489.25 MHz, respectively (Tab. 2). When the *fourfit* algorithm searches for the multiband delay, it assumes a flat cross-power spectrum and refers the phase of each channel to its reference frequencies (8446.99 MHz and 8485.99 MHz). However, in the case of DOR tones, the respective reference frequency has to be that of the tones at 8450.75 MHz and 8489.25 MHz. So, two things are incorrect at the same time, the phase and frequency relation ($\phi(\omega)$) and the spanned bandwidth which is taken as 39.0 MHz while correctly it is only 38.5 MHz, thus affecting the $\tau = d\phi/d\omega$ relationship.

A complication for the test is that for the whole session OCEL-01, signals were also transmitted on the data communication channel. Since this signal was very strong, its sidelobes have interfered with the DOR channels, especially at the +19.25 MHz channel (see Fig. 11).

For excluding the influence of RFI and studying only the effect of incorrect spanned bandwidth, the interference signal in channel #5 (+19.25 MHz) has to be mitigated before the data are entered into *fourfit*. This is done by identifying the frequency lag, where the DOR

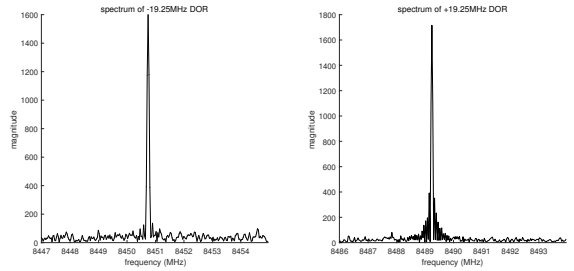

Fig. 12 Cross-power spectrum of DOR tones channel #1 and #5 after elimination of interference in channel #5.

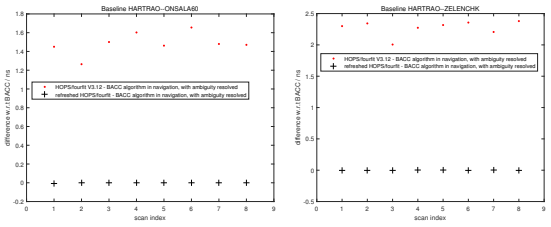

Fig. 13 Comparison of the two algorithms using BACC group delay determinations as reference. Scans are displayed in a regular sequence.

peak sticks out, and replacing all the other visibilities with white noise with similar power than that of the −19.25 MHz DOR tone channel (Fig. 12). All the data were kept strictly in Mark IV type 1 binary data format to be used as input of both, *fourfit* and *fourfit-DOR*.

As a result, systematic differences of a few nanoseconds between the two fringe fitting programs can be identified in Fig. 13 where the group delay determinations of BACC serve as reference (Kikuchi et al., 2004; Tang, 2012).

It should be mentioned here that the BACC delay determinations work with the phases of the correlated DOR tones directly, first using the phases of the two nearest channels (-3.85, +3.85 MHz) to produce a first group delay approximation. Extending the $d\phi/d\omega$-slope to the phases of the -19.25 and +19.25 MHz tones identifies the most probable, ambiguity-free phase values for these frequencies. The final residual group delay for a single accumulation period (AP) of normally 1 s duration is then computed just from the two channels furthest apart according to $\tau = d\phi/d\omega$. For all APs, the arithmetic mean represents the residual group delay of a single scan. This procedure is commonly used in spacecraft navigation. Therefore, they are a good reference for our studies.

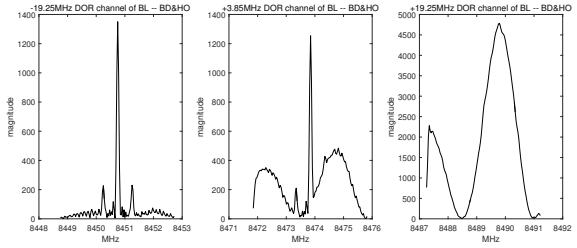

Fig. 14 Cross-power spectrum of DOR tones channel #1, #4, and #5 of OCEL-09.

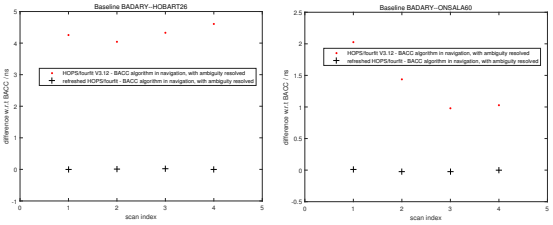

Fig. 15 Comparison of different algorithms.

The *fourfit-DOR* results agree at the level of about 10 ps with the group delay determinations realized at BACC while the *fourfit* results are off by a few nanoseconds. This is attributed to the incorrect frequency spacings in the first four OCEL sessions.

Test 2

The second test concerns the influence of moderate interference where the signal itself has a level which is a factor of two or more of the interference signal. In OCEL-09 as an example, the frequency setup follows exactly the spacing of the DOR tones with a 4 MHz channel bandwidth and the center frequencies matching the nominal DOR tone (Tab. 2). However, in some scans (e.g., on 2016-01-21 from 15:00 to 15:30 UT), the DOR tone signal is interfered by other signals (most probably by the data communication signal) as shown in Fig. 14. The DOR tones in the +19.25 MHz DOR channel could not be identified because of this interference, so we chose the +3.85 MHz DOR channel (frequency 8471.85 MHz) instead. Although the spanned bandwidth is now reduced to 23.1 MHz and channel #4 shows some level of interference, the resulting group delays determined with the two algorithms can still be compared (Fig. 15). The differences are at the level of several nanoseconds. Again, the reference is the BACC realization mentioned above.

As in the test before, the *fourfit-DOR* results are close to the BACC results while the *fourfit* results are offset by a few nanoseconds. It is not the differences w.r.t. the BACC results but the differences between the two *fourfit* results which demonstrate the effect of the interference.

The signal interference mainly comes from the strong data communication signal which is transmitted by another antenna on the lander. It is not coherent with the carrier and the DOR tones. This interference exists quite common in OCEL-01/-02/-03/-04 and for parts of the scans of OCEL-05 to -12. In some cases the +19.25 MHz DOR tones are totally submerged and could not be identified any more. In this case only the +3.85 MHz DOR tone is used instead to achieve maximum channel separation.

Test 3

Here, we just focus on the random errors of the two algorithms in cases where interference does not exist and the frequency setting is the one as used from OCEL-09 onwards. In principle, the *fourfit* algorithm does a three dimensional fit over all delays and accumulation periods (AP) by transforming the visibilities from the frequency domain into the delay domain through Fourier transformation. This ignores some of the information content and inevitably induces more noise which then distributes over the whole frequency band within the channel.

Taking again baseline NYALES20–ONSALA60 in OCEL-09 as an example, Fig.16 and Fig. 17 show the differences of the residual delay (and residual delay rate) w.r.t. reference values from the BACC algorithms used in navigation. The RMS (root mean square) errors of the residual delays are 0.198 ns and 0.009 ns, and the RMS of residual delay rates are 0.0559 ps/s and 0.0258 ps/s for the *fourfit* and *fourfit-DOR* fringe fitting, respectively.

Assuming that the BACC DOR processing (Kikuchi et al., 2004; Tang, 2012) provides a ground truth, the results presented here demonstrate that *fourfit-DOR* can better deal with (a) low SNR, (b) RFI issues, and (c) observing channel allocations which do not agree exactly with the DOR tone separations.

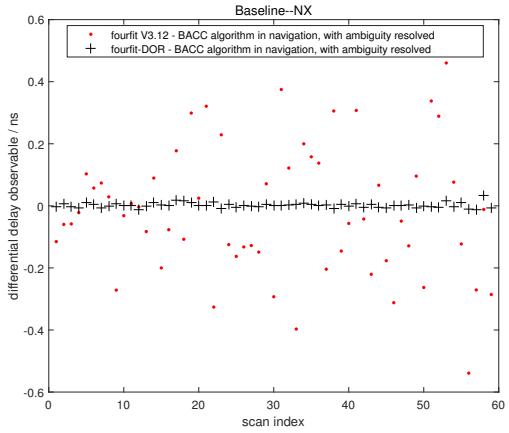

Fig. 16 Residual delay comparison.

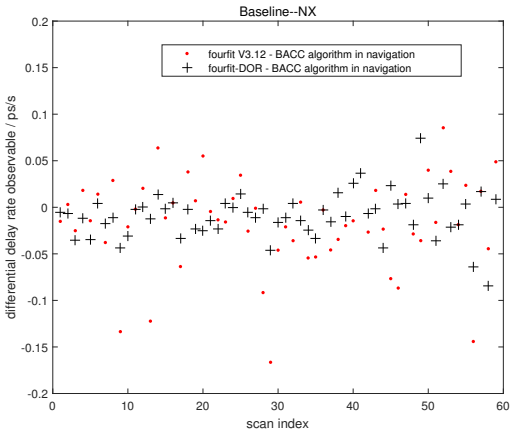

Fig. 17 Residual delay rate comparison.

7.2 PIMA

PIMA is a software for processing the correlator output visibilities data from VLBI experiments, which performs data inspection, data calibration and fringe fitting (Petrov et al., 2011). Similar to the Haystack HOPS software or the NRAO AIPS and CASA software packages, PIMA is designed for batch processing of VLBI experiments for astronomy and geodesy applications. As a tool for fringe fitting, we used PIMA to process the OCEL sessions for testing.

7.2.1 General Algorithm

The concept of PIMA aims at wide-band baseline-based fringe fitting across all the bands of a bandwidth synthesis setup (Petrov et al., 2011). According to the PIMA source code and a related guide, the program reads the correlator output data in FITS-IDI format. This contains the complex spectra of the auto-correlation function and the spectrum of the cross-correlation function for each accumulation period (AP). After a spectrum re-normalization, PIMA first does a coarse fringe search. For this, a Fast 2D Fourier transform (FFT) is performed using time and frequency as dimensions. This produces coarse estimates of the group delay and delay rate whose accuracy depends on the grid resolution. To refine the estimates, a 3D Fourier transform is performed cycling through group delay rate, group delay, and phase delay rate to compute a 3D delay resolution function. This is then searched for its maximum amplitude to determine an intermediate group delay rate, group delay, and phase delay rate.

Since normally imperfections of the baseband filters exist at any of the stations, the spectrum of a channel may be distorted by phase and amplitude variations. This then also applies to the cross-power spectrum of the correlation process. Consequently, a non-rectangular shape of the amplitude response will cause the group delay to vary with time (Petrov et al., 2011). In the case where bandpass calibration from a reference source is available, a complex bandpass calibration may be performed in PIMA after the coarse search. With one station selected as the reference station, the complex bandpass function for each of the other stations can be computed and applied to correct for instrumental frequency-dependent delays and fading of the amplitude with increasing frequency.

After bandpass calibration, a fringe search is performed again to obtain the final residual phase delay, group delay and their time derivatives for a baseline at a given time with respect to the a priori delay model. The a priori delay model is usually the same as that used for the correlation. However, when the a priori delay model used for correlation is not continuous, PIMA can generate its own a priori delay model based on the one used for correlation. Then according to the scan reference time (SRT), which is normally within 1 second of the middle of the observation duration, the total path delay is computed by adding the residual delay to the a priori delay. PIMA also allows to specify independent fringe reference times (FRT).

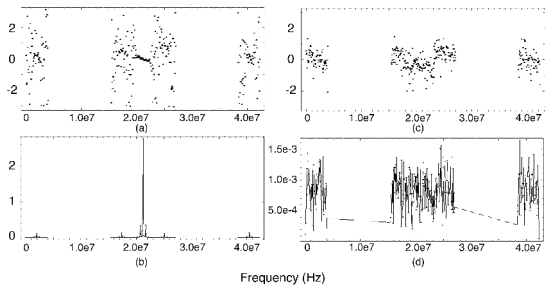

Fig. 18 (a) X-band fringe phases vs. **frequency** of 5 DOR tone channels of baseline BADARY–ONSALA60, (b) respective fringe amplitudes, (c) fringe phases vs. **frequency** of 5 DOR tone channels for source 0507+179, (d) respective fringe amplitude.

7.2.2 Preliminary Results

PIMA (version 2.22, 29.02.2016) was applied to do the fringe fitting of the OCEL-09 session. To process the OCEL observations, we changed the mode from baseline-based to geocenter-based fringe fitting to keep it comparable to the *fourfit* results. In a first test, we used all channels (8448.75 MHz, 8464.15 MHz, 8468.00 MHz, 8471.85 MHz and 8487.25 MHz) for both, the Chang'E-3 lunar lander and the delay referencing source 0507+179, on baseline BADARY–ONSALA60 (Fig. 18). It should be mentioned that 64 spectral lags had been computed in the Fourier transform of the correlation process with DiFX for this example. The amplitudes and phases of the cross-power spectrum are reasonably balanced for the quasar fringe fit, though not optimal. In contrast to that the lander's DOR frequencies appear as sharp peaks in the amplitude spectrum with the phases showing a rather arbitrary scatter. Only the carrier frequency band which has a much higher signal strength has a well defined sequence of phases. Looking at the 3D fringe plot of PIMA for this setup (Fig. 19), we see that it displays a smooth wave form of a series of maxima. This suggests that the final group delay determination becomes rather uncertain. In a series of test combinations, we discovered that the tone on the carrier frequency is responsible for this behavior. Most probably it is the increased intensity of this channel

which causes the delay resolution function to become so awkward.

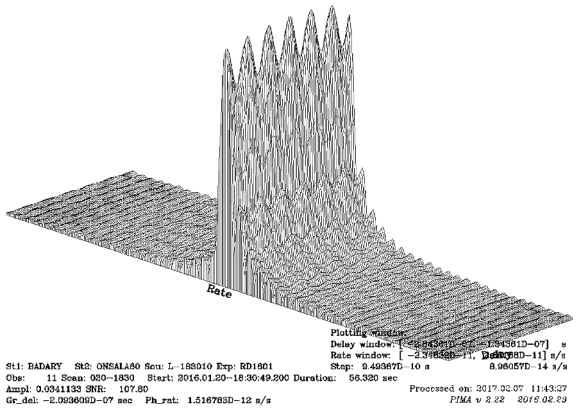

Fig. 19 PIMA 3D fringe plot of all five DOR tone channels for the Chang'E-3 lunar lander on the BADARY–ONSALA60 baseline.

For this reason, we had a look at channel combinations which might be more suitable for a reliable group delay determination. The starting point is to choose just the outer two channels #1 and #2 spanning a total of 39.0 MHz. Here, the basic figure of phases versus frequencies (Fig. 20) looks the same as for all five channels, just taking out the three central bands. At the same time, we can also look at the phases versus time (Fig. 21). The phase and amplitude behavior calculated from a 3-dimensional delay resolution function with frequency, channel and time as dimensions in which the phase rotation and counter rotation are applied looks much more stable for the lunar lander (left column) than for the quasar (right column). It should be pointed out that the scan length of about 240 s is rather long and the radio source thus seems to be rather weak (SNR 12.1). The delay resolution function (Fig. 22) shows pronounced peaks about every 12.7 ns. This appears to be about half of the theoretical ambiguity spacing of 1/38.5 MHz = 25.974 ns. Looking at Fig. 23 for some more insights, we see sidelobes here also at about half of the natural ambiguity spacing. So, we assume that every second peak is a sidelobe rather than a full ambiguity peak. The reason for theses sidelobes are still unknown so far because the theoretical delay resolution function from a pure Fourier transformation of two or three frequency bands does not show these extreme sidelobes.

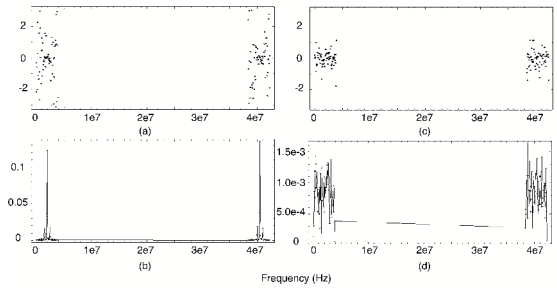

Fig. 20 (a) X-band fringe phases vs. **frequency** of DOR tone channels #1, and #5 of baseline BADARY–ONSALA60, (b) respective fringe amplitudes, (c) fringe phases vs. **frequency** of DOR tone channels #1, and #5 for source 0507+179, (d) respective fringe amplitude.

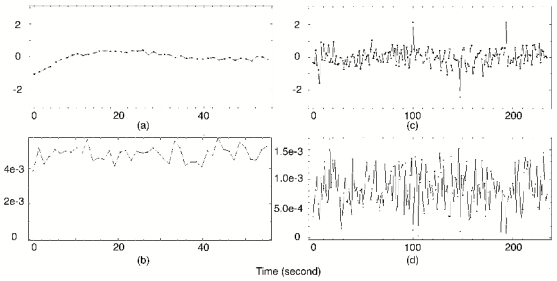

Fig. 21 (a) X-band fringe phases vs. **time** of DOR tone channels #1, and #5 of baseline BADARY–ONSALA60, (b) respective fringe amplitudes. (c) fringe phases vs. **time** of DOR tone channels #1, and #5 for source 0507+179, (d) respective fringe amplitude.

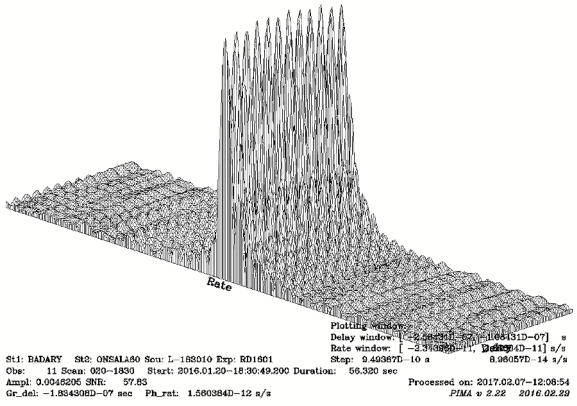

Fig. 22 PIMA 3D fringe plot of DOR tone channels #1, and #5 for Chang'E-3 lunar lander on the BADARY–ONSALA60 baseline.

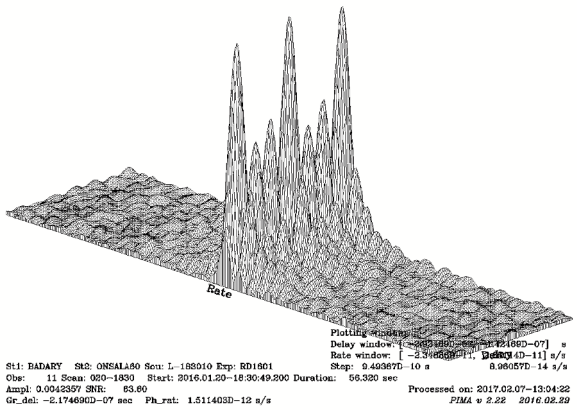

Fig. 23 PIMA 3D fringe plot of DOR tones channel #1, #2, and #4 for the Chang'E-3 lunar lander on the BADARY–ONSALA60 baseline.

The final choice of selected frequency channels for the group delay determination with PIMA is actually #1, #2, and #4. Here, the delay resolution function looks rather promising in shape with a single pronounced maximum (Fig. 22). The last channel (#5) is de-selected because it was shown in Sec. 7.1 that this channel is often compromised by RFI. Unfortunately, there are still two rather large side lobes which may produce sub-ambiguities in the group delay determination. However, we hope to be able to cope with them in the lunar parameter estimation process because the natural ambiguity spacing is 129.870 ns.

Before we look at the estimated group delays, we should also contemplate our expectations. The frequency setup of the channels for the DOR tones #1, #2 and #4 produces an RMS bandwidth ν_{rms} of 9.6 MHz. Entering this into the approximation of the standard deviation of the group delay σ_τ

$$\sigma_\tau = \frac{1}{2\pi \cdot SNR \cdot \nu_{rms}}, \tag{1}$$

with a signal to noise ratio (SNR) of 50 results in a standard deviation of approximately 330 ps. To be on the safe side, 0.5 ns appears to be a good first estimate of the delay determinations.

From the different PIMA fringe fitting processes, we deduce a few example delays (Tab. 3). These do not show a clear picture. For the HARTRAO–ONSALA60 scan, the group delays with and without channel #3 (Columns 4 and 5) may differ by one ambiguity spacing. Omitting also channel #5 (Column 3) produces a delay which is 3.6 ns off the first two determinations. However, considering the RFI effect of channel #5 may well explain this small discrepancy. Although a bit larger, we see a similar discrepancy on the BADARY-ONSALA60 baseline. In both cases, columns 2 and 3 differ by some arbitrary number which can only be attributed to some linear combination of ambiguities with a lot of imagination.

8 Delay Referencing

During the scheduling process specific care was taken that a good number of extra-galactic objects could be observed which are close to the direction to the Moon. With these radio sources a special delay referencing will be applied in the final analysis steps. The idea of delay referencing is to compute delay calibration values for the lunar observations from neighboring radio source observations. The total lunar observation will be composed of the initial lunar observation $\tau^{\mathrm{L}}_{\mathrm{Obs}}$ and a lunar delay correction $\Delta\tau^{\mathrm{L}}$

$$\tau^{\mathrm{L}}_{\mathrm{Obs,Corr}} = \tau^{\mathrm{L}}_{\mathrm{Obs}} - \Delta\tau^{\mathrm{L}}, \tag{2}$$

with

$$\Delta\tau^{\mathrm{L}} = \Delta\tau_{\mathrm{Clock}} + \Delta\tau_{\mathrm{Atm,w}} + \Delta\tau_{\mathrm{Atm,h}} + \Delta\tau_{\mathrm{Ion}}. \tag{3}$$

The first term, the clock contribution consists of the difference of the two clock values to be computed from the estimates according to Eq. (5) applying the respective observing epoch of the lunar observation t for telescopes a and b

$$\Delta\tau_{\mathrm{Cl}}(t) = \tau_{\mathrm{Cl_b}}(t) - \tau_{\mathrm{Cl_a}}(t), \tag{4}$$

with

$$\Delta\tau_{\mathrm{Cl}_*}(t) = T_{0_*} + T_{1_*}(t-t_0) + T_{2_*}(t-t_0)^2. \tag{5}$$

In principle, the same applies to the atmospheric corrections, where the zenith wet component $\tau_{\mathrm{Atm,W}}$ could be taken from the estimates. Since normally time derivatives in the form of piece-wise linear polygons are estimated as well, the lunar corrections for the zenith wet component for each station can be computed from

Table 3 Residual group delay and SNR results with different IF combinations of Chang'E-3 lander for HARTRAO–ONSALA60 and BADARY–ONSALA60 baselines.

IFs	#1,#5	#1,#2,#4	#1,#2,#4,#5	#1,#2,#3,#4,#5
HARTRAO–ONSALA60				
Residual group delay (ns)	-20.026	34.507	30.977	-99.258
SNR	46.4	46.0	55.7	115.7
BADARY–ONSALA60				
Residual group delay (ns)	-183.431	-217.469	-209.723	-209.361
SNR	57.8	63.6	76.4	107.8

$$\Delta\tau^{z}_{\mathrm{Atm,w}}(t) = \frac{\Delta\tau^{z}_{\mathrm{Atm,w}}(t_{n+1}) - \Delta\tau^{z}_{\mathrm{Atm,w}}(t_n)}{t_{n+1}-t_n}\cdot(t-t_{n+1}) + \Delta\tau^{z}_{\mathrm{Atm,w}}(t_{n+1}), \quad (6)$$

where t_n is the epoch of the polygon before and t_{n+1} the epoch of the polygon after the lunar observation. The final correction for the wet component then reads

$$\Delta\tau_{\mathrm{Atm,w}} = \Delta\tau^{z}_{\mathrm{Atm,w}}\cdot m_w(\varepsilon), \quad (7)$$

with $m(\varepsilon)$ being the mapping function computed for the elevation of the lunar observation. The hydrostatic correction $\Delta\tau_{\mathrm{Atm,h}}$ is computed as usual from the hydrostatic correction in zenith direction $\Delta\tau^{z}_{\mathrm{Atm,h}}$ according to the modified Saastamoinen formula (Davis et al., 1985) and the hydrostatic mapping function $m_h(\varepsilon)$.

The ionospheric correction is a bit more tricky because the observations of the extra-galactic radio sources only provide baseline-related and not station-related ionosphere corrections. Furthermore, the elevation angles at both stations differ for the quasar and the lunar observations. To cope with these intricacies we devised the following scheme. First, the ionosphere and its total electron content at both stations is extracted from total electron content (TEC) maps[3] for the epochs of the quasar observation directly before and the one directly after the lunar scan. From that theoretical ionosphere corrections are computed for the pairs of quasar directions. Quite naturally the theoretical ionosphere corrections deviate from the ones computed from the S and X band group delays because the latter corrections are based on observed values which might be biased by instrumental effects. Consequently, each baseline has a unique bias between modeled and observed ionosphere corrections of approximately 50 to 250 ps. Setting the station-based bias of one of the stations to zero, relative station-related biases can be computed from the baseline-related biases with a simple adjustment program.

The station based biases can then be applied as corrections for the model values from the TEC maps. If the reference station is selected very carefully, these corrections are consistent with the observed ionosphere corrections of the observations of the "delay referencing sources" because they also contain the effects of the systematic differences between the S and X band observations due to instrumental effects.

[3] available, e.g., at `https://cddis.nasa.gov/Data_and_Derived_Products/GNSS/atmospheric_products.html#iono`

9 First results

Considering that not all correlation, fringe fitting, and calibration options have been tested yet, we are nevertheless able to produce the first interim results already. These are the observed minus computed delays (O-C) produced in the analysis software ivg::ASCOT. No parameter estimation module for near-field targets is available yet in ivg::ASCOT.

Out of the many baselines observed, the O-C values of two example baselines of the OCEL-09 session, which was carried out on January 20–21, 2016, are depicted in Fig. 24 as representative results. In both cases we show that results using the Duev et al. (2012) model and the Sekido and Fukushima 2006 model look identical. For both baselines a constant offset in the microsecond regime for all observations has been subtracted from the data as indicated in the figure caption to center them around zero, a measure which can also be considered as subtraction of a constant clock offset.

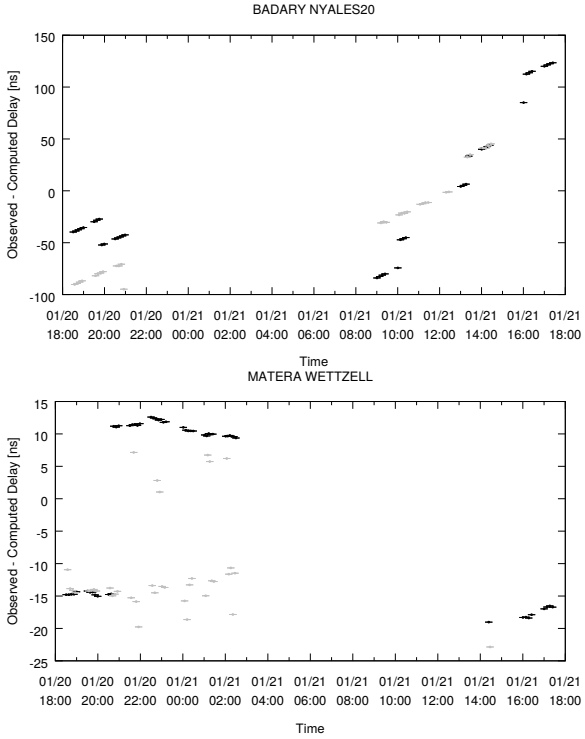

Fig. 24 Two example baselines, as indicated in the plot titles, for the Chang'E-3 observations (OCEL-09 session, carried out on January 20–21, 2016). Data points for the lunar lander are plotted in black, for the quasars in gray. Top: Both lunar and quasar observables follow the same trend, but the lunar ones are offset from the quasar ones and are subject to jumps. For this baseline a constant offset of -161 μs has been subtracted from the data. Bottom: In this example the overall variance is much less than in the data shown in the top panel. However, here it is worth of note that while the lunar data follow a systematic trend the quasar data are also subject to random variations. For this baseline a constant offset of -32 μs has been subtracted from the data.

On the baseline Badary–Ny-Ålesund (top panel of Fig. 24) both lunar and quasar observables mostly follow the same trend. However, there is a distinct offset between the two in the order of $\sim$10 ns. In addition, the lunar lander data are subject to occasional jumps, not present in the quasar data here.

In the bottom panel of Fig. 24 the data for the baseline Matera–Wettzell are shown. The overall variance is much less here than in the data presented above (hundreds of ns in the top panel compared to tens of ns in the bottom panel). However, in this example it is striking that the lunar lander data are dominated by a systematic trend while the quasar data are also subject to random variations.

10 Conclusions

We developed a chain of processes to include observations of an artificial radio source on the Moon, the Chang'E-3 lunar lander, into geodetic VLBI sessions to benefit from relative observations of nearby quasars and from directly observed auxiliary information such as observed UT1–UTC and nutation offsets of date. The scheduling strategy alternates between 30 minutes long slots of standard geodetic observations and 30 minutes long lunar lander observations. During the latter the lunar lander DOR-signal is observed, alternating with close-by radio sources in order to allow for phase- and/or delay-referencing.

In total twelve so-called OCEL sessions were scheduled and observed during 2014 to 2016, involving networks with between 7 and 12 worldwide IVS stations. However, constraints due to station availability sometimes made it impossible to observe the lunar lander for several hours due to the Pacific gap in the IVS network.

The choice of a suitable frequency setup that allows both observations of the DOR tones of the lunar lander and normal natural radio sources turned out to be rather difficult. Various approaches were tested during the different OCEL sessions. Based on the experience gained, a suitable frequency setup was finally developed and used in the two most recent OCEL sessions.

The correlation of the lunar lander observations was done with DiFX, the standard software correlator used for geodetic VLBI. The necessary a priori delays were calculated with state-of-the-art near-field delay models. While the correlation is rather straightforward with the standard version of DiFX, the special signal structure of the Chang'E-3 lunar lander required to modify the standard fringe fitting software *fourfit* in order to handle the DOR tones properly. Besides fringe-fitting with *fourfir-DOR* also tests with the fringe-fitting software *PIMA* were performed.

Two near-field models were introduced into two independent VLBI data analysis software packages. The two near-field models show some level of disagreement, which is however not of importance for the data correlation but will be of interest for the future data

analysis. Since so far no OCEL session is completely correlated and fringe-fitted, VLBI databases for further analysis are not yet available. However, the data analysis software packaged ivg::ASCOT and c5++ have been extended and prepared for data analysis, for c5++ also including parameter estimation Klopotek et al. (in prep.).

The work will continue with a thorough comparison and evaluation of the different approaches for fringe-fitting and to determine group delay observables. After that the VLBI observables for all twelve OCEL-sessions will be produced and analyzed. Meanwhile, we aim for further OCEL sessions to make use of this target-of-opportunity, the Chang'E-3 lunar lander, as long as it is working.

Acknowledgements

We want to thank the personnel of the radio telescopes at Badary, Fortaleza, Hartebeesthoek, Hobart, Kokee Park, Kunming, Matera, Medicina, Ny-Ålesund, Onsala, Seshan, Urumqi, Wettzell, and Zelenchukskaya for participating in the OCEL sessions. We appreciate their positive attitude towards this research and development effort, and their willingness to observe these rather non-standard VLBI sessions. The flexibility to incorporate last-minutes changes in the .vex files is greatly acknowledged.

References

Bates JR, Lauderdale WW, Kernaghan H (1979) ALSEP Termination Report. NASA Reference Publication 1063

Bertarini A (2013) DiFX Correlation and Post-Correlation Analysis, IVS VLBI School. http://www.evga.org/teaching/VLBI_school_2013/VLBI-school-2013_08_Bertarini.pdf

Barache C, Bouquillon S, Carlucci T, Francou G (2015) Lunar Laser Ranging Observations from 1969 to 30 December 2015. http://pola.obspm.fr/llrdatae.html

Barbosa RC (2013) China's Chang'e-3 and Jade Rabbit duo land on the Moon. December 2013. https://www.nasaspaceflight.com/2013/12/china-jade-rabbit-lunar-arrival/

Border JS (2009) Innovations in Delta Differential One-way Range: from Viking to Mars Science Laboratory. In: *Proc. 21st Int. Sym. Space Flight Dynamics*, Toulouse, France, 28 Sept.–02 Oct., http://issfd.or/ISSFD_2009/OrbitDeterminationI/Border.pdf

Bouquillon S, Francou G, Manche H, Torre JM, Féraudy D, Le Poncin-Lafitte C, Lhotka C (2013) Lunar Laser Ranging: Recent Activities of the Paris Observatory Lunar Analysis Center. http://cddis.gsfc.nasa.gov/lw18/docs/papers/Session9/13-04-03-Bouquillon.pdf

Cao J, Zhang Y, Hu S, Huang Y, Chen M (2016) An Analysis of Precise Positioning and Accuracy of the CE-3 Lunar Lander Soft Landing. Geomatics and Information Science of Wuhan University, 2016, doi:10.13203/j.whugis2014123 (In Chinese)

Cappallo R (2016) Post-correlation analysis and fringe-fitting. 2nd IVS VLBI School, http://www.evga.org/teaching/IVS_school_2016/L08.pdf

Counselman III CC, Hinteregger HF, King RW, Shapiro II (1973) Lunar baselines and libration from differential VLBI observation and ALSEPs. *The Moon*, 8:484–489

Davis JL, Herring TA, Shapiro II, Rogers AEE, Elgered G (1985): Geodesy by radio interferometry: Effects of atmospheric modeling errors on estimates of baseline length, Radio Sci, 20(6), pp. 1593–1607

Deller AT, Tingay SJ, Bailes M, West C (2007a) DiFX: A Software Correlator for Very Long Baseline Interferometry Using Multiprocessor Computing Environments. *Publications of the Astronomical Society of the Pacific*, 119:318–336

Deller AT, Brisken WF, Philips CJ, Morgan J, Alef W, Cappallo R, Middelberg E, Romney J, Rottmann H, Tingay SH, Wayth R (2007b) DiFX-2: a more flexible, efficient, robust, and powerful software correlator. *Publications of the Astronomical Society of the Pacific*, doi:10.1086/658907

Duev DA, Molera Calvés G, Pogrebenko SV, Gurvits LI, Cimó G, Bocanegra Bahamon T (2012) Spacecraft VLBI and Doppler tracking: algorithms and implementation. *Astronomy & Astrophysics*, 541, A43, doi:10.1051/0004-6361/201218885

Duev DA, Pogrebenko SV, Cimó G, Molera Calvés G, Bocanegra Bahamon TM, Gurvits LI, Kettenis MM, Kania J,

Tudose V, Rosenblatt P, Marty J-C, Lainey V, de Vicente P, Quick J, Nickola M, Neidhardt A, Kronschnabl G, Plötz C, Haas R, Lindqvist M, Orlati A, Ipatov AV, Kharinov MA, Mikhailov AG, Lovell JEJ, McCallum JN, Stevens J, Gulyaev SA, Natush T, Weston S, Wang WH, Xia B, Yang WJ, Hao L-F, Kallunki J, Witasse O (2016) Planetary Radio Interferometry and Doppler Experiment (PRIDE) technique: A test case of the Mars Express Phobos fly-by. *Astronomy & Astrophysics*, 593, A34, doi:10.1051/0004-6361/201628869

Fey A, Gordon D, Jacobs C, Ma C, Gaume R, Arias F, Bianco G, Boboltz D, Boeckmann S, Bolotin S, Charlot P, Collioud A, Engelhardt G, Gipson J, Gontier AM, Heinkelmann R, Kurdubov S, Lambert S, Lytvyn S, MacMillan DS, Malkin Z, Nothnagel A, Ojha R, Skurikhina E, Sokolova J, Souchay J, Sovers OJ, Tesmer V, Titov O, Wang G, Zharov V (2015) The Second Realization of the International Celestial Reference Frame by Very Long Baseline Interferometry. *The Astronomical Journal*, 150:58 (16 pp), doi:10.1088/0004-6256/150/2/58

Folkner WM, Williams JG, Boggs DH (2008) The planetary and lunar ephemerides DE421. *JPL IOM 343R-08-003*

Folkner WM, Williams JG, Boggs DH, Park RS, Kuchynka P (2014) The planetary and lunar ephemerides DE430 and DE431. *Interplanet. Netw. Prog. Rep*

Kikuchi F, Kono Y, Yoshikawa M, Sekido M, Ohnishi M, Murata Y, Ping JS, Liu QH, Matsumoto K, Asari K, Tsuruta S, Hanada H, Kawano N (2004) VLBI observation of narrow bandwidth signals from the spacecraft. *Earth, Planets and Space*, 56, 11: 1041–1047, doi:10.1186/BF03352546

Han, ST, Tang GS, Cao JF, Chen L, Ren TP (2015) Monitoring CE3 Rover Movement Using Same-Beam Interferometry with Chinas Deep Space Network. In: *Proc. Second International Conference on Mechatronics and Automatic Control*, Lecture Notes in Electrical Engineering, Vol. 334, Springer International Publishing, Berlin, 651-659

Han ST, Nothnagel A, Zhang ZK, Tang G: Fringe Fitting and Group Delay Determination for Geodetic VLBI Observations of DOR Tones, in prep.

Hobiger T, Otsubo T, Sekido M, Gotoh T, Kubooka T, Takiguchi H (2010) Fully automated VLBI analysis with c5++ for ultra rapid determination of UT1. *Earth, Planets and Space*, 62, 12: 933–937, doi:10.5047/eps.2010.11.008

Jaron F, Nothnagel A, Iddink A, Halsig S, Planck L, Near-field VLBI delay models, this volume

JPL's HORIZONS system (2016) `http://ssd.jpl.nasa.gov/horizons.cgi`

King RW(1979) Precision Selenodesy via Differential Very-Long Baseline Interferometry. Ph.D. Thesis, Massachusetts Institute of Technology, Cambrige, Mass.

King RW, Counselman III CC, Shapiro II (1976) Lunar dynamics and selenodesy: Results from analysis of VLBI and laser data. *Journal of Geophysical Research*, doi:10.1029/JB081i035p06251

Klopotek G, Hobiger T, Haas R (2017) Implementation of VLBI near-field delay models in the c5++ analysis software, this volume

Klopotek G, Hobiger T, Haas R (2017), Geodetic VLBI with an artificial radio source on the Moon – a simulation study, in preparation

Müller J, Hofmann F, Fang X, Biskupek L (2013): Lunar Laser Ranging: recent results based on refined modelling., In: Earth on the Edge: Science for a Sustainable Planet (eds. C. Rizos, P. Willis). IAG Symposia Series, Vol. 139, Springer, Berlin

Munghemezulu C, Combrinck L, Botai JO (2016) A review of the lunar laser ranging technique and contribution of timing systems. *South African Journal of Science*

Nothnagel A, Artz T, Behrend D, Malkin Z (2016) International VLBI Service for Geodesy and Astrometry – Delivering high-quality products and embarking on observations of the next generation. *Journal of Geodesy*, doi:10.1007/s00190-016-0950-5

IERS Conventions (2010). Gérard Petit and Brian Luzum (eds.). (IERS Technical Note 36), Frankfurt am Main: Verlag des Bundesamts für Kartographie und Geodäsie, 2010, 179 pp., ISBN 3-89888-989-6

Petrov L, Kovalev YY, Fomalont EB, Gordon D (2011) The Very Long Baseline Array Galactic Plane SurveyVGaPS. *The Astronomical Journal*, doi:10.1088/0004-6256/142/2/35

Radio Fundamental Catalog. `http://astrogeo.org/rfc/`

Rogers AEE, Moffet AT, Backer DC, Moran JM (1984) Coherence limits in VLBI observations at 3-millimeter wavelength. *Radio Science*, 19, 1552

Sekido M, Fukushima T (2006) A vlbi delay model for radio sources at a finite distance. *Journal of Geodesy*, 80, 137–149, doi:10.1007/s00190-006-0035-y

GSFC VLBI SKED Software Package, `http://lupus.gsfc.nasa.gov/software_sked.htm`

Slade MA, Preston RA, Harris AW, Skjerve LJ, Spitzmesser DJ (1977) ALSEP-quasar differential VLBI. *The Moon*

Sovers OJ, Fanselow JL, Jacobs CS (1998) Astrometry and geodesy with radio interferometry: experiments, models, results. *Reviews of Modern Physics*, 70, 1393, doi:10.1103/RevModPhys.70.1393

Tang G (2012) Radiometric Measurement Technique for Deep Space Navigation. China, Beijing: National Defense Industry Press

Tang G, Cao J, Han S, Hu S, Ren T, Chen L, Sun J, Wang M, Li Y, Li L (2014) Research on Lunar Radio Measurements by Chang'E-3. In: *IVS 2014 General Meeting Proceedings "VGOS: The New VLBI Network"*, Eds. D. Behrend, K.D. Baver, K.L. Armstrong, Science Press, Beijing, 473–477, 2014, `ftp://ivscc.gsfc.nasa.gov/pub/general-meeting/2014/pdf/101_Tang_etal.pdf`

Taylor DB, Bell SA, Hilton JL, Sinclair AT (2010) Computation of the quantities describing the lunar librations in the astronomical almanac. Naval Observatory Washington DC

VEX2 – VLBI Experiment definition, `http://vlbi.org/`

Will CM (2014) The confrontation between general relativity and experiment. Living Rev. Relativity

Zheng W, Huang Y, Chen Z, Wang G, Liu Q, Tong F, Li P, Tong L, Shu F (2014) Real-time and High-Accuracy

VLBI in the CE-3 Mission. In: *IVS 2014 General Meeting Proceedings "VGOS: The New VLBI Network"*, Eds. D. Behrend, K. D. Baver, K. L. Armstrong, Science Press, Beijing, 473–477, ftp://ivscc.gsfc.nasa.gov/pub/general-meeting/2014/pdf/100_Zheng_etal.pdf

In der Schriftenreihe des Instituts für Geodäsie und Geoinformation der Rheinischen Friedrich-Wilhelms-Universität Bonn sind erschienen:

Heft 54 2017	Proceedings of the First International Workshop on VLBI Observations of Near-field Targets
Heft 53 2016	Christian Eling Entwicklung einer direkten Georeferenzierungseinheit zur Positions- und Orientierungsbestimmung leichter UAVs in Echtzeit
Heft 52 2016	Maike Schumacher Methods for assimilating remotely-sensed water storage changes into hydrological models
Heft 51 2015	Christoph Holst Analyse der Konfiguration bei der Approximation ungleichmäßig abgetasteter Oberflächen auf Basis von Nivellements und terrestrischen Laserscans
Heft 50 2015	Lutz Rolf Roese-Koerner Convex Optimization for Inequality Constrained Adjustment Problems
Heft 49 2015	Jan Martin Brockmann On High Performance Computing in Geodesy Applications in Global Gravity Field Determination
Heft 48 2015	Judith Leek The application of impact factors to scheduling VLBI Intensive sessions with twin telescopes
Heft 47 2015	Thomas Artz Determination of Sub-daily Earth Rotation Parameters from VLBI Observations
Heft 46 2015	Roelof Rietbroek Retrieval of Sea Level and Surface Loading Variations from Geodetic Observations and Model Simulations: an Integrated Approach
Heft 45 2014	Ehsan Forootan Statistical Signal Decomposition Techniques for Analyzing Time-Variable Satellite Gravimetry Data
Heft 44 2014	Erich Weiß Lebensbilder der preußischen Verwaltung des 19. und 20. Jahrhunderts im Wandel Eine Sammlung biographischer Miniaturen
Heft 43 2014	Neysa Jacqueline Setiadi Assessing People´s Early Warning Response Capability to Inform Urban Planning Interventions to Reduce Vulnerability to Tsunamis Case Study of Padang City, Indonesia
Heft 42 2013	Nils Leber Entwicklungsperspektiven metropolitaner Peripherien im Rahmen Stadtregionaler Planungs- und Entwicklungsprozesse am Beispiel Nordrhein-Westfalen
Heft 41 2013	Sophie Schetke Socio-environmental impacts of settlement growth under conditions of fostered infill development: a methodological framework for a multicriteria assessment
Heft 40 2013	Ribana Roscher Sequential Learning Using Incremental Import Vector Machines for Semantic Segmentation

Heft 39 2013	Michael Ying Yang Hierarchical and Spatial Structures for Interpreting Images of Man-made Scenes Using Graphical Models
Heft 38 2013	Sabine Daniela Bauer Automatische Detektion von Krankheiten auf Blättern von Nutzpflanzen
Heft 37 2013	Martin Drauschke Ein hierarchischer Ansatz zur Interpretation von Gebäudeaufnahmen
Heft 36 2013	Timo Dickscheid Robust Wide-Baseline Stereo Matching for Sparsely Textured Scenes
Heft 35 2013	Alexander Barth Vehicle Tracking and Motion Estimation Based on Stereo Vision Sequences
Heft 34 2013	Richard Steffen Visual SLAM from image sequences acquired by unmanned aerial vehicles
Heft 33 2013	Till Rumpf Finding spectral features for the early identification of biotic stress in plants
Heft 32 2012	Christian Siemes Digital Filtering Algorithms for Decorrelation within Large Least Squares Problems
Heft 31 2012	Silvia Becker Konsistente Kombination von Schwerefeld, Altimetrie und hydrographischen Daten zur Modellierung der dynamischen Ozeantopographie
Heft 30 2013	Annette Eicker / Jürgen Kusche (eds.) Lecture Notes from the Summer School of DFG SPP1257 Global Water Cycle
Heft 29 2012	Matthias Siemes Ein Beitrag zur koordinatengesteuerten Aussaat von Rübenpflanzen mittels Multi-Sensor-System und Filteransatz
Heft 28 2012	Jörg Schmittwilken Attributierte Grammatiken zur Rekonstruktion und Interpretation von Fassaden
Heft 27 2012	Markus Rembold Die Anerkennung und Feststellung von Grundstücksgrenzen Ein Beitrag zur Entwicklung des Liegenschaftskatasters im Lande Nordrhein-Westfalen in Vergangenheit, Gegenwart und Zukunft
Heft 26 2012	Lihua Li Separability of deformations and measurement noises of GPS time series with modified Kalman filter for landslide monitoring in real-time
Heft 25 2012	Benedikt Frielinghaus Ökonomisches Entscheidungstool zur Wohnbaulandentwicklung Wirtschaftlichkeitsanalysen potenzieller Wohnbauflächen auf der Ebene des Flächennutzungsplanes
Heft 24 2011	Enrico Kurtenbach Entwicklung eines Kalman-Filters zur Bestimmung kurzzeitiger Variationen des Erdschwerefeldes aus Daten der Satellitenmission GRACE
Heft 23 2011	Sarah Böckmann Robust determination of station positions and Earth orientation parameters by VLBI intra-technique combination
Heft 22 2011	20th Meeting of the European VLBI Group for Geodesy and Astronomy Proceedings

Heft 21 2011	Philipp Zeimetz Zur Entwicklung und Bewertung der absoluten GNSS-Antennenkalibrierung im HF-Labor
Heft 20 2011	Alessandra Roy Effects on the Geodetic-VLBI Observables Due to Polarization Leakage in the Receivers
Heft 19 2011	Dietmar Weigt Auswirkungen von Flughäfen insbesondere von Fluglärm auf den Immobilienmarkt am Beispiel des Marktsegments „individuelles Wohnen“
Heft 18 2011	Anno Löcher Möglichkeiten der Nutzung kinematischer Satellitenbahnen zur Bestimmung des Gravitationsfeldes der Erde
Heft 17 2010	Basem Elsaka Simulated Satellite Formation Flights for Detecting the Temporal Variations of the Earth’s Gravity Field
Heft 16 2010	2nd International Conference on Machine Control & Guidance Proceedings
Heft 15 2009	Alexandra Weitkamp Brachflächenrevitalisierung im Rahmen der Flächenkreislaufwirtschaft
Heft 14 2008	Akbar Shabanloui A New Approach for a Kinematic-Dynamic Determination of Low Satellite Orbits Based on GNSS Observations
Heft 13 2008	Frank Friesecke Stadtumbau im Konsens!? Zur Leistungsfähigkeit und Fortentwicklung des städtebaulichen Instrumentariums unter Schrumpfungsbedingungen
Heft 12 2008	Heinz Rütz Zur Kostenanalyse der privaten Umlegung als Teil der konsensualen integrierten Baulandentwicklung
Heft 11 2008	Gaby Alexandra Boele-Keimer Kommunales Kennzahlenmanagement am Beispiel von Vermessungs- und Katasterämtern in Nordrhein-Westfalen
Heft 10 2008	Annette Eicker Gravity Field Refinement by Radial Basis Functions
Heft 9 2008	Torsten Mayer-Gürr Gravitationsfeldbestimmung aus der Analyse kurzer Bahnbögen
Heft 8 2008	Boris Kargoll On the Theory and Application of Model Misspecification Tests
Heft 7 2008	Hamza Alkhatib On Monte Carlo Methods
Heft 6 2008	Klaus Borchard Annäherungen an Städtebau und Raumentwicklung
Heft 5 2008	Jens Jähnke Zur Teilmarktbildung beim Landerwerb der öffentlichen Hand
Heft 4 2008	Atef Abd-Elhakee Makhloof The Use of Topographic Isostatic Mass Information
Heft 3 2008	Markus Vennebusch Singular Value Decomposition and Cluster Analysis

Heft 2
2007
Christian Beder
Grouping Uncertain Oriented Projective Geometric Entities

Heft 1
2007
Klaus Börger
Geodäsie und Quantenphysik

Vertrieb Rheinische Friedrich-Wilhelms-Universität Bonn
Institut für Geodäsie und Geoinformation
· Bibliothek ·
Nußallee 17
53115 Bonn

Tel.: #49 (0)228 73-3566
Fax: #49 (0)228 73-2988

Internet: http://www.igg.uni-bonn.de

ISSN 1864-1113